# Characterization Of The Primitive Neuroectodermal Tumor Genome Using Transposon-Mediated Insertional Mutagenesis

A DISSERTATION
SUBMITTED TO THE FACULTY OF THE GRADUATE SCHOOL
OF THE UNIVERSITY OF MINNESOTA
BY

**Jon David Larson**

IN PARTIAL FULFILLMENT OF THE REQUIREMENTS
FOR THE DEGREE OF
DOCTOR OF PHILOSOPHY

**Dr. David Andrew Largaespada**

December, 2011

## ACKNOWLEDGEMENTS

I absolutely thank my mentor, Dr. David A. Largaespada, for his mindful vision in science and life, endless levels of patience, guidance, respect and ambition to achieve enjoyable excellence. Thank you for the opportunity to be '1-1 in 2011.' It has been a privilege and pleasure to work with and learn from you during this journey, and it is your example that will continue to motivate me. I am very grateful to my committee members Dr. Walter Low, Dr. John Ohlfest and Dr. Dan Vallera for their superb direction and support over the years. Many thanks and respect to members of the Largaespada lab past and present for all their collaboration and camaraderie. I hold in high regard our time together during business and pleasure. I thank the Microbiology, Immunology and Cancer Biology graduate program for the opportunity to be a MICaBer with special acknowledgement to Louise Shand, Dr. Yoji Shimizu, Dr. Christopher Pennell and Dr. Sandra Armstrong for your leadership and encouragement. Thank you to the University of Minnesota community, especially members of the Brain Tumor Program, Masonic Cancer Center and Center For Genome Engineering for your consistent collaboration and solid support. It is with great pride that I represent you and the UMN. These are days I will always look back on with great fondness.

## DEDICATION

I dedicate my time and effort to my wife Siga, and our family near and far. Your support and caring means everything. We have experienced amazing adventures over the years, but the journey has only begun and I look forward to more adventures we will share together.

## ABSTRACT

Primitive neuroectodermal tumors (PNET) include medulloblastoma and supratentorial primitive neuroectodermal tumor subtypes that share histological features yet differ at the genomic level and in clinical outcome. Delineation of the genetic anomalies between PNET subtypes is a current challenge for establishing effective targeted therapeutic strategies against these aggressive tumors. Current efforts have demonstrated specific molecular pathways drive a minority of medulloblastoma and supratentorial PNET but the genetic basis of the majority of these tumors remains poorly understood and anecdotal. To better define the genetic causes of medulloblastoma and supratentorial PNET, we have developed a single *Sleeping Beauty* transposon insertional mutagenesis mouse model that recapitulates the morphological similarities and genetic heterogeneity of these tumor types capable of identifying genetic drivers important for PNETagenesis. This work has revealed biologically relevant candidate oncogenes and tumor suppressor genes for both medulloblastoma and supratentorial PNET in mice and humans. *ARHGAP36* is a novel oncogene implicated in poorly understood MB molecular subgroups, and multiple RAS pathway effector genes were identified to be important for sPNET formation. Ultimately, these results present new understanding of the genetic basis for medulloblastoma and supratentorial PNET development and offer potential targets for therapeutic testing to improve patient clinical outcome.

## TABLE OF CONTENTS

**Page**

**Page**

## LIST OF TABLES

**Page**

**CHAPTER 2**

## LIST OF FIGURES

**Page**

**Page**

## LIST OF ABBREVIATIONS

| Term | Abbreviation |
|---|---|
| Adenomatous Polyposis Coli | APC |
| Avian Leukosis Virus | ALV |
| Beta-Catenin | CTNNB1 |
| Candidate Cancer Genes | CCG |
| Central Nervous System | CNS |
| Coding Sequence | CDS |
| Common Insertion Sites | CIS |
| Comparative Genomic Hybridization | aCGH |
| Deoxyribonucleic Acid | DNA |
| *Discosoma sp*. Red Fluorescent Protein | DSRED |
| Embryonal Tumor With Abundant Neuropil and True Rosettes | ETANTR |
| External Granule Cell Layer | EGL |
| Glycogen Synthase Kinase-3-Beta | GSK3β |
| Gray Unit | Gy |
| Granule Neuron Precursor Cell | GNPC |
| Green Fluorescent Protein | GFP |
| Hematoxilin and Eosin | H and E |
| Histone 3 Lysine 9 | H3K9 |
| Horse Radish Peroxidase | HRP |
| Immunohistochemistry | IHC |

| | |
|---|---|
| Inverted Terminal Repeat | ITR |
| Internal Granule Cell Layer | IGL |
| Internal Ribosome Entry Site | IRES |
| Isochromosome 17 | i17q |
| Long Terminal Repeat | LTR |
| Luciferase | LUC |
| Medulloblastoma | MB |
| Myristoylated AKT | myrAKT |
| N-(2-chloroethyl)-N-cyclo-hexyl-N-nitrosurea | CCNU |
| Nevoid Basal Cell Carcinoma Syndrome | NBCCS |
| Patched | PTCH |
| Phosphoglycerate Kinase | PGK |
| *PiggyBac* | PB |
| Polyadenylation | PA |
| Polyethylenimine | PEI |
| Primitive Neuroectodermal Tumor | PNET |
| Replication-Compotent ALV Splice Acceptor | RCAS |
| Restriction length polymorphism | RFLP |
| Retinoblastoma 1 | RB1 |
| Ribonucleic Acid | RNA |
| Simian Virus 40 Large T Antigen | SV40-LgTAg |
| Single Nucleotide Polymorphism | SNP |

| | |
|---|---|
| *Sleeping Beauty* | SB |
| Smoothened | SMO |
| Sonic Hedgehog | SHH |
| Splice acceptor | SA |
| Supratentorial Primitive Neuroectodermal Tumor | sPNET |
| Suppressor of Fused | SUFU |
| Tumor Suppressor Gene | TSG |
| Wingless and Int | WNT |
| World Health Organization | WHO |

# CHAPTER 1

# Introduction

## Pediatric Brain Tumor Development

### Clinical Presentation of Medulloblastoma and sPNET

Malignant brain tumors are the most frequent solid cancer in children and consist of several different subtypes that pose distinct clinical challenges (Packer, 2008). Medulloblastoma (MB) and supratentorial primitive neuroectodermal tumor (sPNET) are intracranial primitive neuroectodermal tumors (PNET) subtypes defined by the World Health Organization (WHO) with useful guidelines for diagnosing their heterogeneous histological characteristics and malignancy grade (Louis et al., 2007). MB and sPNET are WHO grade IV embryonal tumors that occur most frequently in children and share several histopathological features including poorly differentiated small round cells of dense cellularity, high nucleus-to-cytoplasm ratio with frequently observed Homer-Wright rosettes (Inda et al., 2006). Despite their similarities, MB are more common comprising approximately 20% of all childhood malignant brain tumors compared to the more rare sPNET affecting approximately 3% of pediatric brain tumor patients (Reddy et al., 2000). MB and sPNETs have also been observed in rare adult patients (Brandes et al., 2009; Gessi et al., 2011). Other fundamental differences include physiological location with MB always occurring in the cerebellum, while sPNET arise in the cerebrum. sPNET patients also suffer an overall poorer prognosis (Li et al., 2005; Pfister et al., 2010). Furthermore, MB can be subdivided into five histology subtypes with varying frequencies: classic (~70%), desmoplastic (7%), anaplastic (2-4%), large cell (10-22%), and medulloblastoma with extensive nodularity (3%) (Gilbertson and Ellison, 2008; Louis et al., 2007). Although rare, sPNET are also being subdivided into histological

variants including CNS neuroblastoma, ganglioneuroblastoma and "embryonal tumor with abundant neuropil and true rosettes" (ETANTR) (Li et al., 2009; Pfister et al., 2009; Pfister et al., 2010; Eberhart, 2011). Classic MB is the most common subtype and shares the most histology overlap with sPNET. Although somewhat subjective, the clinical significance of these histological subtypes indicates a more favorable prognosis for non-metastatic MB displaying desmoplastic or nodular features, while anaplastic tumors provide a worse outcome (Eberhart et al., 2002; Pfister et al., 2010). The differences between MB and sPNET continue to be a focus of attention to delineate their clinical behavior.

Although very rare, patients with sPNET experience a relatively low 5-year overall survival of 50% compared to approximately 80% for MB patients (Inda et al., 2006). sPNETs are large tumors that can present with distant spread throughout the central nervous system (CNS), and patients commonly suffer increased intracranial pressure, enlarged head circumference and seizures. MB also cause increased intracranial pressure and increased head circumference due to hydrocephalus stemming from tumor growth and compression in the cerebellar fourth ventricle (Crawford et al., 2007). Subsequent symptoms for MB patients include headache, vomiting, irritability, and ataxia (Crawford et al., 2007).

**Current Medulloblastoma and sPNET Treatment Strategies**

Current risk stratification for MB patients after initial surgical resection is based on several criteria: age at diagnosis, extent of residual tumor tissue and presence of metastasis (Crawford et al., 2007). Patients less than 3 years of age or having residual

tumor mass larger than 1.5cm$^2$, or presenting with metastatic disease at time of diagnosis are considered high-risk, and patients that do not fit these criteria are considered average-risk. (Karajanni et al., 2008). Current average-risk MB patients over the age of 3 generally experience an 80% 5-year disease-free survival after receiving low-dose (23.4 Gy) craniospinal and local boost radiotherapy (5.58 Gy) plus adjuvant chemotherapy in an effort to eradicate potential undetected microscopic disease and control disease recurrence (Packer and Vezina, 2008). Chemotherapeutic drugs include cisplatin, N-(2-chloroethyl)-N-cyclo-hexyl-N-nitrosurea (CCNU), vincristine, cyclophosphomide, and etoposide. High-risk MB patients over the age of 3 undergo a similar treatment regimen with the exception of a high-dose (3.6 Gy) craniospinal radiotherapy and have approximately 60% 5-year disease-free survival (Packer and Vezina, 2008). Children under the age of 3 with MB pose a particularly difficult risk assessment as they do not receive radiation therapy to avoid severe neurological morbidity due to the delicate developmental stage of the brain. General strategy includes a chemotherapeutic approach to delay or preclude radiation if the patient reaches 3 years of age. Clinical management of this group is further complicated because up to 40% of these patients will present with metastatic disease at diagnosis (Packer et al., 2008). One benefit for this group is the high frequency of desmoplastic histotype MB that responds well to chemotherapy (Packer et al., 2008). Despite overall significant disease-free survival, current therapeutic strategies cause long-term morbidity among most MB survivors including neurological, neurocognitive and neuroendocrine problems. sPNET patients receive treatment similar to high-risk MB patients and benefit from a 5-year disease-free survival up to 60%,

however suffer a high frequency of recurrence (Reddy et al., 2000). Clear differences in the clinical behavior between MB and sPNET has spurred significant research to identify how these tumors differ on a genetic level, and possibly uncover molecular features predicating better risk stratification and potential target-specific therapeutic strategies to improve clinical response and reduce treatment induced morbidity.

## Genetic Origins Of Primitive Neuroectodermal Tumors

Current understanding of the genetic basis for MB and sPNET can be attributed to multiple studies of patients with heritable disease and genomic analysis of sporadic forms of these tumors.

### Familial Syndromes: Higher Risk For Medulloblastoma And sPNET

Patients with nevoid basal cell carcinoma syndrome (NBCCS), or Gorlin syndrome, suffer an increased incidence of malignancy including basal cell carcinoma, meningioma and medulloblastoma (Gorlin, 1987; Taylor et al., 2000). Gorlin syndrome is an autosomal dominant disorder manifested through mutations in the transmembrane receptor *PATCHED1* (*PTCH1*) gene located on chromosome 9q, a negative regulator of the SONIC HEDGEHOG (SHH) pathway. Interestingly, most medulloblastomas driven by SHH have a desmoplastic histotype. Lack of active PTCH1 results in derepression of the serpentine receptor SMOOTHENED (SMO) and subsequent activation of GLI transcription factors that help drive expression of SHH effector genes including *N-MYC*, *MATH1* and *CYCLIND1* (Kessler et al., 2009).

Turcot syndrome Type I patients harbor mutations in deoxyribonucleic acid (DNA)

mismatch repair genes *hMLH1*, *hMSH2*, *hPMS1* and *hPMS2* and develop colorectal adenocarcinoma, glial brain tumors, and have been linked with sPNET (De Vos et al., 2004). Turcot syndrome Type II is characterized by a germline mutation in the chromosome 5q21 *Adenomatous Polyposis Coli* (*APC*) gene and these patients suffer an increased risk of colorectal carcinoma and medulloblastoma (Taylor et al., 2000). Interestingly, most of these medulloblastomas have a classic histotype. APC operates as part of a negative regulation complex of the *Wingless and Int* (*WNT*) signaling pathway. In the absence of WNT signaling, APC complexes with AXIN and Glycogen Synthase Kinase-3-Beta (GSK3β) to phosphorylate the WNT signaling effector molecule Beta-Catenin (CTNNB1). Phosphorylated CTNNB1 is degraded via the ubiquitin-proteosome pathway (Hamilton et al., 1995). Mutant *APC* allows for uncontrolled WNT signaling resulting in stabilized cytosolic CTNNB1 that can translocate into the nucleus where it binds *TCF* transcription factors facilitation transcription of multiple genes including *C-MYC* and *CYCLIND* (Taylor et al., 2000).

Li-Fraumeni syndrome is caused by germline mutation of the *TP53* gene. These patients present with various types of cancer including sarcomas, acute leukemia, breast cancer, and brain tumors (Varley et al., 1997). Li-Fraumeni syndrome is also associated with MB (Pearson et al., 1982) and sPNET (Orellana et al., 1998). Interestingly, sporadic forms of these tumors also contain *P53* mutations associated with increased P53 immunostaining for both medulloblastoma and sPNET (Eberhart et al., 2005; Tabori et al., 2010).

**Sporadic MB And sPNET Contain Distinct Genetic Features**

Pioneering research and retrospective genetic studies have identified additional significant genetic differences between medulloblastoma and sPNET. Pomeroy and colleagues performed seminal experiments comparing the gene expression profiles of several subtypes of pediatric brain tumors including MB and sPNET and confirmed these tumor subtypes indeed harbor distinct gene expression profiles (Pomeroy et al., 2002). This study also demonstrated that MB histopathological subgroups could be distinguished by their gene expression. Namely, desmoplastic MB harbored differentially expressed genes among the SHH pathway including *PTCH1* and *GLI1* and *N-MYC*. Multiple studies using restriction length polymorphism (RFLP) and array comparative genomic hybridization (aCGH) demonstrated isochromosome 17 (i17q) as the most frequent genetic anomaly in MB, while rarely observed in sPNET (Burnett et al., 1997; Inda et al., 2005; Pfister et al., 2007). Differentially expressed candidate genes in this region are being identified (Traenka et al., 2010). Work by Russo et al. also showed this discrepancy as well as an association of 14q and 19q chromosomal loss with sPNET (Russo et al., 1999). Further studies linked focal deletion of 9p21.3, harboring the tumor suppressor gene *CDKN2A*, and amplification of the 19q13.41 miroRNA cluster exclusively to sPNET (Pfister et al., 2007, Li et al. 2009). In addition, Inda and colleagues identified a higher frequency of hypermethylation at the *CDKN2A* locus for *p14/ARF* in sPNET compared to MB (Inda et al., 2006). These studies provide evidence that despite morphological similarities, MB and sPNETs are genetically complex with some similar and distinctive features. Current confounding issues for comparing and contrasting underlying genetic causes of MB and sPNET include the overall rarity of sPNET and that

they harbor greater complexity of DNA copy number changes compared to MB (Li et al., 2005).

As mentioned above, MB are subdivided into five histology subgroups: classic, desmoplastic, anaplastic, large cell, and medulloblastoma with extensive nodularity (Gilbertson and Ellison, 2008) and also exist in distinct molecular subgroups (Thompson et al., 2006; Kool et al., 2008; Cho et al., 2010; Northcott et al., 2011). Notably, these studies identify gene expression signatures indicating aberrant SHH or activated WNT signaling in approximately 25 and 15%, respectively, of all medulloblastomas as well as 2 to 4 other subgroups not associated with SHH or WNT that express high levels of the known MB oncogene *OTX2* (Kool et al., 2008; Northcott et al., 2011). Hallmark characteristics of the SHH molecular subgroup include inactivating mutations in SHH pathway suppressors *PTCH1* or Suppressor of Fused (*SUFU*), loss of chromosome 9q (where *PTCH1* resides) or elevated of *N-MYC* expression. WNT MB can harbor activating mutations in *CTNNB1*, nuclear expression of CTNNB1 protein or monosomy for chromosome 6. Importantly, patients presenting with non-SHH/WNT MB subgroups have an overall poorer prognosis, an increased frequency of metastatic disease, and the critical genetic driver pathways for these tumors are not well defined despite the fact they represent the majority of clinical MB. Molecular characteristics of these MB include i17q, *OTX2* and *MYC* amplification, P53 immunopositivity, and are further subdivided by differential expression of genes involved in neuronal or photoreceptor differentiation. (Thompson et al., 2006; Kool et al., 2008; Cho et al., 2010; Northcott et al., 2011).

Similarly, sPNET subcategories have been identified based on their histological and

genetic characteristics (Pfister et al., 2010). *CDKN2A* deletion is more common in CNS neuroblastoma, and 19q13.42 amplification frequent in ETANTR, both with a dismal prognosis (Pfister et al., 2010). Recently, an immunohistochemistry screen was performed to determine WNT pathway activation by nuclear CTNNB1 staining in a series of MB and sPNET. Rogers et al., 2009 identified 36% sPNETs analyzed were immunopositive for nuclear CTNNB1 similar to 27% of MB and patients with these characteristics tended to have better prognosis.

The age and sex of MB and sPNET patients also contribute to overall tumor burden and have been linked with particular genetic anomalies. MB occur more often in males overall, but SHH and WNT pathway subgroups predominantly effect females (Cho et al., 2010; Northcott et al., 2011). In addition, these studies revealed SHH-driven MB arise most often in infants less than 3 years old or adults over 16 years old. Furthermore, sPNETs have also been observed in adult patients and these tumors contain a higher incidence (5/11, 45%) of *P53* mutations compared to pediatric sPNET (Gessi et al., 2011). Mutations that generate the $IDH1^{R132H}$ mismatch observed in secondary glioblastoma also occur more often in adult sPNET (2/11, 18%, Gessi et al., 2011; 2/6, 33%, Hayden et al., 2008.). Collectively, these studies further demonstrate the demographic and genetic complexity of MB and sPNET providing a challenge for clinicians to establish appropriate treatment strategies.

**Current Mouse Models For Medulloblastoma And sPNET**

Molecules and pathways that are affected in human PNET tumors have also been

manipulated in mice to model PNETagenesis, and have provided insight into potential cells of origin for MB and sPNET.

Normal cerebellum development begins during gestational week 6 and stems from two distinct germinal zones, the ventricular zone and the rhombic lip (Gilbertson and Ellison, 2008). The ventricular zone is the neural stem cell primary germinal zone located at the dorsal aspect of the fourth ventricle and gives rise to GABAergic cells including glia and Purkinje cells that take final residence in the cerebellar cortex. The rhombic lip is a secondary germinal zone comprised of granule neuron precursor cells (GNPC) that migrate rostrally to form the external granule cell layer (EGL) that creates a perimeter around cells derived from the ventricular zone. These precursor cells undergo rapid proliferation and then proceed to migrate inward along Bergmann glial fibers, past the Purkinje cell layer, to form mature neurons of the internal granule cell layer (IGL). This process completes within the second year after birth (Gilbertson and Ellison, 2008). Mouse cerebellum development occurs in a similar fashion beginning at embryonic day 10, with GNPC migration persisting through 2 weeks after birth. This process can be tracked during mouse brain development using specific molecular markers for cells derived from their respective germinal zones (Figure 1.1). At embryonic day 14, GNPC derived from the secondary germinal zone have migrated to form the EGL and express the transcription factor *Math1* (Figure 1.1A, D). Simultaneously, developing cells of the fourth ventricle can be detected by *GFAP* expression (Figure 1.1A, G). At postnatal day 7, GNPCs in the EGL achieve peak expansion and begin migrating to form the IGL (Figure 1.1B, E), and cells derived from the fourth ventricle are observed in the cerebellar

cortex, near the EGL (Figure 1.1B, H). By postnatal day 21, the cerebellum is fully developed (Figure 1.1C). GNPC have completed their migration from the EGL to become mature granule neurons of the IGL, cease to express *Math1* and are marked by the neuronal differentiation marker *NeuN* (Figure 1.1F), and cells derived from the fourth ventricle take final residence in the cortex including the Purkinje and molecular cell layer (Figure 1.1C, I). In addition, a third germinal zone was identified within the white matter of the postnatal cerebellum and can generate astrocytes, oligodendrocytes and neurons other than granule neurons (Lee et al., 2005). Perturbations in the organization and movement of these germinal cells could circumvent normal cerebellum development and lead to pathological conditions, including MB as exemplified in $Ptch1^{+/-}$ mice.

Goodrich et al. created the first MB mouse model through germline mutation of *Ptch1* to genocopy Gorlin syndrome and induce Shh signaling (Goodrich et al., 1997). These $Ptch1^{+/-}$ mice suffered a range of phenotypes seen in Gorlin syndrome including extra digits, soft tissue tumors and MB (15%). Although p53 mutant mice designed to mimic Li-Fraumeni syndrome do not form MB, 95% of $Ptch1^{+/-}p53^{-/-}$ mutant mice develop MB within four months (Wetmore et al., 2001). Reviewed in Wu et al. 2011, many other Shh-activated MB mouse models combine *Ptch1* heterzygosity with *Ink4c*, *Kip1*. or *Hic1* mutants. Other Shh-mediated MB mouse models harbor constitutively active *Smo* or combine mutated *Sufu* with *p53* deficiency. Seminal research by Wechsler-Reya and Scott demonstrated critical regulation of the Shh pathway for proper development of the cerebellum and how altered Shh signaling effects granule cell precursors as a MB cell of origin (Wechsler-Reya and Scott, 1999).

Wechsler-Reya used *Ptch1*$^{+/-}$ mice and showed that Shh is produced and secreted by Purkinje cells and normally received by GNPC via the *Ptch1* receptor for proper regulation of proliferation in the EGL (Wechsler-Reya and Scott, 1999). Subsequent studies revealed that although only a fraction of *Ptch1*$^{+/-}$ mice develop MB, all of these animals possess ectopic, pre-neoplastic lesions located in the EGL further suggesting these cells as a cell of origin for MB and their need for proper Shh signaling (Oliver et al., 2005). Furthermore, the ideas of potential MB cells of origin were expanded through Cre-lox conditional knockout of *Ptch1* using *Math1*-Cre (expressed in GNPC) or *GFAP*-Cre (expressed in neural stem cells that give rise to neuronal and glial cells including GNPC) (Yang et al., 2008). Both experiments yielded MB in a similar fashion suggesting proper Shh pathway regulation is required both in early stem cell populations after they commit to the granule cell lineage and the later GNPC of the EGL. Sporadic mouse models of MB have been developed using the RCAS system (described in Chapter 3) to deliver exogenous oncogene expression to *Nestin*-expressing neural stem cells (Rao et al., 2003; Rao et al., 2004; Browd et al., 2006; Binning et al., 2008). These models employ targeted expression of *c-Myc*, *Igf*, *N-myc* or *Hgf*, respectively, in combination with required Shh overexpression to form tumors. Other mouse models of MB have been generated by combining *p53*$^{-/-}$ with various defective DNA damage repair genes including *Lig4*, *Xrcc4*, *Brca2* and *Parp1* in *Nestin*-Cre expressing neural stem cells (Wu et al., 2011). Interestingly, subsequent expression profiling and chromosomal analysis showed significant defects including loss of *Ptch1* and *Gli1* overexpression, further implicating the Shh pathway in MB development.

One of the first non-Shh MB mouse models developed combined a conditional Cre-lox activation mutant *Ctnnb1* with conditional *p53* deficiency (Gibson et al., 2010). The Brain lipid binding protein (BLBP)-Cre transgene promoted recombination in cells throughout the hindbrain including the ventricular zone, GNPCs of the EGL, and progenitor cells of the lower rhombic lip. Gibson et al., 2010 found MB located in the fourth ventricle with expression profiles comparative to human WNT subgroup tumors including elevated levels of *Dkk1-3*, targets of the WNT pathway. Importantly, they went on to show that these tumors do not derive from GNPCs, but by cells derived from the lower rhombic lip that develop and populate the brainstem. Also, these tumors present a classic morphology similar to their human counterpart and distinct from Shh-derived tumors that often have a desmoplastic morphology. Together, these results indicate WNT subgroup MB harbor distinct molecular profiles and are derived from a specific cell of origin compared to Shh subgroup MB. More recently, mice engineered with the Tet system to overexpress *NMYC* in cerebellum cells expressing *glutamate transporter 1* developed several classic and large cell anaplastic MB histotypes with characteristics of non-Shh mediated tumors including elevated *Otx2* and a lack of *Math1* and *Gli1* expression (Swartling et al., 2010).

Mouse models for sPNET that mimic human tumors are sparse. Mice that lack *p53* and different combinations of *Ink4d* (*Cdkn2d*) and *Ink4c* (*Cdkn2c*) deficiency often suffer vascular tumors, and also develop MB and sPNET at a low frequency implicating proper cell cycle control to suppress these tumors (Zindy et al., 2003). *INK4A* (*CDKN2A*) promoter methylation has been weakly observed in several studies of MB and sPNET

(Frühwald et al., 2001; Ebinger et al., 2004), but *CDKN2A* deletion found to be significantly more common in sPNET (Pfister et al., 2007). Recently, Jacques and colleagues conditionally inactivated *Retinoblastoma1* (*Rb1*) and *p53* in prospective subventricular zone stem cells of adult mice and observed sPNET at a frequency of 19.8% and approximately nine-month latency (Jacques et al., 2010). When combined with conditional *Pten* loss, this model develops sPNET faster (approximately 100 days) and more frequently (51%) further implicating proper cell cycle control, genome stability and PI3K signaling in sPNET development. Interestingly, the phenotype is shifted to glioma when *p53* and *Pten* are deleted in these cells. Furthermore, this study importantly demonstrates subventricular zone stem cells as a potential spatial and temporal sPNET cell of origin requiring the correct genetic insult especially loss of cell cycle control by the *Rb1* pathway. Momota et al. utilized the RCAS system (described in Chapter 3) and delivered *c-Myc* overexpression to *GFAP*-expressing subventricular neural stem cells in $p53^{-/-}$ neonatal mice to generate sPNET within 5 months (11/32, 34%) (Momota et al., 2008). Similar tumor incidence was observed when this model was coupled with stabilized *β-cateninS37A* (10/21, 32%), however with a reduced two month latency, further implicating subventricular neural stem cells as a potential sPNET cell of origin. Although these studies are informative, robust sPNET mouse models are needed to decipher the genome-wide characteristics of sPNET biology.

Overall, these studies provide valuable insight into the heterogeneous molecular basis and histogenesis for MB and sPNET. Nevertheless, sPNET and a majority of MB subgroups associated with poor clinical outcome require further molecular

characterization. Appropriate mouse models are urgently needed to assist this characterization and provide a true biological context for direct comparison to human disease, and ultimately pinpoint clinically relevant genetic targets for better patient stratification and therapeutic applications.

### *Sleeping Beauty* Transposons – The Future Is Now For Delineation Of The PNET Genome

In this era of cancer genomics, an ongoing challenge for identifying genetic anomalies in cancer pathogenesis on a genome-wide scale is distinguishing the genetic changes that directly contribute to disease progression from those that do not play a role in tumor growth. Recent efforts have proven beneficial for this purpose in several human tumors including colorectal and breast (Sjöblom et al., 2006), lung (Ding et al., 2008), glioblastoma (The Cancer Genome Atlas Research Network, 2008; Verhaak et al., 2010) and medulloblastoma (Northcott et al., 2009; Parsons et al., 2010) tumors. These studies combined multiple technologies including gene exon re-sequencing, high-resolution single nucleotide polymorphism (SNP) genotyping, aCGH, and microarray gene expression analysis on a genome-wide scale. Importantly, these studies confirm previously known somatically altered oncogenes and tumor suppressor genes (TSG) as well as genes not previously implicated in tumor development. Northcott and colleagues sampled 201 primary MB using high-resolution SNP arrays reidentified the most common MB chromosomal aberration i17q, characterized by a net loss of 17p and a net gain of one copy of 17q, in 28% of samples (Northcott et al., 2009). Known MB

oncogenes (*MYC*, *GLI1* and *OTX2*) were also amplified, while multiple oncogenes and TSG involved in histone 3 lysine 9 (H3K9) methylation were identified as novel candidate MB genes. In addition to structural genetic anomalies, altered gene expression profiles due to epigenetic forces also significantly contribute to tumor phenotype. Genome-wide expression and methylation profiling studies have also uncovered novel oncogene and TSG candidates in MB (Thompson et al., 2006; Kool et al., 2008; Kongkham et al., 2008). Overall, such studies exemplify the importance of identifying significant changes at the genetic, epigenetic and expression levels of gene regulation for better understanding of the cancer genome to ultimately uncover potential therapeutic drug targets. While informative, such studies are not without caveats including the significant costs and resources required to complete them. Also, specific genetic alterations that possibly create tumorigenic functional portions of genes, transcripts or proteins may be overlooked by mutation, expression or chromosomal structure analysis. Therefore it is important to compliment this research with basic research animal models capable of mimicking the genetic and biological context of human cancer to correctly identify relevant candidate cancer genes (CCG).

Since many cancers are derived from a series of somatic genetic mutations and anomalies, forward genetic somatic mutagenesis screens in mice have become an extremely useful approach to mimic this behavior. Mice are well suited for comparative functional genomics studies that model human disease because of their genetic and physiological similarities and both mouse and human genome sequence are publicly available for comparative analysis (Frese and Tuveson, 2007). Insertional mutagenesis in

mice is an efficient method for inducing tumorigenesis by altering the nascent genome, and subsequent identification of the precise genes and gene loci affected (Kool and Berns, 2009). Retroviruses and transposons have been developed as *in vivo* insertional mutagens and shown to be effective for identifying CCG in a variety of tumors including lymphoma (Mikkers et al., 2002; Dupuy et al., 2005), brain tumors (Johansson et al., 2004; Bender et al., 2010) and sarcomas (Collier and Carlson et a., 2005). Areas of the genome that recurrently harbor integrated provirus or transposons among multiple tumors are referred to as common insertion sites (CIS) and represent gene loci that were important for tumor development. These studies demonstrated biological relevance of insertional mutagenesis because genes that are altered in human cancer were identified as well as previously unknown CCG.

The *Sleeping Beauty* (SB) DNA transposon has emerged as a pioneering tool for somatic genome manipulation including insertional mutagenesis in mice. SB transposon and transposase sequences were originally reconstructed based on dormant *Tc1/Mariner* fish transposon genes harboring inactivating mutations (Ivics et al., 1997). SB operates as a 'cut-and-paste' DNA transposon and was engineered to function as a two-component system consisting of the SB transposon and transposase enzyme shown to be active in mammalian cells (Ivics et al., 1997). SB transposase recognizes inverted repeat/direct repeat (IR/DR) sequences flanking the DNA cargo, binds as a homodimer to these IR/DRs and excises the transposon from its genomic location leaving behind a three base pair footprint (CA/TG) (Figure 1.2 A-B) (Ivics et al., 1997). The transposon is then subsequently reintegrated into a new genomic location anywhere a TA dinucleotide is

present (Figure 1.2 C). Several iterations of the SB transposase and transposon IR/DR sequences have been engineered to increase mobilization activity (Grabundazija et al., 2011). This SB system has been used successfully for multiple experiments in mice including germline transgenesis (Dupuy et al., 2002), forward genetic phenotype screening (Carlson et al., 2003; Guerts et al., 2006), somatic cell gene delivery for *in vivo* cancer induction (Carlson et al., 2005; Wiesner and Decker et al., 2009) or suppression (Ohlfest et al., 2005). These studies have also shed light onto limitations of SB-mediated transposition including the tendency for local hopping of the transposon from its donor chromosomal concatomer and incompletely random nature of TA dinucleotide site integration (Carlson et al., 2003; Guerts et al., 2006). Recent studies have also used SB transposon insertional mutagenesis as a successful method for generating cancer in mice and subsequently identifying CIS as candidate genetic drivers of the tumors (Dupuy, 2010). The transposons T2/Onc and T2/Onc2 operate as insertional mutagens via their murine stem-cell virus long terminal repeat/splice donor sequence (MSCV LTR/SD) and bidirectional splice acceptor/polyadenylation sequences (SA/pA) (Figure 1.3A). These transposons are designed to promote protooncogene (Figure 1.3B) or halt TSG (Figure 1.3B) expression, respectively. Both vectors are effective when mobilized in all somatic cells, combined with the correct predisposing mutant background and a sufficient source of transposase to induce neoplastic prostate lesions, lymphomas and sarcomas (Rahrmann and Collier et al., 2009; Collier and Carlson et al., 2005; Dupuy et al., 2005; Collier et al., 2009). Brain tumors including medulloblastoma, sPNET and high-grade glioma were also observed at low frequency using this strategy (Collier et al., 2009; Dupuy et al., 2005)

with novel candidate glioma genes successfully identified (Bender et al., 2010). Furthermore, T2/Onc mutagenesis has been used to induce hepatocellular carcinoma and gastrointestinal tract cancer when applied in a tissue specific manner utilizing a Cre-lox regulated SB transposase transgene (Keng et al., 2009; Starr et al., 2009). Importantly, subsequent transposon insertion site analysis identified gene targets also altered in human disease, as well as candidate oncogenes and TSG not previously associated with their respective tumors. Therefore, these studies provide proof-of-concept that SB-mediated insertional mutagenesis can successfully model relevant stages of cancer in mice, can be applied to specific tissues for particular tumor development, and is capable of identifying known and novel candidate cancer genes for accurate delineation of the genetic basis of different cancers.

**HYPOTHESIS**

Current efforts to understand and distinguish the genetic basis between medulloblastoma and sPNET are ongoing, but still poorly understood. Models to correctly recapitulate molecular and phenotypic subtypes for these tumors are also lacking. I hypothesize that SB insertional mutagenesis can be applied to generate new mouse models for complete MB and sPNET development, identify novel candidate oncogenes and TSG that better define the heterogeneous genetic basis of these tumors, and ultimately identify clinically relevant targets to treat human disease.

**Figure 1.1. Cells Of Origin For Medulloblastoma**

(A-C) Sagital section of mouse brain at progressive developmental stages. (D-F) Math1 red immunofluorescence. (G-I) GFAP red immunofluorescence. (A) Embryonic-day 14 showing early cerebellum structures in the fourth ventricle (IV) including the ventricular zone (VZ), rhombic lip (RL), external granule cell layer (EGL), choroid plexus (CP). (D) Math1 marking cells of the developing EGL. (G) GFAP marking cell expanding from the VZ. (B) Postnatal day 7 showing advanced cerebellum development. (E) Math1 marking proliferating granule neuron precursor cells of the EGL. (H) GFAP marking Bergmann glia and cells bordering the EGL. (C) Adult day 21. (F) NeuN marking mature EGL cells that have successfully migrated to form the internal granule cell layer (IGL). (I) GFAP marking Bergmann glia and astrocytes of the molecular layer (ML). Figure modified from Schüller et al., 2008 and Yang et al., 2008)

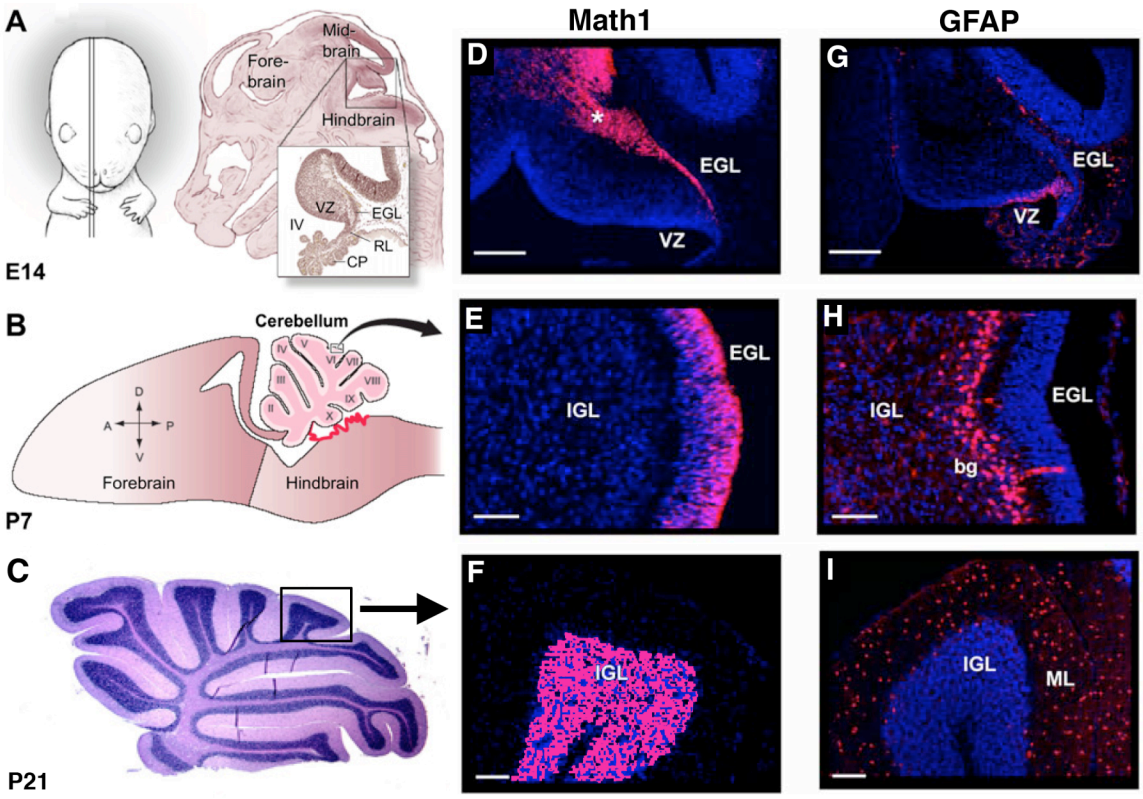
A
Mid-
brain
Fore-
brain
Hindbrain
VZ
EGL
IV
RL
CP
E14
B
Cerebellum
D
A
P
V
Forebrain
Hindbrain
P7
C
P21
Math1
GFAP
D
EGL
VZ
G
EGL
VZ
E
EGL
IGL
H
IGL
EGL
bg
F
IGL
I
IGL
ML

**Figure 1.2. *Sleeping Beauty* Transposon Mechanism Of Mobilization**

(A) SB transposase recognizes and binds as a homodimer to SB transposon IR/DR sequences. (B) SB transposon is excised from its genomic location. (C) Reintegration of the SB transposon into a new TA dinucleotide genomic location. (Adapted from Carlson and Largaespada, 2005).

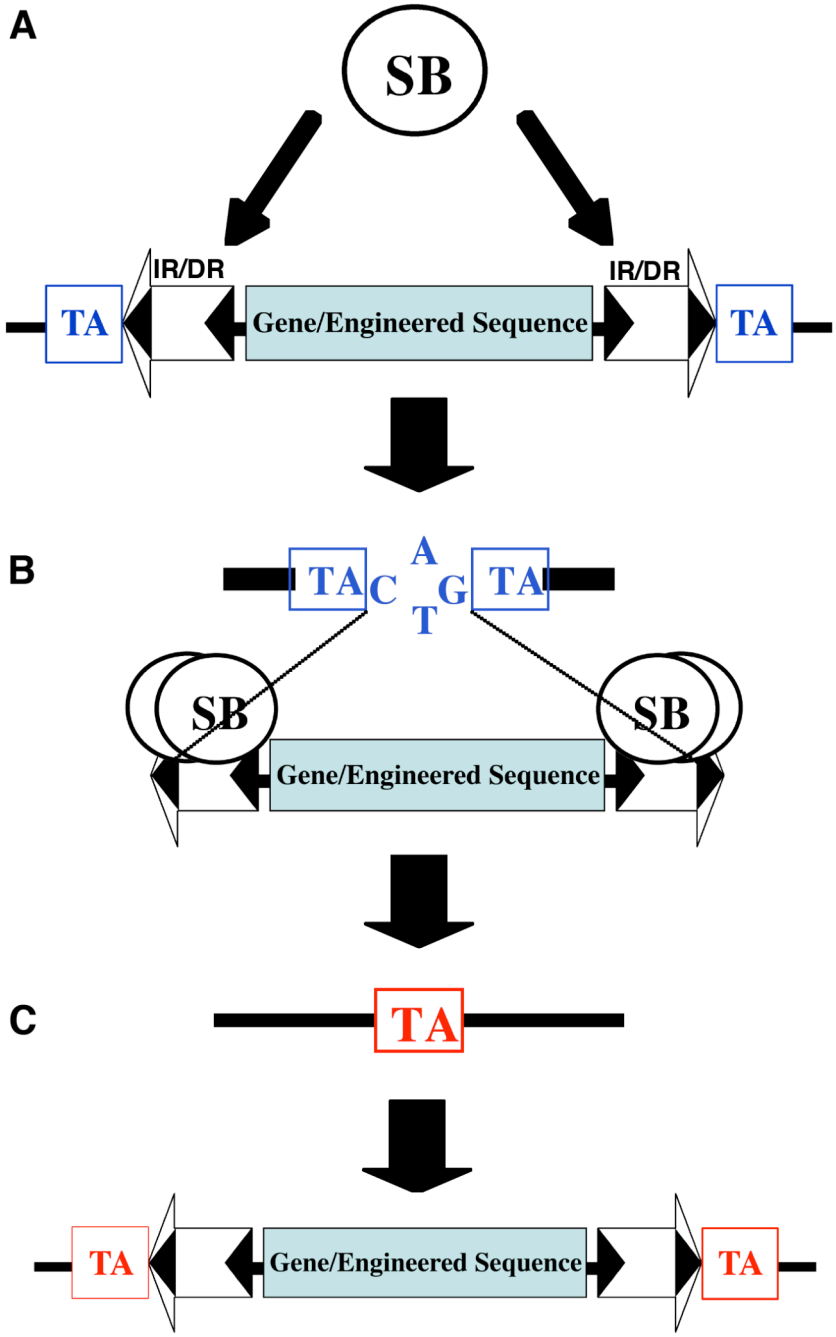
A
SB
IR/DR
IR/DR
TA
Gene/Engineered Sequence
TA
B
TA
C
A
T
G
TA
SB
SB
Gene/Engineered Sequence
C
TA
TA
Gene/Engineered Sequence
TA

**Figure 1.3. Structure And Function Of Mutagenic Transposon**

(A) Schematic of T2/Onc/T2/Onc2. Murine stem cell virus 5′ long terminal repeat with promoter and enhancer elements (MSCV) and splice donor (SD) sequences promote proto-oncogene expression. Bi-directional splice acceptor (SA) and polyadenylation (pA) sequences disrupt expression of tumor suppressor genes. (B) Mutagenic transposon-mediated activation of near full-length (upstream insertion) or truncated form (intronic insertion) of a proto-oncogene. (C) Mutagenic transposon-mediated disruption of tumor suppressor gene (inverse or sense orientation intronic insertion) (Adapted from Dupuy, 2010).

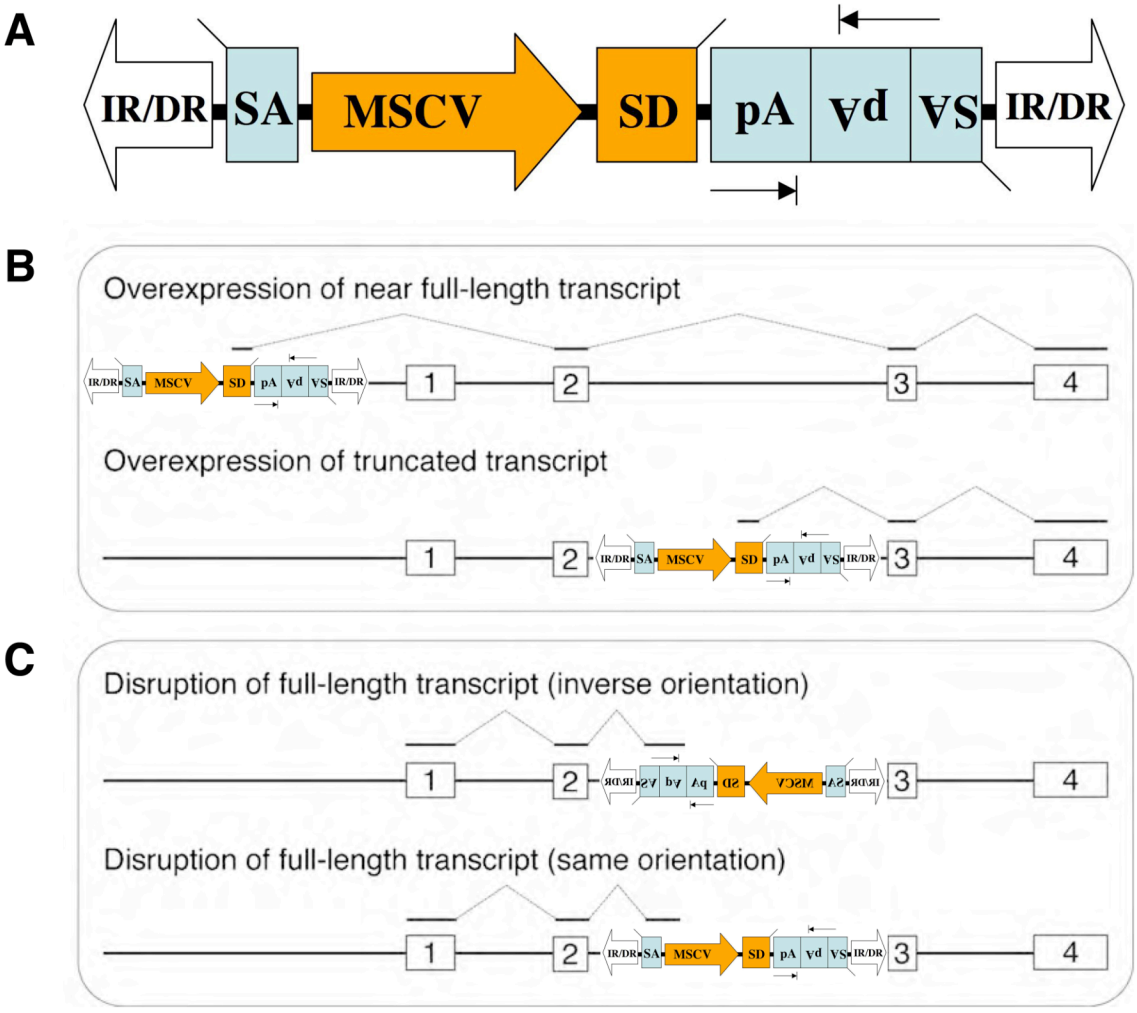
A
IR/DR
SA
MSCV
SD
pA
∀d
∀S
IR/DR
B
Overexpression of near full-length transcript
1
2
3
4
Overexpression of truncated transcript
1
2
3
4
C
Disruption of full-length transcript (inverse orientation)
1
2
3
4
Disruption of full-length transcript (same orientation)
1
2
3
4

# CHAPTER 2

## *Sleeping Beauty* Transposon Insertional Mutagenesis Reveals Distinct Recurrent Genetic Alterations Among Primitive Neuroectodermal Tumors

## Introduction

Primitive neuroectodermal tumors (PNET) are the most common childhood brain malignancies and include MB and supratentorial PNET (sPNET) (Reddy et al. 2000, Dubuc et al., 2010). These tumors share histological characteristics including small round cells of dense cellularity, high nucleus-to-cytoplasm ratio with frequently observed Homer-Wright rosettes (Inda et al., 2006). MB are the most frequent PNET, form in the cerebellum and may arise from ventricular zone stem cells or GNPC of the developing cerebellum (Gilbertson and Ellison, 2008). sPNET are more rare, typically located in the cerebral cortex or pineal gland (Reddy et al., 2000) and may arise from subventricular zone stem cells (Jacques et al., 2010; Momota et al., 2008). Despite their aggressive nature and histological similarities, MB and sPNETs have different clinical outcomes. MB has a 60-80% 5-year survival rate, with survivors facing severe cognitive side effects from current treatment regiments, while sPNET patients suffer poorer prognosis and generally fail to respond to therapy, possibly due in part to inaccessible anatomic location (Northcott et al., 2010). Patients with Gorlin or Turcot syndrome have germline mutations in the *PTCH1* or *APC* genes, respectively, and are at increased risk of MB through aberrant SHH or WNT signaling pathways, respectively (Taylor et al., 2000). Individuals with Li-Fraumeni syndrome harbor *P53* mutations and experience an increased incidence of MB and sPNET among other tumors. Sporadic forms of these tumors also contain genetic mutations affecting these pathways including *P53* mutations associated with increased P53 immunostaining for both MB and sPNET (Eberhart et al., 2005; Tabori et al., 2010). Seminal microarray analysis identified multiple differentially

expressed genes distinguishing sPNET from MB and other tumors (Pomeroy et al., 2002). Loss of *PTEN* through 10q copy loss and mutation has been observed in sPNET (Kraus et al., 2002), and biallelic loss or *PTEN* promoter hypermethylation has been observed in MB (Hartmann et al., 2006). Although i17q is one of the most frequent chromosomal abnormalities occurring in human cancer including MB, it is rarely observed in sPNET (Burnett et al., 1997; Inda et al., 2005; Pfister et al., 2007; Carvalho and Lupski, 2008). Further studies linked focal deletion of 9p21.3, harboring the tumor suppressor gene *CDKN2A*, and amplification of the 19q13.41 miroRNA cluster exclusively to sPNET (Pfister et al., 2007, Li et al. 2009). Recent global analysis of the MB genome using high power SNP array or exon resequencing identified candidate tumor suppressor genes important for proper histone methylation (Northcott et al., 2009; Parsons et al., 2011). Therefore, there is a growing body of evidence that despite morphological similarities, MB and sPNETs are genetically complex and more distinct from each other than previously thought.

In addition to genetic differences that distinguish PNETs, MB and sPNET are further subdivided into histological and genetic subgroups (Thompson et al., 2006; Kool et al., 2008; Gilbertson and Ellison, 2008; Cho et al., 2010; Pfister et al., 2010; Northcott et al., 2011). MB subgroups include those with gene expression signatures indicating aberrant SHH (25%), activated WNT signaling (15%), and tumors not associated with SHH or WNT that express high levels of the known MB oncogene *OTX2* (Kool et al., 2008; Northcott et al., 2011). Importantly, patients presenting with non-SHH/WNT MB or sPNET subgroups have an overall poorer prognosis and the critical genetic driver

pathways for these tumors are not well defined. Further clarification of the genetic differences between MB and sPNET as well as differences amongst subgroups of these tumors is needed for future improvements on current treatment methods for patients suffering from these diseases.

The use of *in vivo* transgenic mammalian models has proven invaluable for dissecting the genetic causes of MB and sPNET, and mouse models have been created to mimic these human diseases based on genetic, molecular and physiological similarities between mice and man. Multiple genetically engineered mouse models of MB have been developed by activating the Shh or Wnt pathways in various cells of origin to recapitulate their corresponding human subgroup MB (Reviewed in Wu et al., 2011). Other mouse models affecting the *Rb1* and *p53* pathways can trigger sPNET formation (Marcus et al., 1991; Jacques et al., 2010). While very useful, these models focus on specific well known molecules and pathways associated with PNET disease. There is currently a need for an *in vivo* model to interrogate the global characteristics of the PNET genome in an unbiased manner to faithfully recapitulate human PNETs and their subgroups, and use for direct comparative genomics approach.

To address these deficiencies, we used SB-mediated insertional mutagenesis to perform a novel, non-biased, forward genetic screen in mice to better understand the genetic differences between MB and sPNET development. We targeted the SB system to the neuronal and glial precursor cells using *Nestin*-Cre as a source of Cre recombinase in otherwise wild type, *Pten* deficient or dominant negative *p53* backgrounds. MB and sPNETs developed in mutagenized mice with the highest frequency occurring on a

dominant negative *p53* background and common insertion sites reveal distinct genetic drivers for each tumor type establishing a new mouse model for interrogating molecular differences between PNET subtypes. Furthermore, we identified a novel candidate MB gene, *Arhgap36,* whose increased expression occurs in a Shh-independent molecular subgroup demonstrating the ability of this new model to faithfully recapitulate and provide potentially novel therapeutic targets for human disease.

## Materials And Methods

### Generation of Transgenic Mice

*Nestin*-Cre mice (Jackson Laboratory #003771, Tronche et al. 1999) were bred to either T2/Onc (chromosome 15 or 1 concatomers, approximately 25 copies, Collier et al., 2005) or T2/Onc2 (TG6057, chromosome 4 concatomer, approximately 148 copies, Dupuy et al., 2005) to generate *Nestin*-Cre:T2/Onc double transgenic mice. *Rosa26-lsl-SB11* (Starr et al., 2009, Keng et al., 2009) were bred to either $p53^{lsl\text{-}R270H}$ (Olive et al. 2004) or $Pten^{flox/flox}$ (Xiao et al. 2005) to generate *Rosa26-lsl-SB11*:$Pten^{flox/flox}$ or *Rosa26-lsl-SB11*:$p53^{lsl\text{-}R270H}$ double transgenic mice. *Nestin*-Cre:T2/Onc mice were then bred to *Rosa26-lsl-SB11*:$Pten^{flox/flox}$ or *Rosa26-lsl-SB11*:$p53^{lsl\text{-}R270H}$ mice to generate mice with and without insertional mutagenesis in combination with different genetic backgrounds: wild type, conditional *Pten* heterozygous, or conditional dominant negative *p53* (Figure 2A, B and C). All mice were bred and cared for under the guidelines of the University of Minnesota Animal Care and Use Committee.

### Genotyping and Excision PCR

PCR primer sequences for each transgene were as follows: *Nestin*-Cre: Forward 5′-CTGATGGACATGTTCAGGGATCG-3′, Reverse 5′-CCCACCGTCAGTACGTGAGATATCT-3′; *Rosa26-lsl-SB11*: Forward 5′-ATGTTTGGAGGAAGAAGGGG-3′, Reverse 5′-CCATTTGCGACCAAGCTTTA-3′; T2/Onc or T2/Onc2: Forward 5′-CGCTTCTCGCTTCTGTTCGC-3′, Reverse 5′-CCACCCCCAGCATTCTAGTT-3′; $Pten^{flox}$: Forward 5′-AAAAGTTCCCCTGCTGATTTGT-3′, Reverse 5′-TGTTTTTGACCAATTAAAGTAGGCTGT-3′; $p53^{lsl\text{-}R270H}$ (detects both wild type and transgenic alleles): wild type Forward 5′-TTACACATCCAGCCTCTGTGG-3′, transgenic Forward 5′-AGCTAGCCACCATGGCTTGAGTAAGTCTGCA-3′, wild type Reverse 5′-CTTGGAGACATAGCCACACTG-3′.T2/Onc and T2/Onc2 excision PCR was performed as previously described (Collier et al. 2005) using primer sequences: Forward 5′-TGTGCTGCAAGGCGATTA-3′, Reverse 5′-ACCATGATTACGCCAAGC-3′.

**Histopathology and Immunohistochemistry**

Tissue samples were fixed in 10% phosphate buffered formalin, paraffin embedded, cut into 5μm sections and stained with Hematoxilin and Eosin (H and E) using standard methods. Unstained tissue microarray sections of formalin-fixed, paraffin-embedded tumor specimens on glass slides were obtained through an IRB-approved mechanism through the University of Minnesota Biological Materials Procurement Network (BioNet; www.bionet.umn.edu), and Johns Hopkins University. Immunohistochemistry was conducted using standard methods with citrate-based antigen retrieval (#H-3300, Vector

Laboratories). Endogenous peroxidase activity was quenched with 3% hydrogen peroxidase. Primary antibodies: SB (#MAB2798, R&D Systems), Ki67 (#NCL-L-Ki67-MM1, Leica) Synaptophysin (clone SY38, ICN Biomedicals), Nestin (#sc-33677, Santa Cruz Biotechnology), GFAP (#Z0334, Dako), Gli1 (#AB3444, Millipore), Otx2 (#AB9566, Millipore), Arhgap36 (#HPA002064, SIGMA), p-AKT(Ser473) (#4060, Cell Signaling Technologies), Pten (#9559, Cell Signaling Technologies), p-Erk (Thr202/Tyr204) (#4370, Cell Signaling Technologies) were used and detected with Vector Laboratories reagents: Vectastain Elite ABC Kit (#PK6100) and 3,3'-diaminobenzidine (DAB) Substrate Kit (#SK-4100).

**Ligation Mediated PCR**

Genomic DNA was carefully isolated from tumor tissue by proteinase K digestion with subsequent phenol-chloroform extraction and ethanol precipitation. Transposon-genomic DNA junction fragments were amplified as previously described (Keng et al., 2009; Starr et al. 2009) and processed by Illumina sequencing.

**CIS Analysis**

Transposon-genomic DNA sequences were loaded into a relational database and database queries were used to identify and remove barcodes denoting the library of origin. Transposon sequences and linker fragments were trimmed off, leaving genomic sequence. Identical sequences derived from the same library were condensed to a single sequence entry, retaining the total count of observations. Potential genomic sequences were mapped to the mouse genome using the bowtie algorithm. Only insertions with flanking genomic sequence beginning with a TA dinucleotide were considered further.

As an additional step to minimize the potential for false positive mapping, bowtie was set to only allow mismatches in lengths of sequences where randomly generated sets of 50000 DNA sequences were unable to map. The empirical cutoffs to eliminate this potential source of error were 33 nucleotides for 3 mismatches, 30 for 2 mismatches, 28 for 1 mismatch and 24 for 0 mismatches. For this rational, sequences of 23 or less bases were discarded from the analyses to increase the stringency of the analyses.

Common transposon integration sites were calculated using the Poisson distribution. The Poisson distribution determined the probability of observing a given number of events within a region assuming that these events occur in an essentially unbiased manner. In this case the transposon insertions were the events, the size of the genome was the region, and the total number of insertions being analyzed for CIS were used to estimate the frequency of event observation. The probability estimate was then corrected based on the total number of windows examined (i.e., the total number of insertions) using Bonferroni correction to ensure statistical rigor.

For CIS analysis, the window sizes used were determined by identifying the maximum window size to generate a corrected p-value $< 0.05$ with an integer number of insertions by examining window sizes from 10000 bases to 300000 bases. If fewer than 1000 insertions or more than 200000 inserts were examined, default window sizes of 12500, 25000,50000,100000 and 200000 bases were used.

**RT-PCR**

Total RNA was extracted from tumor tissues using TRIzol Reagent (#15596-018, Invitrogen). Residual contaminating DNA was removed with TURBO DNA-*free* Kit

(#AM1907, Ambion). RT-PCR was performed with 500ng total RNA using SuperScript III First-Strand Synthesis System (#18080-051, Invitrogen) and an *Arhgap36*-specific primer targeting exon 5 (5′-GCAACAAGTCTCAACAATCTGAGG-3′). Fusion transcripts were amplified using these primers: T2Onc/2 Splice Donor Forward (5′-CTACTAGCACCAGAACGCCC-3′), Arhgap36 Ex5 Reverse (5′-GATTTGTTGAGCAATTGGGTTGAGG-3′), BetaActin Forward (5′-TGGGCCGCCCTAGGCACCA-3′), BetaActin Reverse (5′-CTCTTTGATGTCACGCACGA-3′).

**Results**

***Nestin*-Cre Mediates SB Transposase Expression Throughout the Mouse Brain**

To assess the spatial and temporal activation of the *Rosa26-lsl-SB11* allele in central nervous system cells, we bred *Nestin*-Cre mice with *Rosa26-lsl-SB11* mice. We tested Cre-lox recombination of the *Rosa26-lsl-SB11* allele in brain cells of double transgenic mice by immunohistochemistry using an antibody specific for the SB transposase protein. At postnatal day two, we observed SB expression throughout the brain (Figure 2.1A) including cells of the developing cerebellum: granule cells (Figure 2.1B), white matter (Figure 2.1C), and cells surrounding the fourth ventricle (Figure 2.1D). SB transposase expression was also observed in cells of the subependymal midbrain (Figure 2.1E), subventricular zone (Figure 2.1F) and olfactory bulb (Figure 2.1G). SB transposase expression throughout the brain also persists in adult mice (data not shown). Importantly, we did not observe SB transposase expression in mice harboring only the *Rosa26-lsl-*

*SB11* allele (Figure 2.1B`-G`). We also observed mosaic SB expression in other tissues including pancreas, kidney and testicles (data not shown). These results demonstrated that the *Nestin*-Cre allele successfully activates SB transposase expression in prospective cells of origin for medulloblastoma and sPNET.

**SB Insertional Mutagenesis Promotes Malignant PNET Formation**

In an effort to evaluate tissue-specific SB insertional mutagenesis throughout the brain in combination with *Pten* or *p53* deficiency for PNETagenesis, we bred mice transgenic for *Nestin*-Cre and T2/Onc (or T2/Onc2) concatomer with mice harboring Cre recombinase-responsive transgenes *Rosa26-lsl-SB11* and $Pten^{flox/flox}$ or $p53^{lsl\text{-}R270H}$. These crosses generated three experimental cohorts of mice undergoing tissue-specific SB transposition with distinct genetic backgrounds: wild type (Figure 2.2A), conditional *Pten* heterozygosity (Figure 2B) or conditional dominant negative $p53^{R270H}$ (Figure 2.2C). Important control mice lacking transposition but undergoing *Nestin*-Cre-mediated SB11 transposase expression (Figure 2.2A), *Pten* heterozygosity (Figure 2.2B) or dominant negative $p53^{R270H}$ (Figure 2.2C) were also produced in each cohort. We initiated these cohorts to exclusively harbor two different transgenic lines for T2/Onc (Collier and Carlson et al., 2005) or T2/Onc2 (Dupuy et al., 2005). The T2/Onc transgenic mice harbor a concatomer of approximately 25 transposon copies located on chromosome 1 or 15. T2/Onc2 transgenic mice harbor a concatomer of approximately 148 transposon copies located on chromosome 4. The majority of experimental animals contained either the low copy chromosome 15 T2/Onc concatomer or the high copy chromosome 4 T2/Onc2 concatomer (Supplemental Figure 2.1). All mice were aged and monitored for

signs of neurological symptoms. Animals that developed severe ataxia, enlarged cranium or general morbidity were sacrificed, dissected and carefully examined for tumors.

We observed macroscopic MB only in mice undergoing SB mutagenesis, but at varying frequencies dependant on the genetic background (blue columns, Figure 2.2D): transposition only = 6/68 (9%), transposition and $Pten^{flox/+}$ = 4/90 (4%), transposition and $p53^{lsl\text{-}R270H}$ = 12/64 (19%). The overall average age of mice that died from MB was 143 days. Average latencies (in days) of each cohort were: transposition only = 148, transposition and $Pten^{flox/+}$ = 195, transposition and $p53^{lsl\text{-}R270H}$ = 123 (Figure 2.2E). Mice with SB-induced tumors associated with dominant negative $p53^{R270H}$ showed the greatest acceleration among all the cohorts and developed tumors significantly faster than mice with medulloblastomas associated with *Pten* heterozygosity ($p = 0.0088$). We also observed macroscopic sPNET at varying frequencies among animals undergoing SB mutagenesis (red columns, Figure 2.2D): transposition only = 1/68 (2 %), or transposition and $p53^{lsl\text{-}R270H}$ = 12/64 (19%). In addition, only one microscopic sPNET was also identified in the olfactory bulb of a *Nestin*-Cre; $p53^{lsl\text{-}R270H}$ control mouse: 1/47 (2%) further indicating SB mutagenesis accelerates sPNET formation in conjunction with $p53^{lsl\text{-}R270H}$. The SB-induced sPNETs associated with dominant negative p53 occurred on average at 440 days (Figure 2.2F). The SB-induced sPNET derived on an otherwise wild type background developed at 499 days and control sPNET from the activated dominant negative p53 only occurred at 333 days. We consistently observed a high frequency of T2/Onc2-mediated MB (Supplemental Figure 2.1A, B and C). In contrast, sPNET associated with dominant negative p53 were equally derived from low and high copy

transposon concatomers 15 and 4, respectively (Supplemental Figure 2.1C). However, the SB-induced sPNET observed on an otherwise wild type background harbored the high copy T2/Onc2 chromosome 4 concatomer (Supplemental Figure 2.1A). No brain tumors occurred in mice with low copy T2/Onc resident on chromosome 1, however these animals represented a small percentage of starting experimental mice in transposition only (9%),and transposition and *Pten*$^{flox/+}$ (15%) groups (Supplementary Figure 2.1A and C). Overall, mice that developed SB-induced PNETs died faster compared to control mice in each experimental cohort (Supplemental Figure 2.2).

In addition, several experimental male mice undergoing transposition develop SB-induced testicle tumors at different frequencies depending on the genetic background (Supplemental Figure 2.2A-C and data not shown). Other prominent tumor types observed among all control and experimental cohorts include osteosarcomas and lymphomas and were not SB-derived, but dependent on the genetic background. For example, a significant number of osteosarcomas and lymphomas were observed in mice carrying the *p53*$^{lsl\text{-}R270H}$ allele (Supplemental Figure 2.2C), common phenotypes seen in other *p53*-deficient mouse models (Attardi and Jacks, 1999). Interestingly, lymphomas were observed in over 25% of mice with the *Pten*$^{flox/+}$ transgene and over 50% of mice with both *Nestin*-Cre and *Pten*$^{flox/+}$ transgenes (Supplemental Figure 2.2B) suggesting the *Pten*$^{flox}$ allele may have hypomorphic properties and *Nestin*-Cre mediates Cre expression in cells important for lymphomagenesis (data not shown).

We confirmed that PNET tumors from animals suffering SB mutagenesis were indeed SB-derived. MB and sPNETs express SB transposase protein by

immunohistochemistry (Supplemental Figure 2.3A). In addition, we performed a transposon excision PCR assay that confirmed T2/Onc and T2/Onc2 mobilization from their initial concatomer locations. Transposon excision was observed in all MB and sPNETs tested (Supplemental Figure 2.3C) compared to transgenic tissue lacking Cre recombinase (Supplemental Figure 2.3C). Collectively, PNET formation required SB mutagenesis and was enhanced by dominant negative *p53* genetic background.

**SB Insertional Mutagenesis-Induced Medulloblastomas Mimic Human Medulloblastoma Histological Subtypes**

SB-induced MB were located in the cerebellum (Figure 2.3A, 2.3C). Histopathology revealed morphological characteristics similar to human classic MB including small round cells with high nuclear:cytoplasm ratio, Homer-Wright rosettes (Figure 2.3B), vascularization, and sporadic mitotic cells (Figure 2.3B). Areas of anaplasia were also observed (data not shown). Leptomeningial spread from the primary tumor (Figure 2.3C) with similar morphology (Figure 2.3D) was also observed in 11/22 cases (MB characteristics shown in Supplemental Table 2.1). To further characterize their malignant and neuronal nature, we conducted immunohistochemical analysis on these tumors. They stained positive for the proliferation marker Ki67 (Figure 2.3E), primitive neuronal marker Synaptophysin (Figure 2.3F), and the neural progenitor intermediate filament protein Nestin (Figure 2.3G). In contrast, the MB were negative for the astrocyte marker glial fibrillary acidic protein (GFAP, Figure 2.3E). In addition, we observed 2/4 MB from the transposition plus $Pten^{flox/+}$ cohort that contained both classic morphology and nodular areas consisting of elongated streams of cells resembling human MB with extensive

nodularity (Supplemental Figure 2.4). Similar to classic portion of the tumor, tumor cells within the nodule areas stain positive for Synaptophysin and negative for GFAP (data not shown). However, cells within the nodular areas are overall negative for Ki67 (Supplemental Figure 2.4D) and Nestin (Supplemental Figure 2.4F) compared to cells in the classic area (Supplemental Figure 2.4E and G, respectively). Collectively, these data show SB-induced MB phenocopy heterogeneous features of human medulloblastoma.

**SB Insertional Mutagenesis-Induced sPNET Mimic Human sPNET**

In contrast to MB, SB-induced sPNETs were found in the rostral portion of the brain commonly overwhelming areas of the olfactory bulbs, lateral ventricle and cortex (Figure 2.4A). Histopathology showed morphological characteristics of the bulk tumor similar to human sPNET including small round cells with a high nuclear:cytoplasm ratio, presence of Homer-Wright rosettes (arrow Figure 2.4B), vascularization, and sporadic mitotic cells (arrowhead Figure 2.4B). We also observed tumor cell infiltration into the brain parenchyma (Figure 2.4C). sPNET characteristics shown in Supplemental Table 1. Immunohistochemistry revealed these tumors express Ki67 (Figure 2.4D), Synaptophysin (Figure 2.4E), and Nestin (Figure 2.4F). They are largely negative for GFAP (Figure 2.4G) except for reactive astrocytes entrapped within the bulk tumor. Together, these data demonstrate SB-induced sPNET faithfully recapitulate characteristics of human sPNET.

**Medulloblastoma And sPNET Common Insertion Sites Identify Known And Novel Gene Targets**

To identify candidate MB and sPNET genes that help drive PNETagenesis in our SB mutagenized mice, we recovered transposon insertion sites from 22 MB and 13 sPNET

by linker-mediated PCR using barcoded primers distinct for each tumor followed by sequencing-by-synthesis with the Illumina Genome Analyzer IIx. 22 MB and 13 sPNET generated over 390,000 and 155,000 nonredundant mapped insertions sites, respectively. Sequenced non-redundant insertion sites that represent greater than 0.1% (0.001 stringency) of total number of mapped insertions from each library were used for analysis to generate top candidate common insertion sites that achieve a P-value less than 0.05 for MB and sPNET (Figure 2.5A). From this analysis, 14 and 16 CIS were identified for MB and sPNET, respectively (Figure 2.5A). Ingenuity Pathway Analysis for each CIS group identified top molecular networks for both MB and sPNET including genes involved in: Cancer (MB: *Gli1*, *Pten*; sPNET: *Nf1*, *Pten*) and Nervous System Development and Function (MB: *Chl1*, *Dyrk1a*, *Gli1*, *Pten*; sPNET: *Clcn3*, *Qk*, *Nf1*, *Npas3*, *Pten*).

Several genes that have been previously implicated in human MB are represented with common insertion sites among multiple SB-induced tumors including *Gli1* and *Pten* (asterisks, Figure 2.5A). In human MB, SHH pathway activation marks a molecular subgroup often associated with upregulation of GLI1 (Northcott et al., 2011). Also, biallelic loss or *PTEN* promoter hypermethylation associated with PI3K pathway activation has been observed in MB (Hartmann et al., 2006). *Foxr2* is a member of the forkhead box family of transcription factors related to *FOXG1*, a candidate oncogene amplified in human medulloblastoma (Northcott et al., 2010). CIS-associated genes including *Serinc3*, *Zmynd11*, *Enox2*, *Chl1*, *Dlg1*, *Rreb1* and *Dyrk1a* have been implicated in human cancer but not previously linked with MB (Bossolasco et al., 1999; Yang et al., 2010; Tang et al., 2007; Senchenko et al., 2011; Mori et al., 1998; Nitz et al., 2011; de

Wit et al., 2002). Also, we show here the first association for *Ddx19a*, *Dusp14* and *Vsp45* in any cancer. Strikingly, a completely novel RhoGTPase activating protein *Arhgap36* was the most frequent candidate oncogene identified occurring in 14/22 medulloblastomas across all predisposing genetic backgrounds (wild type: 4/6, 67%; $Pten^{flox/+}$: 4/4, 100%; $p53^{lsl\text{-}R270H}$: 6/12, 50%).

We also identified *Pten* as a candidate gene in SB-induced sPNET, and loss of *PTEN* through 10q copy loss and mutation has been observed in human sPNET (Kraus et al., 2002) (asterisk, Figure 2.5A), Several genes marking different cellular functions were identified and not previously implicated in sPNET development. Notably, *Setd2* and *Setd5* are histone lysine methyltransferase enzymes potentially involved in global gene expression regulation, with human *SETD2* having a tumor suppressor role in breast and renal cell cancer (Newbold and Mokbel, 2010; Varela et al., 2011). *Ambra1* is a predicted tumor suppressor gene that promotes autophagy in the central nervous system (Fimia et al., 2007), a process shown to regulate MB development *in vivo* (Bhoopathi et al., 2010). Additionally, *Ube2d3* and *Usp9x* were also identified implicating protein ubiquitination with sPNET. Multiple genes that play a suppressive or activating functional role in Ras signaling were identified in many sPNETs (arrowheads, Figure 5A). Transposon insertions in these genes predict an overexpression role for the candidate oncogene *Eras*, and expression disruption for tumor suppressors *Nf1*, *Erbb2ip* and *Rasa3*. 10/13 (77%) sPNETs are included in this group and show an increase in p-Erk immunopositivity indicating Ras pathway activation (Figure 2.5B, Supplemental Table 2). Furthermore, 9/10 (90%) of these Ras-activated tumors also harbor $p53^{lsl\text{-}R270H}$. In contrast, tumors that

are not associated with these Ras-pathway genes lack p-Erk staining (Figure 2.5C, Supplemental Table 2). These results implicate Ras pathway activation linked with *p53* deficiency sPNET development.

Collectively, these results reveal genetic alterations previously associated with MB and sPNET. Importantly, multiple genes were also identified in our screen that directly implicate them in PNET development and further distinguish the genetic basis between MB and sPNET. Additional research is warranted to determine how these gene targets function during MB or sPNET development, respectively. Furthermore, novel genes and molecular pathways frequently altered in these tumors may mark potential therapeutic targets in human disease.

**_Arhgap36_ Is The Most Frequent Medulloblastoma Candidate Oncogene And Marks A Sonic Hedgehog/Wnt-Independent Genetic Subgroup**

Out of 22 SB-induced MB, 14 (63% total) harbored transposon insertion sites near the novel GTPase activating protein gene, *Arhgap36*, marking it as a top CIS represented in all three predisposing backgrounds (Supplementary Table 2.2). Interestingly, 3 of the remaining 8 (13% total) tumors contained transposon insertions within intron 5 of the Shh pathway effector gene *Gli1* positioned to induce Gli1 expression and were associated with dominant negative $p53^{lsl\text{-}R270H}$ (Supplementary Table 2.2). Also, 1 of these remaining 8 tumors (5% total) that does not fall into the Arhgap36- or Gli1-mediated subgroups harbors expression-disrupting insertions within intron 1 and 2 of the *Apc* gene (WT459, data not shown). The pattern of *Arhgap36* insertion site loci for each of the 14 tumors are clustered either upstream of exon 1 up to approximately 206Kb away (Figure

2.6A), or within intron 1 (Figure 2.6A). Importantly, the MSCV/SD portion of the transposon is in the sense orientation relative to *Arhgap36* for each of the 14 tumors predicting to drive expression of *Arghap36*. To verify this, we amplified *T2/Onc/2:Arhgap36* fusion transcripts from a subset of tumors containing *Arhgap36* insertions, but not from control tumors without *Arhgap36* insertions (Figure 2.6B). Sequence analysis of the RT-PCR products confirmed a precise fusion transcript containing the T2/Onc/2SD:*Arhgap36* exon 2 boundary with an in-frame ATG codon at 44bp of exon2. We also recovered full-length fusion transcript coding sequence from 2 tumors tested consistent with the largest *Arhgap36* isoform (ENSMUST00000114904, data not shown). The slightly larger band amplified from tumor P53184 contains a similar fusion transcript which also contains a 90bp fragment of Gm14696 intron 1 between the transposon SD and *Arhgap36* exon 2 (Figure 2.6B and data not shown). In addition, immunohistochemistry revealed robust Arhgap36 expression in tumors with corresponding *Arhgap36* insertions (Figure 2.6C) compared to control tumors (Figure 2.6D). Arhgap36 expression was observed in cells of the primary tumor (Figure 2.6C) and tumor cells that spread through the leptomeninges (Figure 2.6C). 8/14 (57%) *Arhgap36*-driven tumors displayed a metastatic phenotype compared to 3/8 (38%) for Arhgap36 negative tumors, and only 1/3 (33%) observed in Gli1 immunopositive tumors (Supplementary Table 2.2). Arhgap36 protein was localized to the cytoplasm in cells from insertion-positive MB (Figure 2.6E) compared to sparse nuclear positive cells found in *Arhgap36* insertion-negative MB tissue (Figure 2.6F) similar to expression in normal granule cells of the same tissue (data not shown). Conversely, immunohistochemistry

demonstrated tumors with *Gli1* insertions display Gli1 nuclear expression (Figure 2.6H), while tumors without *Gli1* insertions fail to express Gli1 (Figure 2.6G). Arhgap36 positive tumor P53176 also showed Gli1 expression without *Gli1* insertions indicating an alternative mechanism of induced expression (Supplemental Table 2.2). We then compared the expression of Otx2 between the SB-induced MB. *OTX2* is a transcription factor amplified and overexpressed in SHH-independent MB (Adamson et al., 2010). We observed nuclear Otx2 expression in all the SB-induced MB (Figure 2.6I) except those driven by Gli1 expression (Figure 2.6J). Furthermore, tumors harboring *Pten* loss via the $Pten^{flox}$ allele or transposon insertions also exhibit transposon-mediated *Arhgap36* expression (Supplemental Table 2.2). Among Arhgap36 positive tumors, we observed reduced Pten and elevated p-Akt cytoplasmic expression in 3/4 $Pten^{flox/+}$ MB and MB P53720 (Supplementary Table 2.2, Figure 2.6K). These data indicate that our SB-induced MB include a *Gli1*-mediated Shh molecular subgroup, disrupted *Apc*-mediated Wnt molecular subgroup, and a Shh/Wnt-independent molecular subgroup driven by a novel oncogene *Arhgap36* that may cooperate with *Pten* loss.

**ARHGAP36 Expression is Elevated in Poor Prognosis Human Medulloblastomas**

To determine if *ARHGAP36* is involved in human MB development, we assessed *ARHAGP36* RNA expression levels from the Affymetrix HG-U133 microarray dataset generated previously from a panel of 62 tumors (Kool et al., 2008). Cluster analysis of these tumors revealed 10 tumors with the highest and 10 with the lowest *ARHGAP36* expression segregated into the 5 subgroups established by Kool et al. (Figure 2.7A). Interestingly, 8 of the ten lowest expressors clustered into subgroup A (WNT) or B

(SHH), 8 of the top 10 highest expressors could be found in subgroups C and D, and 2 of each were found in subgroup E (Figure 2.7A). This data is consistent with observations from the SB-induced MB showing high *Arhgap36* expression is associated with Shh-independent tumors. We next assessed ARHGAP36 expression levels in a spatial-temporal manner in human MB using immunohistochemistry on two separate tissue microarrays prepared at the University of Minnesota, and Johns Hopkins University. We analyzed 65 samples and observed tumors with areas of ARHGAP36 expression localized in the nucleus, cytoplasm, or both, and a fraction of tumors were ARHGAP36 negative (Figure 2.7B). From this data, 37/65 (56%) of the samples displayed areas of cytoplasmic ARHGAP36 expression similar to what we observed in the *Arhgap36*-driven mouse MB, and 8/65 samples showed strong nuclear expression. Furthermore, overall 5-year survival analysis of MB patients immunopositive for ARHGAP36 revealed a trend of poorer survival during the first two years after diagnosis compared to patients lacking ARHGAP36 immunopositive expression (All, Figure 2.7C). This trend is exacerbated in patients with cytoplasmic ARHGAP36 expression. Similarly, deceased MB patients showing ARHGAP36 immunopositivity (n = 14) suffer significantly faster mortality compared to ARHGAP36 negative patients (n = 12) and this mortality rate significantly shorter when ARHGAP36 expression is localized to the cytoplasm (n = 11) (Deceased, Figure 2.7C). 4/5 (80%) patients with confirmed metastatic disease also showed cytoplasmic ARHGAP36 expression. In addition, we noted several human MB containing cells of classic morphology with cytoplasmic ARHGAP36 staining as well as nodular areas demonstrating streaming cells with sporadic weak nuclear expression

(Figure 2.7D). We saw a similar expression pattern in the two mouse MB harboring both classic and nodular morphologies indicating a predominance of cytoplasmic Arhgap36 expression in MB cells with a primitive and proliferative phenotype. This observation indicates these tumors bear both histological and molecular heterogeneity that can influence clinical behavior. Taken together these data show that *ARHGAP36* expression is elevated in human MB at the RNA and protein levels and contributes to SHH and WNT pathway independent high-risk molecular subgroups.

**ARHGAP36 Is Expressed In Normal Developing And Adult Cerebellum**

To further investigate the biological relevance of *ARHGAP36* to MB development, we determined the spatial and temporal expression pattern of ARHGAP36 protein during normal developing and adult cerebellum tissue. We observed cells in the developing cerebellum of both mouse and human that express nuclear localized ARHGAP36. Cells of the developing cerebellum that express ARHGAP36 include those throughout the molecular layer (ML), Purkinje cell layer (PC) and internal granule cell layer (IGL) (Figure 2.8A-B). In adult cerebellum, we observed a similar expression pattern in the mature ML, PC and IGL (Figure 2.8C-D). Interestingly, we did not see detectable staining in cells of the developing external granule cell layer (EGL).

**Discussion**

MB and sPNET are central nervous systems tumors that often occur in pediatric patients. Although similar on a histological level, these tumors pose different levels of treatment response and survivability. This is due in part to genetic disparity observed

through genomic structural changes, expression profiling and epigenetic alterations. As described in Chapter 1, several key similarities and differences have been identified, including those used to determine MB and sPNET molecular subgroups. Although multiple studies show sPNET are genetically distinct from MB, little is known about which genetic factors drive sPNET formation and how this relates to clinical outcome. Also, we lack a concise view of to what extent specific molecules and pathways determine the pathogenesis of a majority of MB.

We report here a novel SB insertional mutagenesis mouse model that helps address these deficiencies in MB and sPNET tumor research. This model recapitulated histological and molecular features of human MB and sPNET development as well as previously reported mouse models. Interestingly, we observed MB amongst all three genetic backgrounds with a higher frequency associated with $p53^{lsl\text{-}R270H}$. Also, a higher rate of mutagenic transposition effected MB frequency because overall fewer mice were generated harboring the high-copy T2/Onc2 transposon concatomer, yet a majority of MB formed in these animals (14/22, 64%) (Supplemental Figure 1). We did not see as obvious a trend in mice that developed sPNET as the overall frequency of T2/Onc2-mediated sPNET associated with $p53^{lsl\text{-}R270H}$ was 50%, however, T2/Onc2 was required for sPNET development associated with a wild type background. Overall, this argues for an advantage of higher-frequency mutagenic transposition to mediate PNET formation. The lack of Nestin and Ki67 immunopositivity in the biphasic nodular areas of SB-induced MB associated with $Pten^{flox/+}$ indicates a more differentiated phenotype. Similar results are reported in other MB mouse models employing *Pten* heterozygosity

(Hambardzumyan et al 2008; Castellino et al 2010) Although these studies show *Pten* heterozygosity accelerates MB formation in the context of activated Shh signaling via constitutively active *SmoA1* (Castellino et al., 2010), $Pten^{flox/+}$ increased the latency of SB mutagenesis-derived MB. This observation could be attributed to the true unbiased nature of SB mutagenesis, the overpowering strength of constitutively active *SmoA1*, or a combination of both. Alternatively, the nodular areas these tumors contain reflect a desmoplastic morphology observed in human patients that tend to have a better clinical outcome. Importantly, we identified candidate oncogenes and tumor suppressor genes biologically relevant for MB and sPNET. We identified multiple RAS- regulating genes directly implicating this pathway in sPNET development. Furthermore, molecular subgroups for MB were also observed including Shh, WNT, and especially non-Shh/WNT groups crucial for better molecular definition of this poorly understood subgroup. Interestingly, the Shh molecular subgroup identified by *Gli1* insertions occurred in association with $p53^{lsl\text{-}R270H}$ (Supplemental Table 2) similar to other MB mouse models that combine activated Shh pathway via $Ptch^{-/-}$ with loss of *p53* to achieve higher tumor frequency (Wetmore et al., 2001; Lee et al., 2007) indicating the ability of SB mutagenesis to faithfully recapitulate Shh-derived MB subgroup. Importantly, we also identified a novel Rho-GTPase Activating Protein (RhoGAP) *Arhgap36* as a top candidate MB oncogene playing a role in non-SHH subgroup tumors.

Human RhoGAPs comprise a super family of more than 70 proteins of which over half have been characterized (Tcherkezian and Lamarche-Vane, 2007). The canonical function of the GAP domain is facilitating the native GTPase activity of Ras

homologue GTPase (Rho GTPase) proteins. Rho-family GTPases are intracellular signaling proteins that regulate multiple cellular functions including cell growth, cell cycle progression, cytoskeletal remodeling, gene expression, apoptosis and intracellular membrane trafficking (Grogg and Zheng, 2010). They contain lipid modifications that target them to the cell membrane and operate as molecular switches for signal transduction pathways by cycling between active GTP-bound and inactive GDP-bound states. The GDP-GTP cycle is regulated by Rho-guanine nucleotide exchange factors (RhoGEFs) that promote GDP-to-GTP exchange, RhoGAPs that facilitate intrinsic GTPase activity leading to GTP-to-GDP bound form of RhoGTPase, and guanine nucleotide-dissociation inhibitors (GDIs) that isolate RhoGTPases in their GDP-bound state and regulate their intracellular localization (Tcherkezian and Lamarche-Vane, 2007). RhoGTPase protein family includes 18 members with RhoA, Rac1 and Cdc42 as the most commonly studied (Sahai and Marshall, 2002).

Proper regulation of these RhoGTPases requires timely interaction with their respective effectors in the correct cellular compartment of a given cell including neurons of the developing central nervous system. RhoGTPases play essential roles in neuronal morphogenesis including axon growth and guidance, and migration (Luo 2000). Extracellular attractive guidance cues activate Cdc42 and Rac1 while inhibiting RhoA activity (Guan and Rao, 2003). One consequence of RhoGTPase regulation includes the balance between Rac1 and RhoA signaling and how this effects cell actin cytoskeleton and subsequent morphology. Rac1 activity promotes actin polymerization and subsequent cell elongation through lamelipodia formation in melanoma cells (Symons and Segall,

2009). Conversely, RhoA activity mediated via RhoA-associated kinase (ROCK) induced actomyosin contraction and subsequent amoeboid morphology of these cells. Elucidating this phenomenon, Sanz-Mareno et al. showed that ARHGAP22 helped drive ROCK-mediated amoeboid behavior and reduce Rac1-GTP levels, while WAVE2 acted as a downstream Rac1 effector protein for actin polymerization indicating the complicated molecular nature of the balance between Rac1 and RhoA (Sanz-Moreno et al., 2008). Woo and Gomez also demonstrated the need for Rac1 and RhoA balance in neuron morphogenesis by showing that constitutively active Rac1 and ROCK inhibition both produced defective lamellipodia in frog spinal neurons (Woo and Gomez, 2006). Morphological defects are also seen *in vivo* when these pathways are altered. In the cerebellum, mice engineered with constitutively active Rac1 in Purkinje cells resulted in defective axon outgrowth of these cells in the Purkinje cell layer (Luo et al., 1996). Rock-mediated RhoA signaling prevents axonal initiation of cultured cerebellar granule cells (Luo 2000). Several studies using MB cell lines demonstrate that functionally active Rac1 helps promote tumor cell elongation, lamellipodia formation, and subsequent migration *in vitro* via Erk activation (Zavarella et al., 2009; Yuan et al., 2010; Chen et al., 2011). *Slit2*, a secreted protein important for repulsive axon guidance, deters medulloblastoma cell migration by downregulating Cdc42 activity (Werbowetski-Ogilvie et al., 2006). Recently, Bhoopathi et al. correlated an inhibition of RhoA activity with a loss of MB cell proliferation and cell migration (Bhoopathi et al., 2011). Understanding normal mechanisms behind RhoGTPase regulation is ongoing and how these pathways become altered in a cancer context remains valuable.

*Arhgap36* is a novel protein with unknown function, but protein domains and cellular localization provide insight to its potential role. Arhgap36 contains a GAP domain most similar to the RhoGAP family member *ARHGAP6.* GAP domains are characterized by a conserved arginine residue that work directly in the hydrolysis reaction and stabilize GTP/GDP transition (Prakash et al., 2000). Lysine and asparagine residues are also conserved in the GAP domain and located in the putative G-protein binding pocket important for physical interaction with RhoGTPases (Li et al., 1997). Overexpression of ARHGAP6 in HeLa cells reduced GTP-bound RhoA levels and promoted subsequent formation of cellular process elongation and motility (Prakash et al., 2000). Interestingly, ARHGAP6 engineered with a catalytically inactive GAP domain abolished the GAP activity, but did not affect its ability to promote cellular process outgrowth suggesting multiple functions for cell structure organization. Aside from the GAP domain, Arhgap6 contains several putative SH3-binding sites that may mediate protein-protein interactions. $p27^{Kip1}$ is a molecule that does not contain a GAP domain, but was shown to inhibit RhoA when localized to the cytoplasm by preventing RhoGEF-RhoA binding, resulting in increased cell motility in mouse embryonic fibroblasts and breast cancer cells (Larrea. et al., 2009). Furthermore, cytoplasmic $p27^{Kip1}$ was shown to play a role in defective GNPC proliferation and migration in the context of the constitutively active *SmoA1*, Shh-mediated MB mouse model indicating this interaction with RhoA *in vivo* (Bhatia et al., 2010). Arhgap36 may operate in a similar fashion as it contains a GAP domain, a nuclear localization signal and a putative SH3-binding site located within an arginine-rich region. Interestingly, the conserved arginine in the GAP

domain is replaced with a threonine, however the lysine and asparagine residues are present presumably providing RhoGTPase binding ability. Furthermore, many phosphorylation sites are located throughout the protein sequence as predicted by PROSITE (http://prosite.expasy.org/) and Center For Biological Sequence Analysis (http://www.cbs.dtu.dk/services/). Although not previously implicated in human MB, several *ARHGAP36* mutations in ovarian cancer are listed by the Catalogue Of Somatic Mutations In Cancer (COSMIC, http://www.sanger.ac.uk/genetics/CGP/cosmic/) with one occurring within the GAP domain. Nuclear ARHGAP36 protein expression in cells of the developing and adult cerebellum in mice and man indicating a conserved role for this protein during cerebellum growth. Moreover, this expression was found in a subset of Purkinje cells, prospective Bergmann glia and post-migratory granule neurons suggesting a role for nuclear ARHGAP36 in regulating cells derived from the primary cerebellum germinal zone. Moreover, oncogenic expression shifted from the nucleus to the cytoplasm in both mouse and human MB associated with aggressive tumor burden further suggesting multiple roles depending on subcellular location. Cytoplasmic ARHGAP36 may then be free to inhibit RhoA or other RhoGTPases in the cytosol or at the plasma membrane through its GAP or SH3 binding domains or by another unknown mechanism. We reveal here ARHGAP36 as an attractive target for targeted therapy in patients suffering non-SHH-mediated, poor prognosis MB. Current efforts for viable drug development has included targeting molecules involved in RhoGTPase signaling pathways including ROCK and Rac1 (Lu et al., 2009), but inhibitors focused on additional RhoGTPase signaling pathways and effector molecules are lacking.

In an effort to reveal biological cooperation for tumorigenesis, we sought to identify tumors harboring co-occurring CIS or background mutation. We found a significant relationship between animals that harbor the *Pten*$^{flox/+}$ allele or disruptive transposon insertion sites within the *Pten* gene and transposon-mediated expression of Arhgap36. Of significance, PTEN localization and activity can be regulated via phosphorylation by ROCK and this relationship influences leukocyte directional movement (Li et al., 2005; Meili et al., 2005). RhoGTPases are key effector molecules during cellular chemotaxis and they demonstrate PTEN colocalizes with GTP-bound Rho on the back-side of migrating leukocytes, while active Cdc42 resides on the front side excluding PTEN from that location. This occurs through RhoA-mediated activation of ROCK, which then forms a complex with and phosphorylates PTEN activating its phosphatase activity silencing PI3K-mediated activation of Akt ultimately leading to coordinated migration. Assuming Arhgap36 has effector function towards RhoGTPases, it is feasible that loss of *Pten* could cooperate with elevated levels of ARHGAP36 disrupting this precise process leading to uncontrolled cellular movement, a hallmark cancer phenotype. Additional experiments are needed to explore this hypothesis in the context of MB, namely whether ARHGAP36 has GAP activity. Interestingly, in addition to elevated ARHGAP36 expression observed in non-SHH derived MB detailed here, human *PTEN* is located on chromosome 10q and 10q loss is frequent in SHH and Group C MB (Northcott et al.), and the non-SHH molecular subgroup c5 defined by Cho et al. 2010. Similarly, transposon-mediated expression of *Arhgap36* was identified in 6/12 (50%) MB from mice harboring the *p53*$^{lsl\text{-}R270H}$ allele (Supplemental Table 2) suggesting

interaction between Arhgap36 and p53 function in this context. Of note, transposon-mediated expression of *Arhgap36* was also observed in 4/6 (67%) MB from mice with a wild type background (Supplemental Table 2). 3/4 (75%) of these tumors also harbored transposon insertions predicting to drive expression of the anti-apoptosis molecule *Bcl2l1* (data not shown) further implicating a functional relationship between Arhgap36 and p53 signaling during MB development. Indeed, proper p53 activity is important for normal cerebellum development and MB suppression *in vivo* (Wetmore et al., 2001; Malek et al., 2011).

Strikingly from the mouse sPNET, *Nf1* was a top CIS and several other Ras-regulating genes were also represented and highly correlated with the *p53*-deficient background. indicating a propensity of these tumors to form in the absence of cell cycle control and/or functional apoptosis and cell growth. We subsequently observed Ras pathway activity in these tumors determined by positive positive p-Erk immunostaining. Active Ras cooperates with inactive *p53* to promote tumorigenesis in mouse models of tumors and Neurofibromatosis 1 (Hundley et al., 1997; Vogel et al., 1999). Defects in *NF1* and *P53* have mainly been observed in a subset of patients with high grade-glioblastomas (The Cancer Genome Atlas Research Network, 2008; Verhaak et al., 2010), and thought to mark distinct mesenchymal and proneural molecular subtypes, respectively (Verhaak et al., 2010). Several tumors showed combined *NF1* and *P53* anomalies (Verhaak et a., 2010) and many mouse models with body wide or conditional *Nf1* and *p53* co-disruption develop high-grade glioma (Reilly et al., 2000; Kwon et al., 2008) indicating a functional relationship for brain tumor development. Active RAS

signaling promotes neurogenesis from multipotent precursors in the neocortex prior to gliogenesis when JAK-STAT signaling and NF1 simultaneously repress neurogenesis and promote gliogenesis by unknown mechanism (Miller et al., 2007). This fact contributes to the notion that subventricular stem cells are the cell of origin (spatial) and loss of Ras pathway control during early neurogenesis (temporal) to the development of sPNET instead of glioma in our mouse model. Contrary to this notion is a study by Phi et al. who analyzed 12 sPNETs and found JAK-STAT3 pathway activation and expression enrichment for genes involved in gliogenesis including *SOX2*, *NOTCH1* and *ID1* (Phi et al., 2010). Human sPNET are commonly associated with P53 immunopositivity indicating defective function (Li et al., 2005).

Altered RAS signaling may also play a significant role in human sPNET development. Mochizuki and colleagues identified a predominance of *NF1* type I transcript present in sPNETs as well as glioblastomas compared to *NF1* type II transcripts associated with normal, differentiated cerebrum (Mochizuki et al., 1992). *NF1* type II transcripts contain an additional 63 base pair insert within the GTPase activating protein related domain altering its hydrophobicity, secondary structure and possibly its function *in vivo*. Additionally, a secondary sPNET tumor was reported in a neurofibromatosis 1 patient who underwent radiation treatment for a brainstem astrocytoma (Raffel et al., 1989). Several sPNET tumors harbor *NF1* disruption at the genetic level (Dr. Annie Huang, unpublished results). Furthermore, subsequent sPNET developed in patients treated with irradiation for other brain tumor subtypes including pediatric astrocytomas (Hader et al., 2003) or lymphoma (Brüstle et al., 1992). Interestingly, these secondary

sPNETs were also associated with an activated form of *KRAS*. Moreover, the RAS effector molecule *RASSF1* was methylated in a significant number of MB and sPNET tumors (Inda and Castresana, 2007). A recent study by Pfister and colleagues (Pfister et a., 2007) identified multiple chromosomal copy changes in sPNET including loss of *HRASLS3*, a prospective tumor suppressor shown to inhibit *HRAS*-mediated cell transformation (Sers et al., 1997). These studies collectively implicate a role of altered RAS activity in sPNET development and could serve as a viable biological therapeutic target for sPNET patients. Importantly, multiple small molecule inhibitors have been developed and are currently being tested for safety and efficacy in PhaseI/II clinical trials including RAS, RAF and MEK inhibitors (Rauen et al., 2011) and may be useful in treatment strategies.

Collectively, these results provide evidence into underlying genetic causes of MB and sPNET potentially relevant to temporal and spatial control during normal brain development. Specifically, we have provided evidence for *ARHGAP36* as a novel candidate oncogenic driver of non-SHH-mediated MB, a possible marker for high-risk patients, and potential target for therapeutic treatment of these tumors. In addition, further research is warranted to determine what ARHGAP36 domains and sequences are important for its physiological and pathological function and regulation in the context of MB development. We also reveal several candidate oncogenes and tumor suppressor genes that converge on Ras pathway regulation in sPNET development and further analysis of this pathway in the etiology and treatment of these tumors is warranted.

**Figure 2.1. *Nestin*-Cre Mediated SB Transposase Expression Throughout The Mouse Brain**

(A) Immunohistochemistry for SB transposase protein of a *Nestin*-Cre, *Rosa26-lsl-SB11* double transgenic mouse. Sagital section at p2 reveals SB expression throughout the brain. (B-G) High-power magnification of specific areas in (A) demonstrating nuclear SB expression in (B) granule cells, (C) white matter, (D) fourth ventricle, (E) subependymal midbrain, (F) subventricular zone, (G) olfactory bulb. (B`-G`) High-power magnification of corresponding areas in (B-G) from a *Rosa26-lsl-SB11* single transgenic mouse lacking SB transposase protein expression. Scale bar = 50μm.

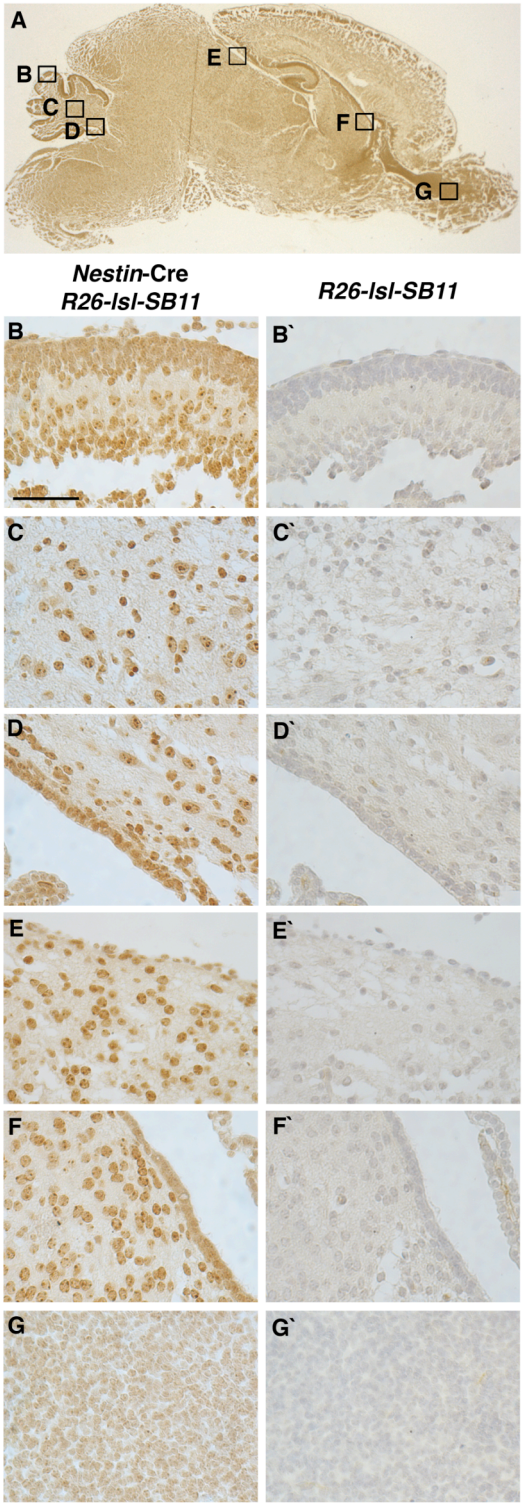
A
B
C
D
E
F
G
Nestin-Cre
R26-lsl-SB11
R26-lsl-SB11
B
B`
C
C`
D
D`
E
E`
F
F`
G
G`

**Figure 2.2. SB Insertional Mutagenesis Causes Malignant PNET**

(A-C) Breeding strategies for generating experimental and control mice on different predisposing genetic backgrounds. Mice double transgenic for *Nestin*-Cre and T2/Onc or T2/Onc2 were mated with mice harboring Cre-regulated transgenes to generate mice undergoing (A) transposition on a wild type background, (B) transposition on a *Pten* heterozygous background, (C) transposition on a dominant negative *p53* background. (D) Percent frequency of macroscopic SB-induced medulloblastoma (blue columns) and sPNET (red columns) tumors observed on wild type, *Pten* heterozygous, or dominant negative *p53* genetic backgrounds. sPNET also occurred at low frequency in *Nestin*-Cre, $p53^{lsl\text{-}R270H}$ control mice. (E) Medulloblastoma latency for experimental groups. (F) sPNET latency for experimental groups and single *Nestin*-Cre, $p53^{lsl\text{-}R270H}$ control tumor.

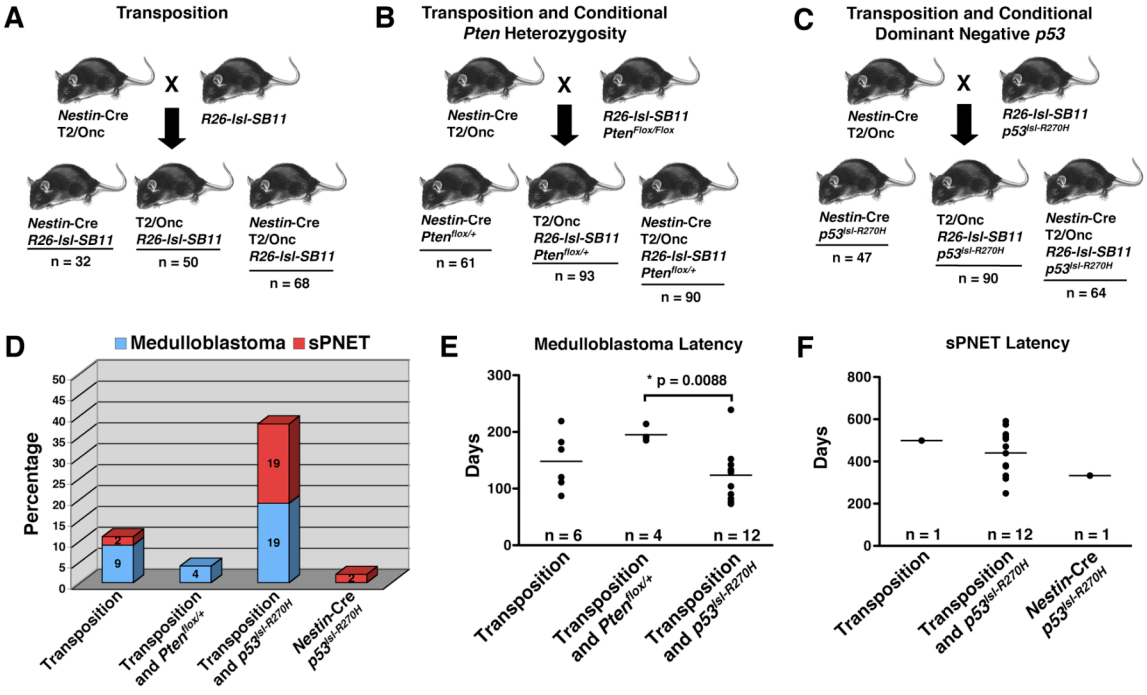
A
Transposition
Nestin-Cre T2/Onc
X
R26-lsl-SB11
Nestin-Cre R26-lsl-SB11
n = 32
T2/Onc R26-lsl-SB11
n = 50
Nestin-Cre T2/Onc R26-lsl-SB11
n = 68
B
Transposition and Conditional Pten Heterozygosity
Nestin-Cre T2/Onc
X
R26-lsl-SB11 Pten Flox/Flox
Nestin-Cre Pten flox/+
n = 61
T2/Onc R26-lsl-SB11 Pten flox/+
n = 93
Nestin-Cre T2/Onc R26-lsl-SB11 Pten flox/+
n = 90
C
Transposition and Conditional Dominant Negative p53
Nestin-Cre T2/Onc
X
R26-lsl-SB11 p53 lsl-R270H
Nestin-Cre p53 lsl-R270H
n = 47
T2/Onc R26-lsl-SB11 p53 lsl-R270H
n = 90
Nestin-Cre T2/Onc R26-lsl-SB11 p53 lsl-R270H
n = 64
D
Medulloblastoma sPNET
Percentage
50
45
40
35
30
25
20
15
10
5
0
9
2
4
19
19
2
Transposition
Transposition and Pten flox/+
Transposition and p53 lsl-R270H
Nestin-Cre p53 lsl-R270H
E
Medulloblastoma Latency
* p = 0.0088
Days
300
200
100
0
n = 6
n = 4
n = 12
Transposition
Transposition and Pten flox/+
Transposition and p53 lsl-R270H
F
sPNET Latency
Days
800
600
400
200
0
n = 1
n = 12
n = 1
Transposition
Transposition and p53 lsl-R270H
Nestin-Cre p53 lsl-R270H

**Figure 2.3. SB Insertional Mutagenesis-Derived Medulloblastomas Display Classic Histopathology Characteristics**

(A-D) H and E staining. (A) Coronal section of representative medulloblastoma located in the cerebellum. (B) High-power magnification area from (A) depicting small, round tumor cells, rosette formation (arrows) and mitotic nuclei (arrowheads). (C) Sagital section of representative classic medulloblastoma located in the cerebellum (arrow) with leptomeningial spread (arrowhead). (D) High-power magnification of leptomeningial spread in (C) depicting similar classic histology. (E-H) Immunohistochemistry illustrating tumors stain positive for (E) Ki67, (F) Synaptophysin, (G) Nestin, and negative for (H) GFAP. Scale bars = 50μm.

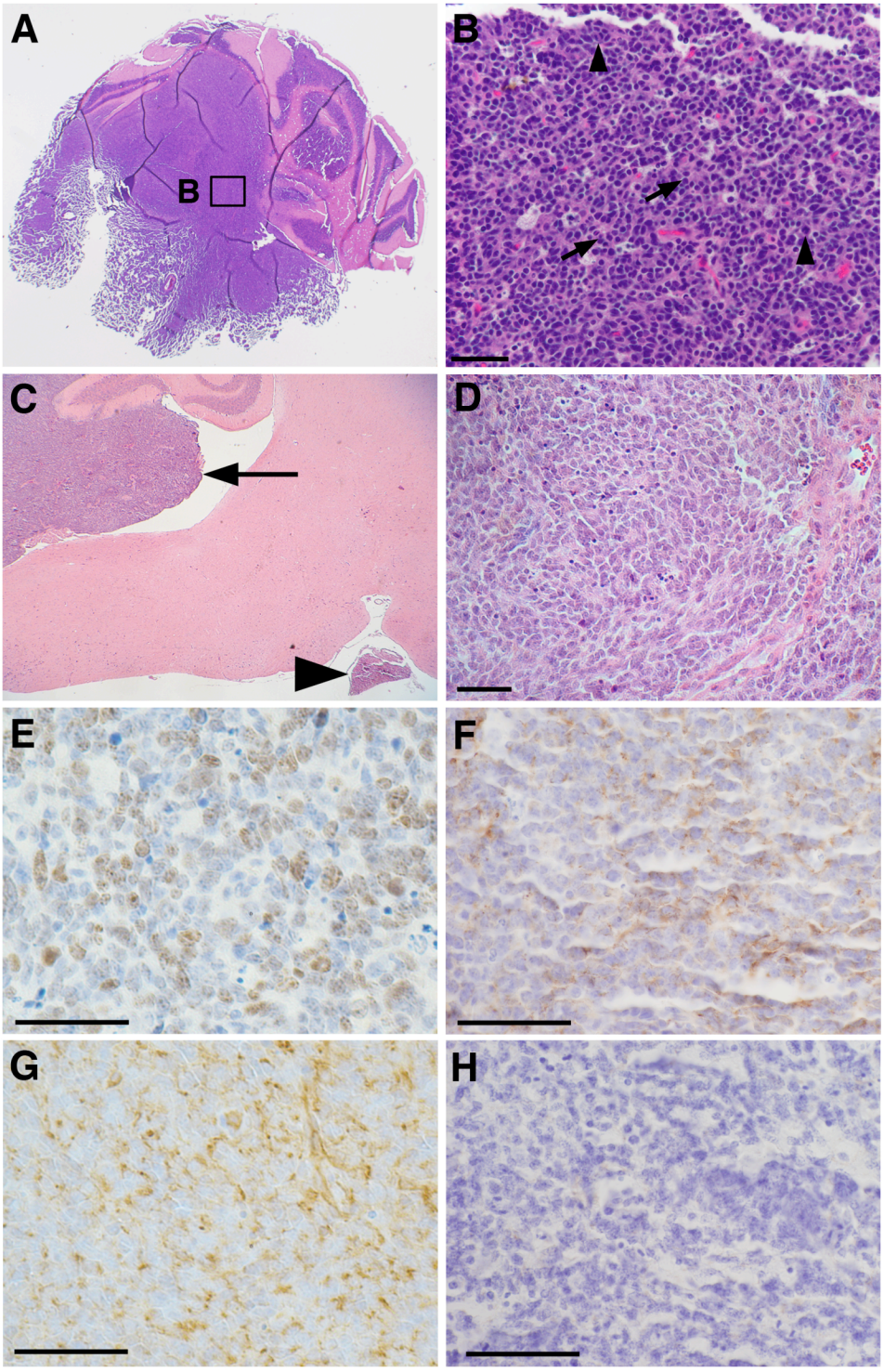
A
B
B
C
D
E
F
G
H

**Figure 2.4. SB Insertional Mutagenesis-Derived sPNET Histopathology Characteristics**

(A-C) H and E staining. (A) Coronal section of representative sPNET located in the right hemisphere dominating the cerebral cortex (ctx), hippocampal formation (hpf), and dentate gyrus (dg). Inset shows sagital section of representative sPNET dominating the lateral ventricle and olfactory bulb (arrow). (B) High-power magnification area from bulk tumor in (A) depicting small, round tumor cells, rosette formations (arrows) and mitotic nuclei (arrowheads). (C) High-power magnification area from (A) depicting tumor cell parenchyma infiltration. (D-G) Immunohistochemistry illustrating tumors stain positive for (D) Ki67, (E) Synaptophysin and (F) Nestin and (G) GFAP in reactive astrocytes. Scale bars = 50μm.

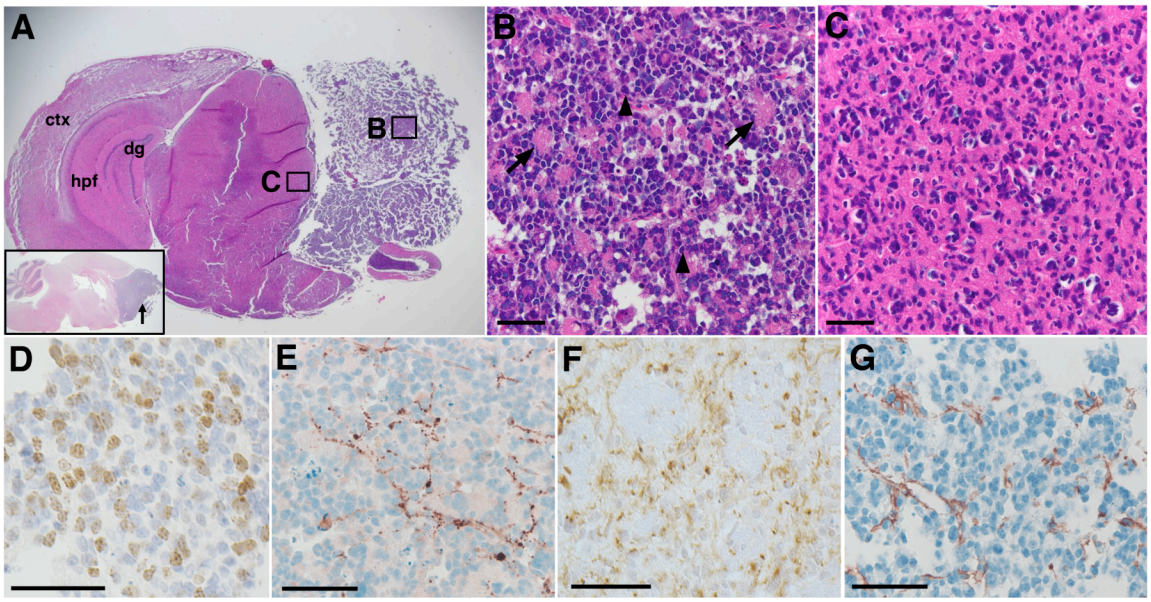
A
ctx
dg
hpf
B
C
B
C
D
E
F
G

**Figure 2.5. Medulloblastoma And sPNET Common Insertion Sites Identify Known And Novel Genes And Molecular Pathways**

(A) CIS identify candidate medulloblastoma and sPNET genes. Asterisks = known genes associated with human PNET. Arrowheads = Ras-pathway genes associated with sPNET. (B-C) Immunohistochemistry illustrating p-Erk nuclear staining. (B) p-Erk positive staining among sPNET tumors harboring transposon insertions in Ras-pathway effector genes. (C) p-Erk negative staining in sPNETs lacking transposon insertions within Ras-pathway genes. Scale bars = 50μm.

**A** **Common Insertion Sites For PNET Variants**

**Medulloblastoma**

| Candidate Gene | Chromosome | Position | Tumor Count | Pvalue | Predicted Gene Effect |
|---|---|---|---|---|---|
| *Arhgap36* | X | 46667600-46867600 | 10 | 6.10E-16 | Overexpress |
| *Foxr2* | X | 149413700-149613700 | 5 | 1.10E-05 | Overexpress |
| *Serinc3* | 2 | 163468400-163480900 | 4 | 1.27E-08 | Disrupt |
| *Ddx19a* | 8 | 113503700-113603700 | 3 | 0.005786256 | Overexpress |
| ★ *Gli1* | 10 | 126774200-126786700 | 3 | 0.007988638 | Overexpress |
| *Zmynd11* | 13 | 9699400-9711900 | 2 | 0.007988638 | Disrupt |
| *Enox2* | X | 46617300-46629800 | 2 | 0.007988638 | Disrupt |
| *Chl1* | 6 | 103599200-103611700 | 2 | 0.007988638 | Disrupt |
| *Dlg1* | 16 | 31713300-31725800 | 2 | 0.007988638 | Disrupt |
| ★ *Pten* | 19 | 32884500-32897000 | 2 | 0.007988638 | Disrupt |
| *Dusp14* | 11 | 83873800-83886300 | 2 | 0.007988638 | Disrupt |
| *Rreb1* | 13 | 37952600-37977600 | 2 | 0.031815022 | Overexpress |
| *Dyrk1a* | 16 | 94886400-94911400 | 2 | 0.031815022 | Disrupt |
| *Vps45* | 3 | 95855500-95880500 | 2 | 0.031815022 | Overexpress |

**sPNET**

| Candidate Gene | Chromosome | Position | Tumor Count | Pvalue | Predicted Gene Effect |
|---|---|---|---|---|---|
| *Nf1* ◀ | 11 | 79206700-79256700 | 7 | 5.03E-14 | Disrupt |
| *Ambra1* | 2 | 91608700-91808700 | 5 | 7.61E-06 | Disrupt |
| *Erbb2ip* ◀ | 13 | 104606900-104706900 | 3 | 0.0045335 | Disrupt |
| *Eras* ◀ | X | 7500000-7512500 | 3 | 9.11E-06 | Overexpress |
| *Setd5* | 6 | 113049200-113061700 | 3 | 9.11E-06 | Overexpress |
| *Serinc3* | 2 | 163468400-163480900 | 3 | 9.11E-06 | Disrupt |
| *Rfwd2* | 1 | 161209300-161221800 | 2 | 0.006644047 | Disrupt |
| *Npas3* | 12 | 54553200-54565700 | 2 | 0.006644047 | Disrupt |
| *Ube2d3* | 3 | 135110400-135122900 | 2 | 0.006644047 | Disrupt |
| *Qk* | 17 | 10448600-10461100 | 2 | 0.006644047 | Disrupt |
| ★ *Pten* | 19 | 32870300-32882800 | 2 | 0.006644047 | Disrupt |
| *Agap1* | 1 | 91471900-91496900 | 2 | 0.026467055 | Overexpress |
| *Rasa3* ◀ | 8 | 13632000-13657000 | 2 | 0.026467055 | Disrupt |
| *Clcn3* | 8 | 63414600-63439600 | 2 | 0.026467055 | Disrupt |
| *Setd2* | 9 | 110439100-110464100 | 2 | 0.026467055 | Disrupt |
| *Usp9x* | X | 12710200-12735200 | 2 | 0.026467055 | Disrupt |

**B**

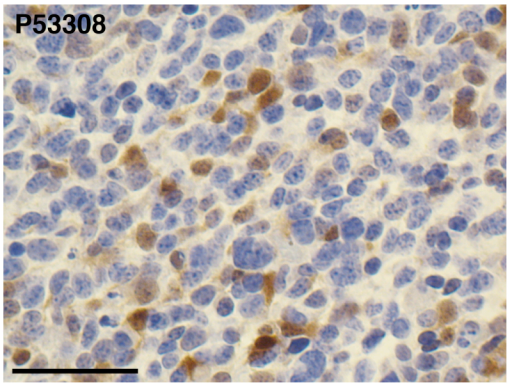


**C**

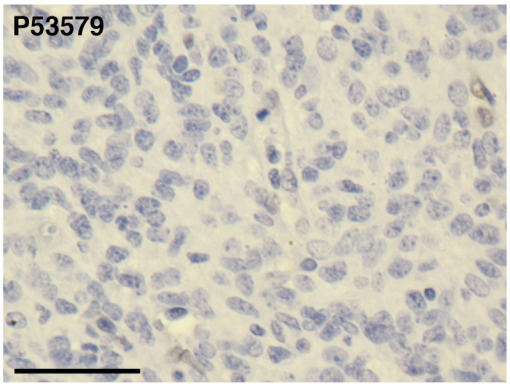

**Figure 2.6. Arhgap36-Driven Tumors Mark a SHH-Independent Medulloblastoma Subgroup**

(A) Mutagenic transposon insertion sites (green arrowheads) are located upstream of the endogenous start site in exon 1 (black arrowhead) or within intron 1 of *Arhgap36*. Direction of green arrowheads indicate sense orientation of the transposon MSCV/SD relative to *Arhgap36*. (B) RT-PCR illustrates only tumors with *Arhgap36* insertions express a *transposon:Arhgap36* fusion transcript. (C) Sagital section of representative medulloblastoma with *Arhgap36* activating insertions express Arhgap36 throughout cells of the primary tumor (asterisk) and leptomeningial spread (arrowhead), localized to the cytoplasm (E). (D) Lack of Arhgap36 expression in control tumors (asterisk) without *Arhgap36* insertions. (F) Residual Arhgap36 nuclear expression in sporadic control tumor cells (arrow). (G) Lack of nuclear Gli1 expression in tumors without Gli1 insertions. (H) Nuclear Gli1 expression in tumors with *Gli1* insertions. (I) Nuclear Otx2 expression in tumors without *Gli1* insertions. (J) Tumors with *Gli1* activating insertions lack Otx2 expression. (K) Arhgap36 positive medulloblastoma Pten164 demonstrating a lack of Pten and robust cytoplasmic p-Akt(S473) immunostaining. Scale bars = 50μm.

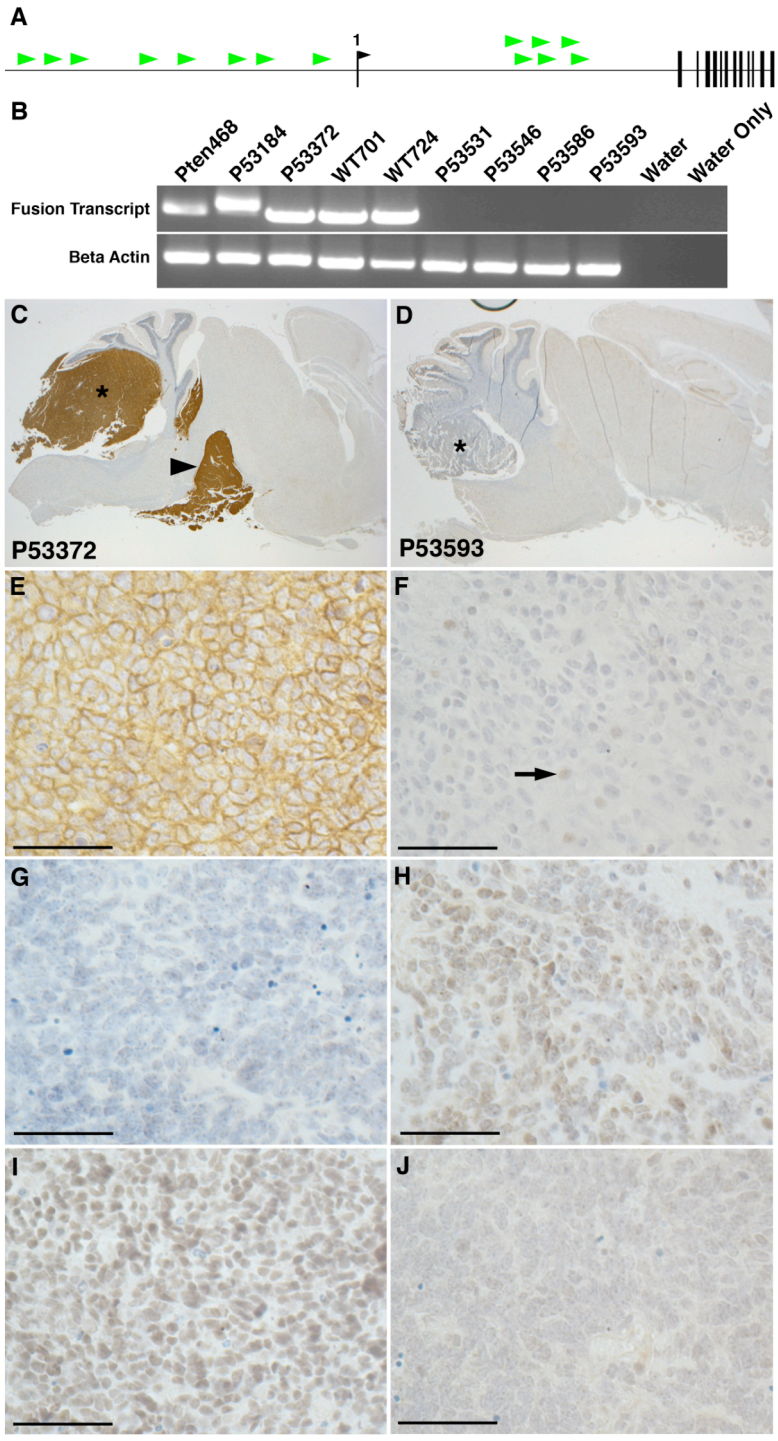
A
1
B
Pten468
P53184
P53372
WT701
WT724
P53531
P53546
P53586
P53593
Water
Water Only
Fusion Transcript
Beta Actin
C
P53372
D
P53593
E
F
G
H
I
J

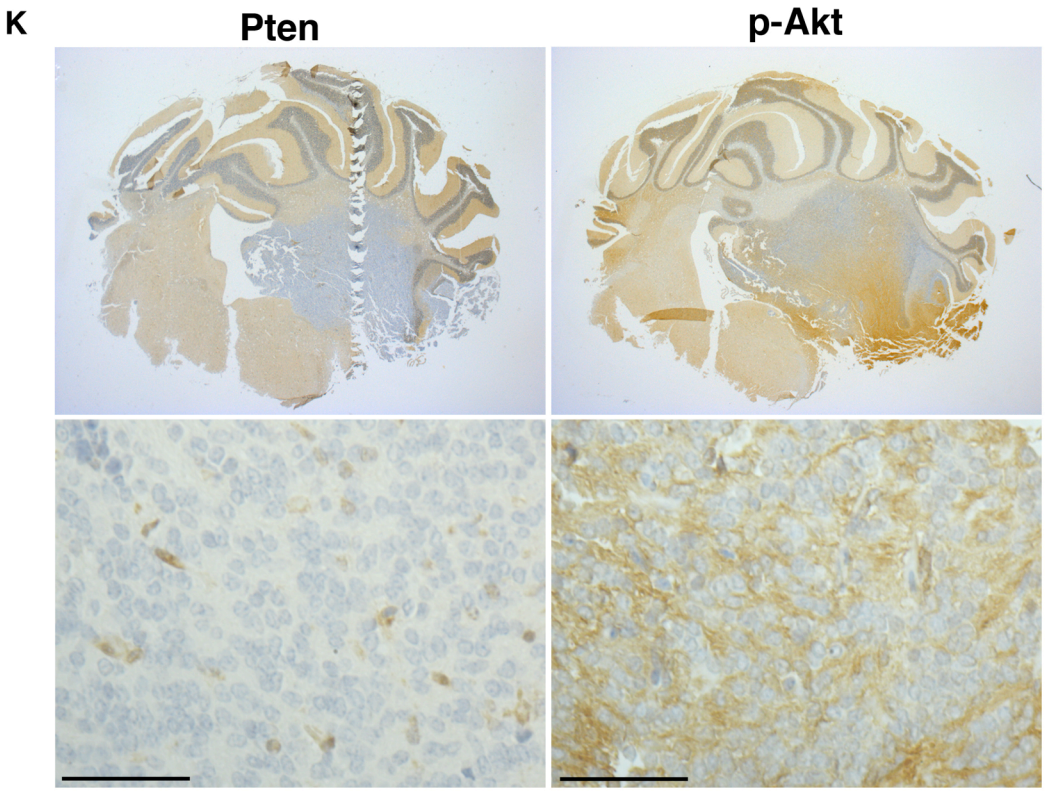
K
Pten
p-Akt

**Figure 2.7. ARHGAP36 Expression Is Elevated In Poor Prognosis Human Medulloblastoma**

(A) Medulloblastomas have increased ARHGAP36 RNA expression and segregate into molecular subgroups C, D and E (Kool et al. 2008). (B) Tissue microarray immunohistochmistry demonstrates ARHGAP36 expression in medulloblastoma. Tumors contained nuclear, cytoplasmic, a combination of both or no staining for ARHGAP36. (C) Kaplan-Meier analysis identifies an inverse association between ARHGAP36 expression and reduced overall survival in All and Deceased patients analyzed. (D) MB with obvious classic and nodular areas show cytoplasmic ARHGAP36 in classic portion and sparse nuclear ARHGAP36 in nodular areas. Statistical significance calculated by Mantle-Cox Log-rank test. Scale bars = 50μm.

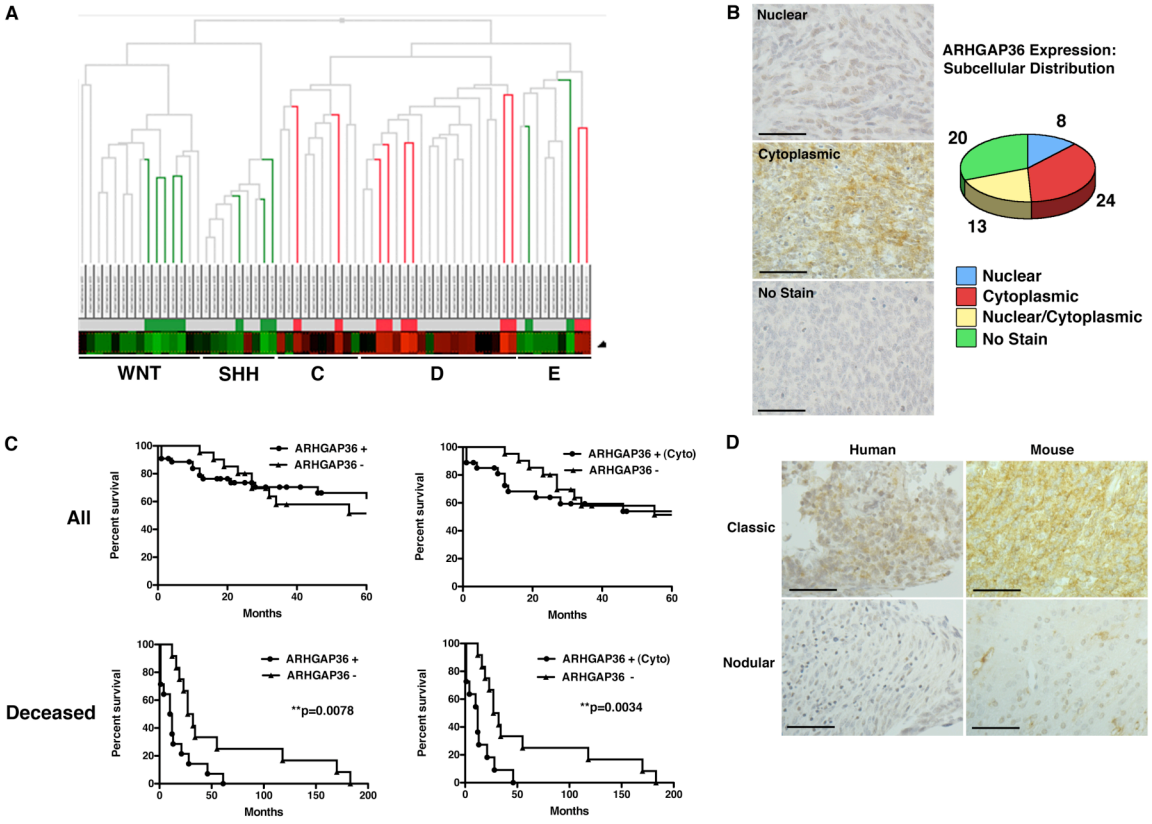
A
WNT
SHH
C
D
E
B
Nuclear
Cytoplasmic
No Stain
ARHGAP36 Expression:
Subcellular Distribution
8
20
24
13
Nuclear
Cytoplasmic
Nuclear/Cytoplasmic
No Stain
C
All
Deceased
Percent survival
Months
ARHGAP36 +
ARHGAP36 -
ARHGAP36 + (Cyto)
**p=0.0078
**p=0.0034
D
Human
Mouse
Classic
Nodular

**Figure 2.8. Endogenous ARHGAP36 Expression In Developing And Adult Cerebellum**

(A-D) Immunohistochemistry expression analysis for ARHGAP36 in mouse (A and C) and human (B and D) cerebellum. (A) Mouse neonatal day 7 and (B) human 32 week perinatal cerebellum illustrating ARHGAP36 nuclear positive cells in the developing molecular layer (ML), Purkinje cell layer (PC) and internal granule cell layer (IGL). (C) Mouse adult day 63 and (D) human adult cerebellum illustrating ARHGAP36 nuclear positive cells throughout the ML, PC and IGL. Scale bars = 50μm.

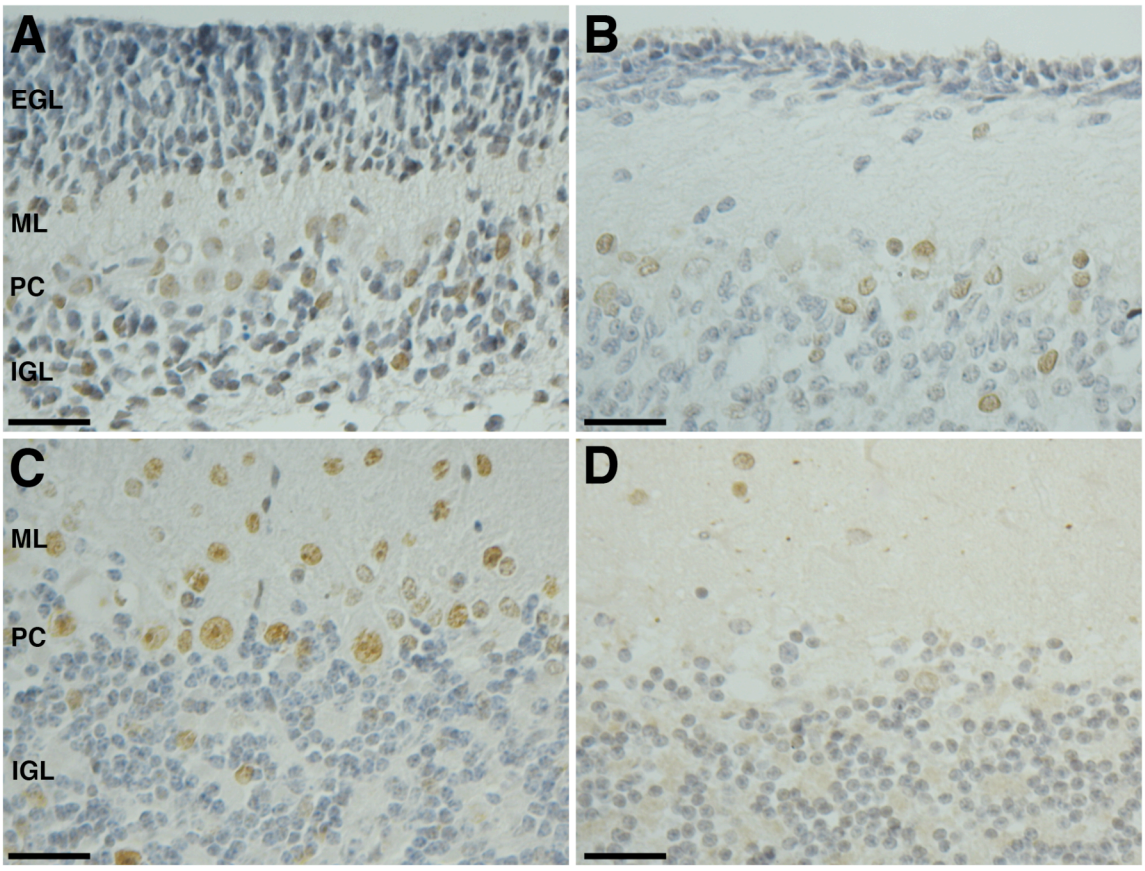
A
EGL
ML
PC
IGL
B
C
ML
PC
IGL
D

**Supplemental Table 2.1. SB-Induced PNET Characteristics**

Itemized list of SB-induced medulloblastomas (top) and sPNET (bottom) tumor characteristics including mouse identifier, gender, age at death, tumor histology and observed metastasis.

## Supplemental Table 1

| MEDULLOBLASTOMA | Sex | Age (Days) | Histology | Observed Metastasis |
|---|---|---|---|---|
| **Transposition Only** | | | | |
| WT22 | F | 120 | Classic | |
| WT363 | F | 181 | Classic | Leptomeningial spread |
| WT459 | F | 219 | Classic | |
| WT523 | F | 87 | Classic | |
| WT701 | M | 111 | Classic | |
| WT724 | F | 169 | Classic | Parenchyma infiltration |
| **Transposition and *Pten*$^{flox/+}$** | | | | |
| Pten49 | F | 190 | Classic | Leptomeningial spread |
| Pten164 | M | 214 | Classic with nodular region | |
| Pten241 | F | 185 | Classic with nodular region | Parenchyma infiltration |
| Pten468 | F | 191 | Classic | |
| **Transposition and *p53*$^{lsl-R270H}$** | | | | |
| P53184 | F | 133 | Classic | Leptomeningial spread |
| P53176 | M | 129 | Classic | |
| P53372 | M | 142 | Classic | Leptomeningial spread |
| P53531 | M | 239 | Classic | |
| P53546 | M | 104 | Classic | |
| P53586 | M | 90 | Classic | |
| P53593 | F | 82 | Classic | Brainstem infiltration |
| P53634 | F | 73 | Classic | |
| P53690 | F | 133 | Classic | Leptomeningial spread |
| P53691 | F | 77 | Classic | Leptomeningial spread |
| P53720 | F | 129 | Classic | Leptomeningial spread |
| P53812 | M | 152 | Classic | Parenchyma infiltration |

| sPNET | Sex | Age (Days) | Histology | Observed Metastasis |
|---|---|---|---|---|
| ***Nestin*-Cre, *p53*$^{lsl-R270H}$** | | | | |
| P53198 | M | 333 | sPNET - Olfactory bulb | |
| Transposition Only | | | | |
| WT722 | M | 499 | sPNET - Olfactory bulb, cortex | Leptomeningial spread |
| **Transposition and *p53*$^{lsl-R270H}$** | | | | |
| P53163 | M | 319 | sPNET - Cortex, Lateral Ventricle | Parenchyma infiltration |
| P53209 | F | 332 | sPNET - Cortex, Lateral Ventricle | Parenchyma infiltration, Leptomeningial spread |
| P53301 | M | 381 | Cortex | Cortex infiltration |
| P53308 | M | 471 | sPNET - Olfactory bulb | Cortex infiltration |
| P53323 | M | 513 | sPNET - Olfactory bulb, Cortex | Cortex infiltration |
| P53434 | M | 507 | sPNET - Olfactory bulb | Cortex infiltration |
| P53528 | F | 377 | sPNET with nodular areas - Olfactory bulb | Leptomeningial spread |
| P53566 | F | 591 | sPNET - Lateral Ventricle | Parenchyma infiltration |
| P53579 | M | 575 | sPNET - Olfactory bulb | Leptomeningial spread |
| P53581 | M | 528 | sPNET - Olfactory bulb, Lateral Ventricle | Parenchyma infiltration |
| P53714 | F | 249 | sPNET - Olfactory bulb, Cortex | Cortex infiltration |
| P53819 | F | 439 | sPNET - Cortex | Cortex infiltration |

**Supplemental Table 2.2. MB And sPNET Transposon Insertions Correspond With Immunopositive Expression Characteristics**

(Top) Itemized list of SB-induced medulloblastomas identifying tumors with *Arhgap36*, *Gli1* and *Pten* transposon insertions. Corresponding IHC analysis for Arhgap36, Gli1, Otx2, Pten and p-Akt also listed for each tumor. (Bottom) Itemized list of SB-induced sPNET identifying tumors with transposon insertions in the Ras-pathway genes *Nf1*, *Erbb2ip*, *Eras* and *Rasa3*. Corresponding IHC analysis for p-Erk also listed for each tumor.

## Supplemental Table 2

| MEDULLOBLASTOMA | Observed Metastasis | *Arhgap36* Driving Insertions | *Gli1* Driving Insertions | *Pten* Disrupting Insertions | Immunohistochemistry: Arhgap36 | Gli1 | Otx2 | Pten | p-AKT(S473) |
|---|---|---|---|---|---|---|---|---|---|
| **Transposition Only** | | | | | | | | | |
| WT22 | | Upstream | | | Cyto+ | - | Nuc+ | + | Sparse Nuc+ |
| WT363 | Leptomeningial spread | Upstream | | | Cyto+ | - | Nuc+ | Localized - | - |
| WT459 | | | | | - | - | Nuc+ | + | Sparse Nuc+ |
| WT523 | | | | | - | - | Nuc+ | + | - |
| WT701 | | Intron 1 | | | Cyto+ | - | Nuc+ | + | - |
| WT724 | Parenchyma infiltration | Intron 1 | | | Cyto+ | - | Localized Nuc+ | + | - |
| **Transposition and *Pten*$^{flox/+}$** | | | | | | | | | |
| Pten49 | Leptomeningial spread | Intron 1 | | Intron 1 | Cyto+ | - | Nuc+ | Overall - | Cyto+ |
| Pten164 | | Upstream | | Intron 5 | Classic = Cyto+ Nodular = - | - | Nuc+ | Overall - | Cyto+ |
| Pten241 | Parenchyma infiltration | Intron 1 | | | Classic = Cyto+ Nodular = - | - | Nuc+ | Classic = Localized - Nodular = Localized - | Classic = sparse nuc+ Nodular = Localized cyto+ |
| Pten468 | | Upstream | | | Cyto+ | - | Nuc+ | Localized - | Localized cyto+ |
| **Transposition and *p53*$^{fl/+R270H}$** | | | | | | | | | |
| P53184 | Leptomeningial spread | Upstream | | | Cyto+ | - | Nuc+ | + | - |
| P53176 | | Upstream | | | Cyto+ | Nuc+ | Nuc+ | + | - |
| P53372 | Leptomeningial spread | Intron 1 | | | Cyto+ | - | Nuc+ | + | - |
| P53531 | | | | | - | - | Nuc+ | Localized - | Sparse Nuc+ |
| P53546 | | | Intron 5 | | - | Nuc+ | - | + | - |
| P53586 | | | Intron 5 | | - | Nuc+ | - | + | Sparse Nuc+ |
| P53593 | Brainstem infiltration | | Intron 5 | | - | Nuc+ | - | Localized - | Sparse Nuc+ |
| P53634 | | Upstream | | | Cyto+ | - | Nuc+ | + | - |
| P53690 | Leptomeningial spread | | | | - | - | Localized Nuc+ | + | Sparse Nuc+ |
| P53691 | Leptomeningial spread | Upstream | | | Cyto+ | - | Nuc+ | + | - |
| P53720 | Leptomeningial spread | Intron 1 | | Intron 5 | Cyto+ | - | Nuc+ | Localized - | Localized cyto+ |
| P53812 | Parenchyma infiltration | | | | - | - | Nuc+ | Localized - | Cyto+ |

| sPNET | Observed Metastasis | *Nf1* Disrupting Insertions | *Erbb2ip* Disrupting Insertions | *Eras* Driving Insertions | *Rasa3* Insertions | Immunohistochemistry: p-ERK |
|---|---|---|---|---|---|---|
| ***Nestin*-Cre, *p53*$^{fl/+R270H}$** | | | | | | |
| P53198 | Leptomeningial spread | | | | | - |
| **Transposition Only** | | | | | | |
| WT722 | Cortex infiltration | Intron 8 | | | Intron 1 | Nuc+ |
| **Transposition and *p53*$^{fl/+R270H}$** | | | | | | |
| P53163 | Parenchyma infiltration | | | | | - |
| P53209 | Parenchyma infiltration, Leptomeningial spread | | | | | Nuc+ |
| P53301 | Cortex infiltration | Intron 4 | | | Intron 1 | Localized Nuc+ |
| P53308 | Cortex infiltration | Intron 4 | | | | Nuc+ |
| P53323 | Cortex infiltration | Intron 4 | Intron 4 | Intron 1 | | Localized Nuc+ |
| P53434 | Cortex infiltration | | | Intron 1 | | Nuc+ |
| P53528 | Leptomeningial spread | Intron 5 | | | | Localized Nuc+ |
| P53566 | Parenchyma infiltration | Intron 1 | | | | Nuc+ |
| P53579 | Leptomeningial spread | | | | | - |
| P53581 | Parenchyma infiltration | Intron 5 | | Intron 1 | | Localized Nuc+ |
| P53714 | Cortex infiltration | | | | | - |
| P53819 | Cortex infiltration | Intron 34 | Intron 14 | | | Nuc+ |

**Supplemental Figure 2.1. Transposition Frequency Influences PNET Penetrance**

High copy (T2/Onc2, chromosome 4) and low copy (T2/Onc, chromosome 1 or 15) mutagenic transposon concatomers were represented at different starting percentages in mice undergoing (A) transposition only, (B) transposition and $Pten^{flox/+}$, (C) transposition and $p53^{lsl\text{-}R270H}$. Medulloblastomas derived from T2/Onc2 transposons occur at a higher percentage compared to starting percentage in each experimental cohort (second column, A-C). Transposition only sPNET was derived from T2/Onc2. sPNETs associated with $p53^{lsl\text{-}R270H}$ are equally derived from T2/Onc2 and T2/Onc transposon concatomers (last column, C).

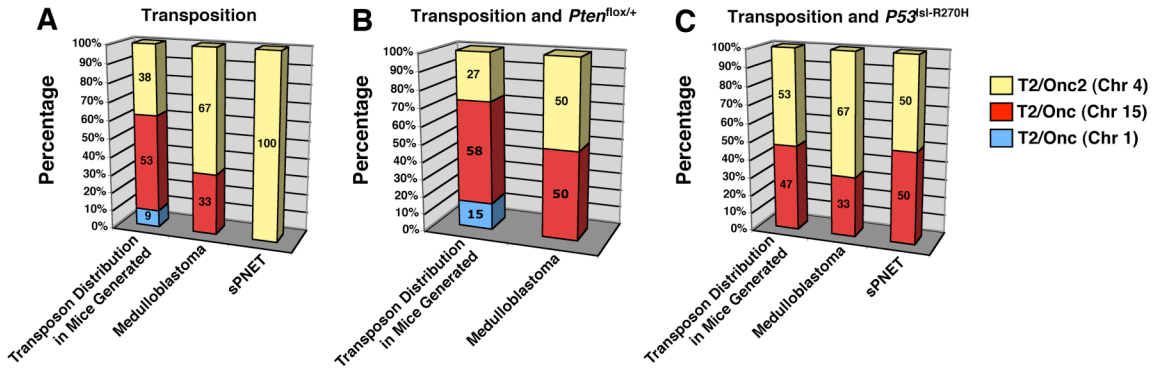
A
Transposition
B
Transposition and Pten flox/+
C
Transposition and P53 lsl-R270H
Percentage
100%
90%
80%
70%
60%
50%
40%
30%
20%
10%
0%
38
53
9
67
33
100
27
58
15
50
50
53
47
67
33
50
50
Transposon Distribution in Mice Generated
Medulloblastoma
sPNET
T2/Onc2 (Chr 4)
T2/Onc (Chr 15)
T2/Onc (Chr 1)

**Supplemental Figure 2.2. Survival Curves And Non-Neural Tumor Burden Among All SB Insertional Mutagenesis Cohorts**

(A-C) Kaplan-Meier survival curves (top) and overall prevalent tumor burden (bottom) for Transposition only (A), Transposition and *Pten*$^{flox/+}$ (B), and Transposition and *p53*$^{lsl\text{-}R270H}$ (C) animal cohorts. Statistical significance: **p<0.05, ***p<0.001 (Log rank Mantel-Cox Test).

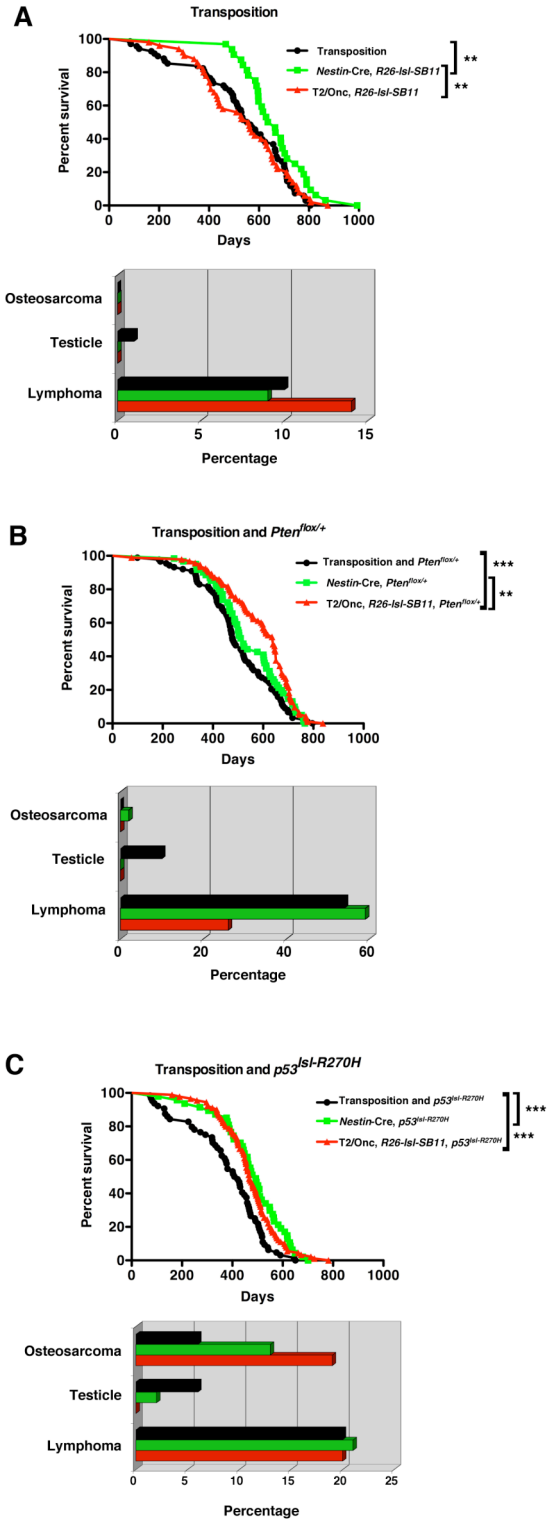
A
Transposition
Percent survival
Days
Transposition
Nestin-Cre, R26-lsl-SB11
T2/Onc, R26-lsl-SB11
**
**
Osteosarcoma
Testicle
Lymphoma
Percentage
B
Transposition and Ptenflox/+
Percent survival
Days
Transposition and Ptenflox/+
Nestin-Cre, Ptenflox/+
T2/Onc, R26-lsl-SB11, Ptenflox/+
***
**
Osteosarcoma
Testicle
Lymphoma
Percentage
C
Transposition and p53lsl-R270H
Percent survival
Days
Transposition and p53lsl-R270H
Nestin-Cre, p53lsl-R270H
T2/Onc, R26-lsl-SB11, p53lsl-R270H
***
***
Osteosarcoma
Testicle
Lymphoma
Percentage

**Supplemental Figure 2.3. PNET Tumors Exhibit SB Mutagenic Transposition**

(A and B) Immunohistochemistry analysis. (A) PNET tumors stain positive for SB. (B) No primary antibody control. (C) Excision PCR assay showing evidence of transposon mobilization in medulloblastoma and sPNET tissue (white arrowhead, 225 bp band) compared to control tissue lacking Cre recombinase (black arrowhead, 2200 bp band). Scale bar = 50μm.

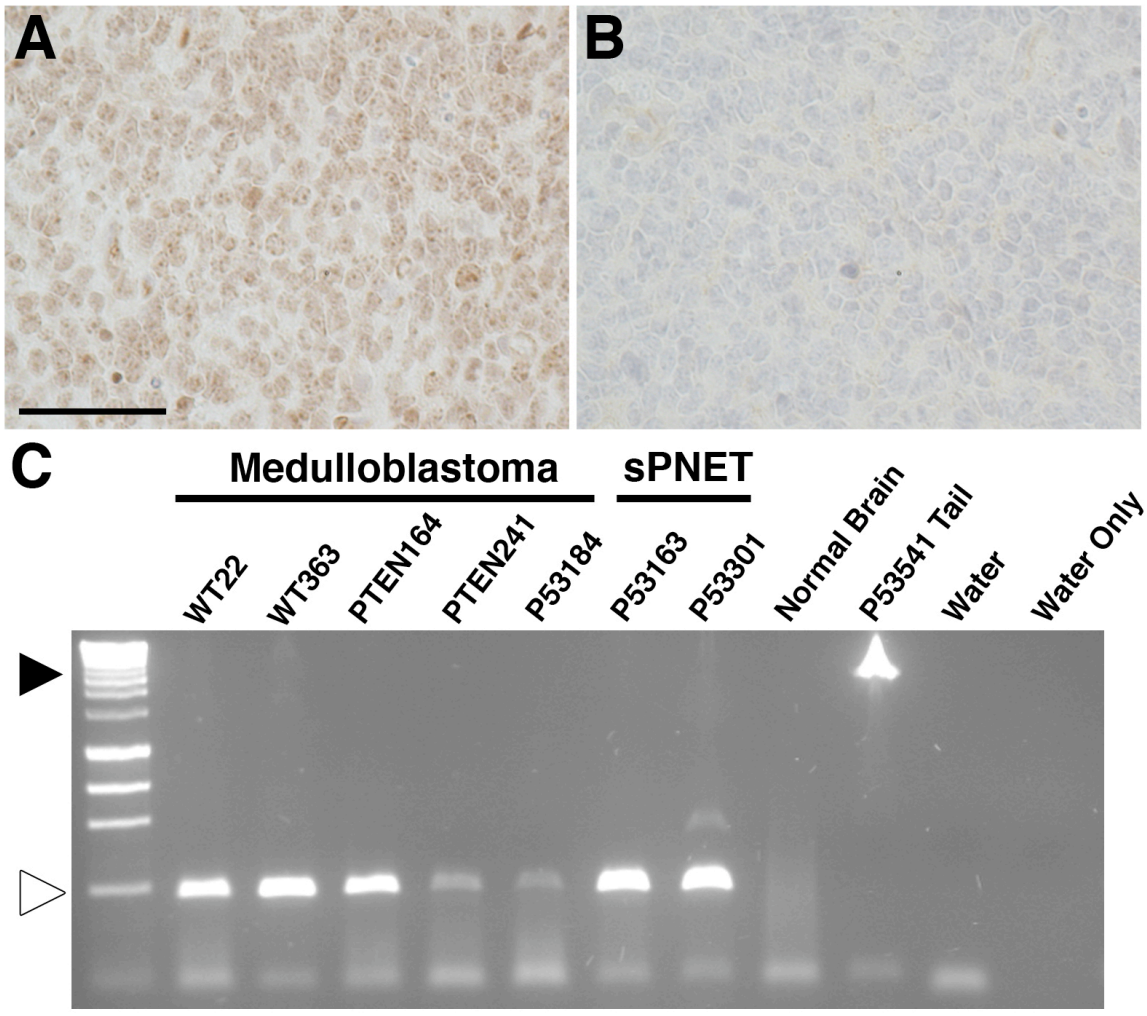
A
B
C
Medulloblastoma
sPNET
WT22
WT363
PTEN164
PTEN241
P53184
P53163
P53301
Normal Brain
P53541 Tail
Water
Water Only

**Supplemental Figure 2.4. SB Insertional Mutagenesis Cooperates With *Pten*$^{flox/+}$ To Generate Biphasic Medulloblastoma**

(A-C) H and E staining. (A) Coronal section of medulloblastoma PTEN241 illustrating two distinct tumor regions. (B) High-power magnification of nodular tumor area. (C) High power magnification of classic tumor area. (D-G) Immunohistochemistry. Nodular tumor area is negative for (D) Ki67 and (F) Nestin (asterisks indicate adjacent classic tumor area). Classic tumor area stains positive for (E) Ki67 and (G) Nestin. Scale bars = 50μm.

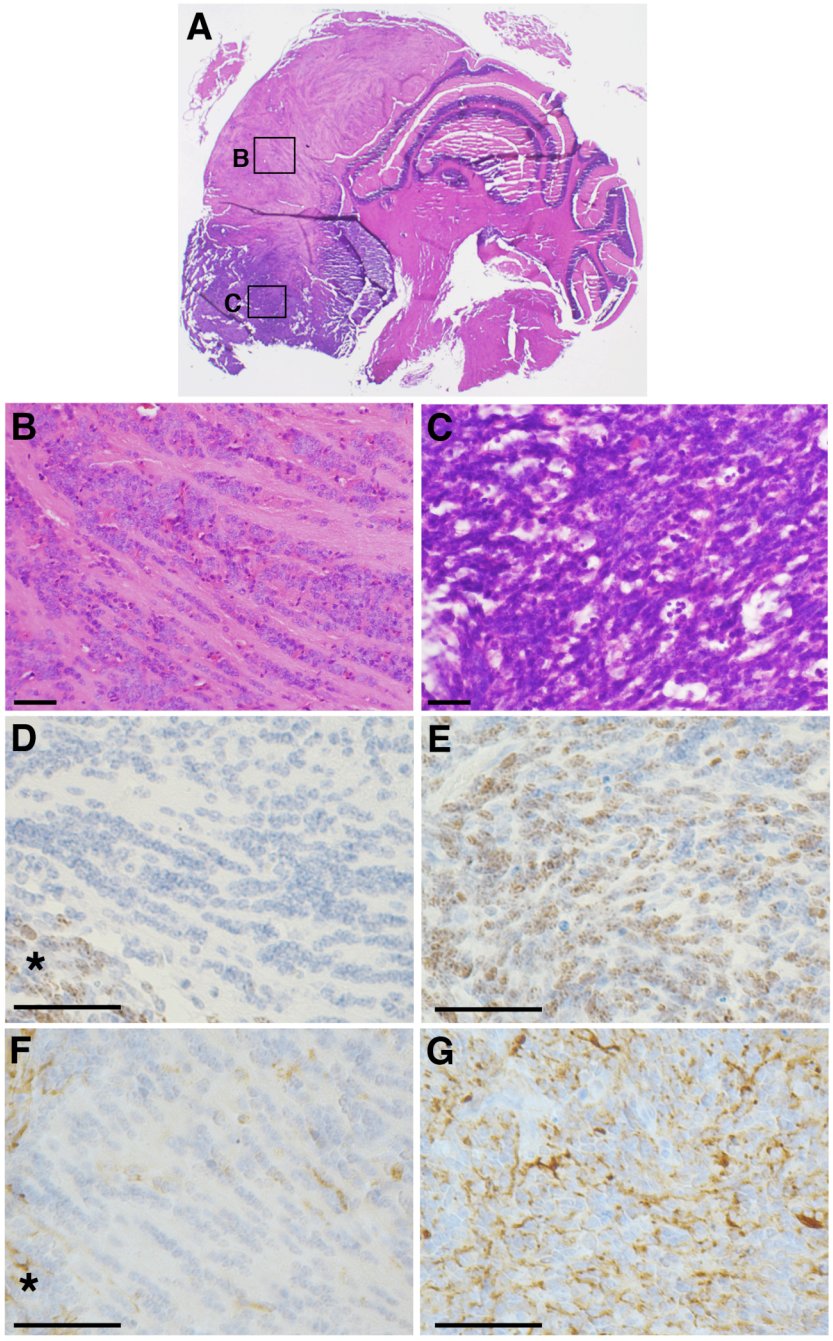
A
B
C
B
C
D
*
E
F
*
G

# CHAPTER 3

## Functional Analysis of Candidate Medulloblastoma Oncogene *Arhgap36*

## Introduction

*Arhgap36* was identified as the most frequent MB candidate oncogene in the SB insertional mutagenesis screen described in Chapter 2. *Arhgap36* was also shown to be upregulated in poorly understood human MB subtypes and associated with poor prognosis. Therefore, we investigated whether *Arhgap36* elicited biological activity upon exogenous overexpression *in vitro* and *in vivo*. We simultaneously tested full-length and truncated versions of human *ARHGAP36* to closely mimic the *Arhgap36* transcripts observed in the SB-induced MB.

NIH3T3 cells are spontaneously immortalized, untransformed mouse embryonic fibroblasts commonly used to test transformation ability of exogenous oncogenes (Rubin et al., 1990). Transformed NIH3T3 cells exhibit morphological changes including round, contracted cells able to form foci in two-dimensional culture. NIH3T3 cells transformed by constitutively active *HRas* expression also demonstrate an increased rate of growth or ability to form anchorage-independent colonies in three-dimensional soft agar culture environment (Qiu et al., 1995; Shang et al., 2007). In addition, NIH3T3 cells have been successfully used to determine transforming abilities of RhoGTPase family genes (Shang et al., 2007; Jaffe and Hall, 2002). Therefore, we used *PiggyBac* (PB) transposon-mediated gene delivery and stable expression of *ARHGAP36* in NIH3T3 cells to test its transforming ability *in vitro*.

Multiple mouse models have been developed in an effort to investigate the histogenesis and molecular mechanisms of MB. Most of these models take advantage of germline or tissue conditional somatic transgenic mice, which can take months to

generate and require significant resources to maintain. We sought to investigate the possibility of transposon-mediated transgene delivery to model spontaneous MB in normal, commercially available mice. This method would be useful for testing tumor-forming ability of candidate MB genes identified in our insertional mutagenesis screen described in Chapter 2. Work from Wiesner and Decker et al. showed SB transposon plasmids could be polyethylenimine (PEI) complexed with a plasmid providing transient SB transposase expression and injected into the lateral cerebral ventricle of neonatal mice to achieve stable transposon integration and subsequent transgene expression (Wiesner and Decker et al., 2009). Individual transposons engineered to express firefly luciferase (Luc), simian virus 40 large T antigen (SV40-LgTAg) and $NRAS^{GV12}$ were combined in this manner to generate high-grade (III and IV) malignant gliomas that could be monitored with live animal bioluminescent imaging. Different combinations of transposons expressing other genes/molecular pathways altered in human glioma including constitutively active EGFRvIII, myristoylated AKT (myrAKT), or a microRNA-based short hairpin RNA to knockdown *p53* expression were also used to induce malignant glioma with varying grade levels. In order to modulate this strategy for MB, we altered the injection site to target the developing cerebellum. Similar *in vivo* postnatal mouse gene transfer has been performed to generate glioblastomas or MB using replication-competent avian leukosis virus-subgroup A (ALV-A) splice acceptor (RCAS) vectors to deliver different combinations of oncogenes (Holland et al., 1998; Holland and Varmus, 1998; Fults, 2005; Rao et al., 2004). The RCAS method works by physically injecting one or more RCAS vector-producing cell lines designed to express exogenous

oncogenes to the brain of a transgenic mouse engineered to express the ALV-A receptor, TV-A, in glial and neural precursor cells. When the RCAS retrovirus infects the respective TV-A-expressing cell, virus replication does not occur, but retroviral RNA is reverse-transcribed to generate a proviral DNA (Fults, 2005). This DNA then integrates into the host genome and the exogenous gene is expressed as a spliced message driven by the constitutive retroviral promoter long terminal repeat (LTR). While extremely elegant, the RCAS method has distinct disadvantages including the requirement of breeding and maintaining the TV-A transgenic mouse, and the limiting 2.6 kilobase cargo capacity of the RCAS vector (Wiesner and Decker et al., 2009). In comparison, distinct advantages of using transposon-mediated transgene delivery include relative ease of transposon plasmid DNA preparation, and the ability of the PEI/DNA complex to transfect cells of any strain of mouse especially commercially available wild type stock strains like FVB/n.

As an initial proof of concept, we tested the ability of SV40 LgTAg transposon to induce spontaneous MB. LgTAg is able to bind and inactivate p53 and Rb1 proteins and has been shown to be expressed in several human MB samples (Huang et al., 1999; Zhen et al., 1999). Additionally, Marino and colleagues created a mouse model for MB by combining a body-wide or conditional *p53*-null mutation with somatic inactivation of *Rb1* in glial and neural precursor cells (Marino et al., 2000). Furthermore, we combined LgTAg expression with a transposon expressing a myristoylated form of AKT as reduced p53 protein expression coupled with activated PI3K pathway activity via phosphorylated Akt (pS437) has been documented to be associated with MB incidence in *Ptch* deficient mice (Pazzaglia et al., 2006). As these experiments helped to establish the ability of

transposon-mediated gene transfer to induce sporadic MB in non-transgenic mice, we further tested tumorigenic effects of *ARHGAP36 in vivo*.

Collectively, these experiments provide evidence that *ARHGAP36* has tumorigenic properties. Moreover, this activity is potentially dependent on the absence of the first 48 amino acids of the endogenous ARHGAP36 sequence indicating important biological regulation.

## Materials And Methods

### Plasmid Vectors

cDNA encoding the full length human *ARHGAP36* (amino acids 1-547) was purchased from OriGene Technologies, Inc. (#SC313948) and subsequently PCR engineered to contain the Kozak sequence 5′-GCCACC-3′ upstream of the start codon. A truncated version of human *ARHGAP36* (amino acids 49-547) was PCR engineered with the same Kozak sequence upstream of the in-frame start codon amino acid 49. Constitutively active human HRasGV12 was purchased from Addgene (http://www.addgene.org). *ARHGAP36* (full length and truncated) and *HRasG12V* fragments were subcloned into Entry Vectors then transferred via LR Clonase (#11791019, Invitrogen) reaction into the PB/SB-CAGGS-loxDsRedlox-DEST-IRES-GFP-PGK-Puro transposon expression vector. To remove the lox-DsRed-lox fragment, the vector was transformed and cultured in *Escherichia coli* expressing Cre recombinase to generate PB/SB-CAGGS vectors expressing *ARHGAP36* (full length), *tARHGAP36* (truncated) or *HRasG12V*. The hyperactive PB transposase PB7 was a kind gift from Dr. Nancy L. Craig. pT/CMV-

*SV40-LgT*, pT2/C-*Luc*/PGK-*SB100*, pKT2/CLP-*myrAKT* vectors were kind gifts from Dr. John Ohlfest. pT3.5-CAGGS-*ARHGAP36* and pT3.5-CAGGS-*tARHGAP36* vectors were constructed via Clonase reaction into T3.5-CAGGS expression vector engineered with attR sites upstream of the polyA.

**Soft Agar Colony Formation Assay**

Bottom agarose layer was prepared with 0.8% Sea Plaque low-melt agarose (#50101, Lonza) in NIH3T3 media and used to coat each 35mm well of a 6-well plate. NIH3T3 cell clones stably transfected with PB/SB-CAGGS-*ARHGAP36*, -*tARHGAP36* or –*HRasG12V* and corresponding control clones were combined with low-melt agarose to make 0.48% top agarose and immediately plated in triplicate at $1x10^4$ cells per well. Polymerized wells were coated with 1mL normal growth media and incubated for two weeks at 37°C in a humidified 5% $CO_2$ incubator. Colonies were visualized by staining with 0.005% crystal violet in 10% phosphate buffered Formalin (#SF100, Fisher) for two hours at room temperature. Colonies larger than 50μm were quantified using ImageJ 1.45r software (National Institutes of Health).

**Mouse Care**

FVB/NJ (#001800, Jackson Labs) were mated and monitored daily until they gave birth. Intracranial injections were performed on neonatal pups within 24 hours of birth. Mice were maintained in a specific pathogen-free facility and experiments were performed according to University of Minnesota Animal Care and Use Committee guidelines.

**Intracranial Injections and Luciferase Imaging**

Plasmid DNA constructs for injections were purified with PureLink HiPure Plasmid

Maxiprep Kit (#K2100-06, Invitrogen) and resuspended in nuclease-free water. PEI (#201-10G, Polyplus Transfection)/DNA complexes were prepared according to the manufacturer's instructions. Injection procedure was performed as previously described (Wiesner and Decker et al., 2009) with coordinate modifications to target the cerebellum: -1.5AP and -1.5DV from λ. A total of 1μg of DNA was consistently delivered in a 2μL volume for all experiments. Live animal *in vivo* Luciferase imaging was performed as described (Wiesner and Decker et al., 2009) to assess successful injection 24 hours after injection and monitor tumor development.

**Histopathology and Immunohistochemistry**

Tissue samples were fixed in 10% phosphate buffered formalin, paraffin embedded, cut into 5μm sections and stained with Hematoxilin and Eosin (H and E) using standard methods. Immunohistochemistry was conducted using standard methods with citrate-based antigen retrieval (#H-3300, Vector Laboratories). Endogenous peroxidase activity was quenched with 3% hydrogen peroxidase. Primary antibodies: Arhgap36 (#HPA002064, SIGMA), p-AKT(Ser473) (#4060, Cell Signaling Technologies), SV40-Tag(v-300) (#sc-20800, Santa Cruz Biotechnology) were used and detected with Vector Laboratories reagents: Vectastain Elite ABC Kit (#PK6100) and 3,3'-diaminobenzidine (DAB) Substrate Kit (#SK-4100).

**Western Blot**

Western blots were performed using standard methods using the following primary antibodies: ARHGAP36 (#ab84010, abcam), GAPDH (#2118, Cell Signaling Technologies). Primary antibodies were probed with HRP-conjugated Donkey-∝-Rabbit

(#SA1-200, Pierce Antibodies) and detected with the Amersham ECL Advance Western Blotting Detection Kit (#RPN2135, GE Healthcare).

## Results

### *Arhgap36* Overexpression Induces *in vitro* Transformation Of NIH3T3 Cells

In an effort to determine if *ARHGAP36* has transformation activity, we developed a transposon plasmid vector designed with the chimeric promoter consisting of chicken β-actin promoter, cytomegalovirus enhancer and β-actin intronic sequences (*CAGGS)* (Okabe et al., 1997) to express cDNA of choice coupled with green fluorescent protein (GFP), after the control *Discosoma sp*. Red fluorescent protein (DsRed) STOP cassette has been removed via Cre recombinase, and Phosphoglycerate kinase (PGK) promoter-mediated Puromycin expression for *in vtiro* drug selection (Figure 3.1A). The transposon was designed with both SB IR/DR and PB inverted terminal repeat (ITR) sequences to facilitate mobilization and stable integration into the genome using either SB or PB transposase. PB transposition is a similar cut-and-paste transposon system derived from the cabbage looper moth (Yusa et al., 2011). Significant differences include PB transposase recognizes and bind the specific ITR sequences to facilitate mobilization, PB transposons target TTAA nucleotide sequences for genome integration, PB transposons predominantly insert at transcription start sites and can carry larger cargo compared to SB (Ivics et al., 2009). We included the PB ITR elements as well because PB-mediated transposition has reported advantages in mammalian cells compared to SB including more efficient transposition with larger cargo (Ivics et al., 2009). We engineered this

vector to express either full length *ARHGAP36* or a truncated isoform 5 (UniProtKB Q6ZRI8-5) of *ARHGAP36* (*tARHGAP36*) to more closely mimic the *Arhgap36* transcript identified in the insertional mutagenesis mice described in Chapter 2. This truncated version lacks the first 144 base pairs, providing transcriptional initiation from the methionine start site at exon 2 amino acid position 49. As a positive control, a vector with a constitutively active form of *HRas* (*HRasGV12*) was also created. These transposon vectors were co-transfected with the hyperactive PB transposase PB7 plasmid (Yusa et al., 2011) into NIH3T3 cells in parallel and individual small colonies were isolated under Puromycin selection to generate distinct clones. Clones harboring the control DsRed-intact transposons readily expressed DsRed, while the experimental transposons with the DsRed sequence removed successfully expressed GFP (3.1B-D). Cells expressing *HRasG12V* display a condensed, round, transformed morphology (bottom brightfield image, Figure 3.1B) as a positive control for transformation that has been documented previously (Shang et al., 2007). Sporadic GFP-expressing foci were commonly observed in these cells as well as clone cultures among all of the experimental groups (Inset, bottom right, Figure 3.1B-D). We performed soft agar colony assays to assess anchorage-independent growth abilities of all the experimental groups and their associated control cells. After two weeks under these conditions, cells expressing *HRasG12V* (GFP) produce multiple robust colonies as expected compared to *HRasG12V* control cells (DsRed) (Figure 3.2A). Interestingly, *ARHGAP36* expressing cells (GFP) did not produce colonies during this time frame, but cells expressing *tARHGAP36* (GFP) generated a significant level of moderate-sized colonies compared to controls (DsRed) (Figure 3.2A).

Quantification of these colonies demonstrated a statistically significant increase in colony formation in cells expressing *tARHGAP36* (Figure 3.2B). These results indicate the ability of ARHGAP36 to induce cellular transformation when N-terminal amino acids 1-48 have been removed from the full-length sequence.

**Transposon-Mediated Oncogene Delivery Generates Spontaneous Medulloblastoma**

To generate MB development, we initially co-injected a transposon expressing LgTAg PEI-complexed with a plasmid expressing a hyperactive SB100X transposase (Mates et al., 2009) and carrying a transposon expressing firefly Luc into the cerebellum of neonatal mice (Figure 3.3A). To determine the successful delivery of the PEI/DNA complex, transient Luc expression from residual plasmid DNA was observed 24 hours after injection (Figure 3.3A). Nine mice were injected in this group (Figure 3.3B). We further combined LgTAg with myrAKT to test cooperation of these oncogenes for medulloblastoma development (Figure 3.3B). We monitored tumor development by careful inspection of mice with a focus on abnormal head shape and neurological morbidity. Tumors were visualized and confirmed with live-animal bioluminescence as a consequence of the firefly Luc transposon included in all injections (Figure 3.4A). Tumors were commonly observed within the $4^{th}$ ventricle including the cerebellum (Figure 3.4B). These tumors contain medulloblastoma histological characteristics including small, round tumor cells with areas of rosette formation and mitotic nuclei (Figure 3.4C). Significant side effects observed in several mice included severe hydrocephaly associated with extreme morbidity within 1 month after injection. These mice did not harbor tumors and were excluded from the analysis (data not shown). To

date, we have observed 1/9 (11%) tumors at 150 days in mice injected with *LgTAg* (Figure 3.4G). Interestingly, mice injected with *LgTAg* and *myrAKT* to date have produced tumors at a similar frequency to *LgTAg* alone (3/30, 10%), but with a decreased latency (67 day average, Figure 3.4G). As expected, animals injected with *myrAKT* alone failed to form tumors (data not shown).

We then tested tumor-forming ability of full-length and truncated forms of *ARHGAP36*. Although these plasmids have thus far failed to form tumors by themselves, we systematically combined them with *LgTAg* and/or *myrAKT* (Figure 3.3B). Thus far, we have observed tumors in mice injected with *LgTAg*, *myrAKT* and *ARHGAP36* with a similar frequency (3/32, 9.4%) and latency (74 days, average) compared to *LgTAg/myrAKT*-injected mice. Interestingly, we have so far observed a tumor (1/25, 4%) in the *LgTAg/tARHGAP36* experimental group occurring faster (103 days) compared to tumors derived form mice injected with *LgTAg* alone (Figure 3.4G). Importantly, tumors injected with *LgTAg*, *myrAKT* and/or variants of *ARHGAP36* express nuclear LgTAg (Figure 3.4D), cytoplasmic p-AKT (S473) (Figure 3.4E) and cytoplasmic ARHGAP36 (Figure 3.4F), respectively. Collectively, these experiments demonstrate the ability of transposon-mediated delivery of oncogenes to the cerebellum of neonatal mice to generate MB. Additionally, current results indicate the ability of a truncated form of *ARHGAP36* to cooperate with *LgTAg* in MB *in vivo*.

**Discussion**

*ARHGAP36* has been implicated as a candidate genetic driver for MB in mouse and man

(Chapter 2). Strikingly, elevated expression of *ARHGAP36* is strongly correlated with MB molecular subgroups independent of SHH and WNT pathway activation that inflict an overall worse patient prognosis, and are poorly understood on a genetic level. In addition, ARHGAP36 is predicted to be a RhoGTPase GAP protein, but there is currently no reported biological function associated with this gene and its transforming ability is unknown.

We tested effects of ARHGAP36 overexpression *in vitro* by engineering NIH3T3 cells to ubiquitously express a full length or truncated isoform version of the protein. Our results here show that truncated ARHGAP36 has a stronger transforming ability compared to the full-length protein as indicated by an increase in anchorage-independent NIH3T3 colony formation. Analysis of the protein features identifies several important characteristics for these isoforms of ARHGAP36. Both harbor the predicted GAP domain and an upstream arginine-rich region containing a bipartite nuclear localization sequence and a predicted SH3 domain (http://cbm.bio.uniroma2.it/SH3-Hunter/). These proteins also contain multiple predicted phosphorylation sites that could be important for subsequent cellular location and function (PROSITE (http://prosite.expasy.org/; Center For Biological Sequence Analysis http://www.cbs.dtu.dk/services/). We observed casein kinase II, tyrosine kinase, Ca2+/calmodulin-dependent protein kinase II, protein kinase C, camp- and cGMP-dependent protein kinase phosphorylation sites in additional to several N-myristoylation sites present throughout the protein sequence (data not shown). Interestingly, several of these features are lost in the truncated ARHGAP36 isoform. Specifically, we noticed one of the N-myristoylation sites (AA 36-41), one of several

potential protein kinase C phosphorylation sites and the potential N-terminal Ca2+/calmodulin-dependent protein kinase II phosphorylation site would all be removed from truncated ARHGAP36. Interestingly, similar sequence changes also occur in the transposon-mediated expression of Arhgap36 seen in the mouse MB described in Chapter 2. Although these sites have unknown function in the context of ARHGAP36, protein phosphorylation is generally known to effect protein function and is a main event in modulating nuclear protein import. Ca2+/calmodulin-dependent protein kinase II-mediated phosphorylation was shown to inhibit the Cdc42 and Rac1-targeting GAP activity of ARHGAP32 (Okabe et al., 2003). Furthermore, Calderilla-Barbosa et al. demonstrated that the nuclear accumulation of a Dystrophin isoform in rat neuronal PC12 cells was mediated by Ca2+/calmodulin-dependent protein kinase II phosphorylation (Calderilla-Barbosa et al., 2006). Therefore it is plausible that the first 48 amino acids of ARHGAP36 have significant purpose for its function regulation and subcellular localization, warranting additional experiments to test this hypothesis.

In effort to create an *in vivo* mouse model for functional testing of candidate MB genes, we further employed the use of transposons as carrier molecules for stable long-term expression of oncogenes and TSG delivered to neonatal stem cells of the fourth ventricle. We report here results of this method demonstrating the ability of LgTAg expression to induce low-penetrance MB, and show that this effect is enhanced and accelerated when combined with constitutively active AKT. These experiments represent the first non-transgenic, spontaneous MB mouse model method that does not utilize the RCAS method or directly manipulate the Shh pathway. It will be important, however, to

examine gene expression profiles of Shh pathway effector molecules such as *Gli1-3*, *Ptch1*, *Shh*, or protein markers in these tumors. This will help determine a Shh pathway role in these tumors similar to previous MB mouse models that develop a Shh molecular signature without directly affecting this pathway by initially targeting *Rb1* and *p53* (Marino et al., 2000; Shakhova et al., 2006). Furthermore, preliminary results combining this method with different isoforms of *ARHGAP36* indicate that truncated ARHGAP36 can cooperate with LgTAg to form MB, indicating a requirement for *ARHGAP36* and *p53* deficiency combined for medulloblastomagenesis in this model similar to that seen in mice from Chapter 2.

Collectively, these data provide further *in vitro* and *in vivo* evidence that *ARHGAP36* does have transforming ability. Intriguingly, these experiments provide insight into what regulatory elements of the *ARHGAP36* sequence can assist in cell transformation and tumorigenesis. Additional experiments identifying and comparing the subcellular localization of the transposon-mediated overexpression of ARHGAP36 isoforms described above will also be beneficial for this purpose. Furthermore, we have developed a new mouse model for MB development capable of straightforward combinatorial analysis of different known and candidate oncogenes. These experiments are ongoing to determine the correct genetic combination and cell of origin for ARHGAP36-mediated MB formation.

**Figure 3.1. Transposon-Mediated Oncogene Delivery Can Induce NIH3T3 Cell Transformation *in vitro***

(A) Schematic of transposon vectors used for oncogene delivery in vitro. (Top) Control transposon contains an intact loxP flanked DsRed sequence preventing expression of gene CDS:IRES-GFP sequences. (Bottom) Experimental transposon with DsRed sequence remove via Cre recombination allowing full expression of gene CDS:IRES-GFP sequences. (B-D) Brightfield and fluorescent images of NIH3T3 cells. (B) Control and experimental *HRasG12V* clones expressing DsRed (top) or GFP (bottom), respectively. Representative colony derived from experimental *HRasG12V* clone (inset, bottom right). (C) Control and experimental *ARHGAP36* clones expressing DsRed (top) or GFP (bottom), respectively. Representative colony derived from experimental *ARHGAP36* clone (inset, bottom right). (D) Control and experimental *tARHGAP36* clones expressing DsRed (top) or GFP (bottom), respectively. Representative colony derived from experimental *tARHGAP36* clone (inset, bottom right).

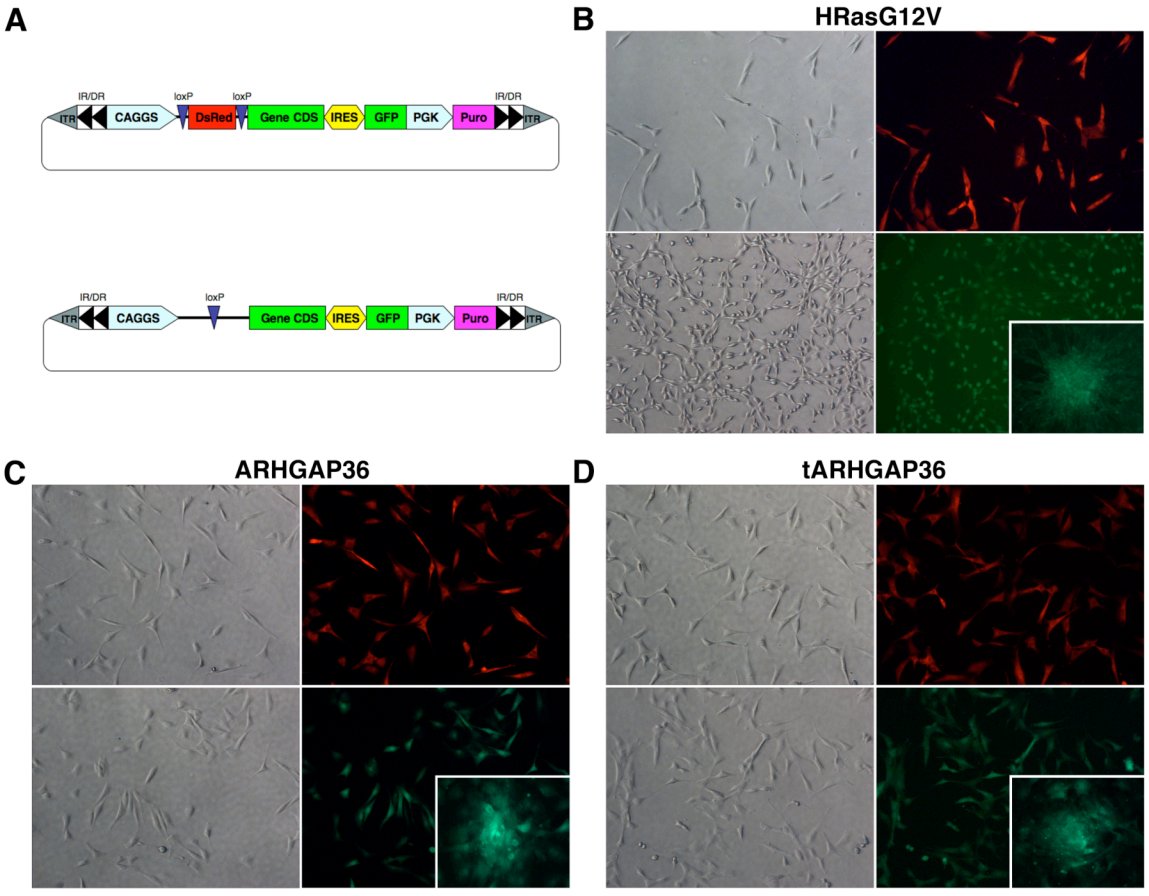
A
IR/DR
loxP
loxP
IR/DR
ITR
CAGGS
DsRed
Gene CDS
IRES
GFP
PGK
Puro
ITR
IR/DR
loxP
IR/DR
ITR
CAGGS
Gene CDS
IRES
GFP
PGK
Puro
ITR
B
HRasG12V
C
ARHGAP36
D
tARHGAP36

**Figure 3.2. Transformation Of NIH3T3 Cells Is Enhanced By *tARHGAP36* Expression**

(A) Representative images of colonies grown in soft agar for *HRasG12V*, *ARHGAP36* and *tARHGAP36* control (top) and experimental (bottom) NIH3T3 clones. Images generated with ImageJ software to remove background (B) Quantification of colonies derived from respective control (DsRed) and experimental (GFP) clones expressing *HRasG12V*, *ARHGAP36* or *tARHGAP36*. Graphs represent data from 2 separate experiments. Error bars are standard deviation values. ***$p<0.001$.

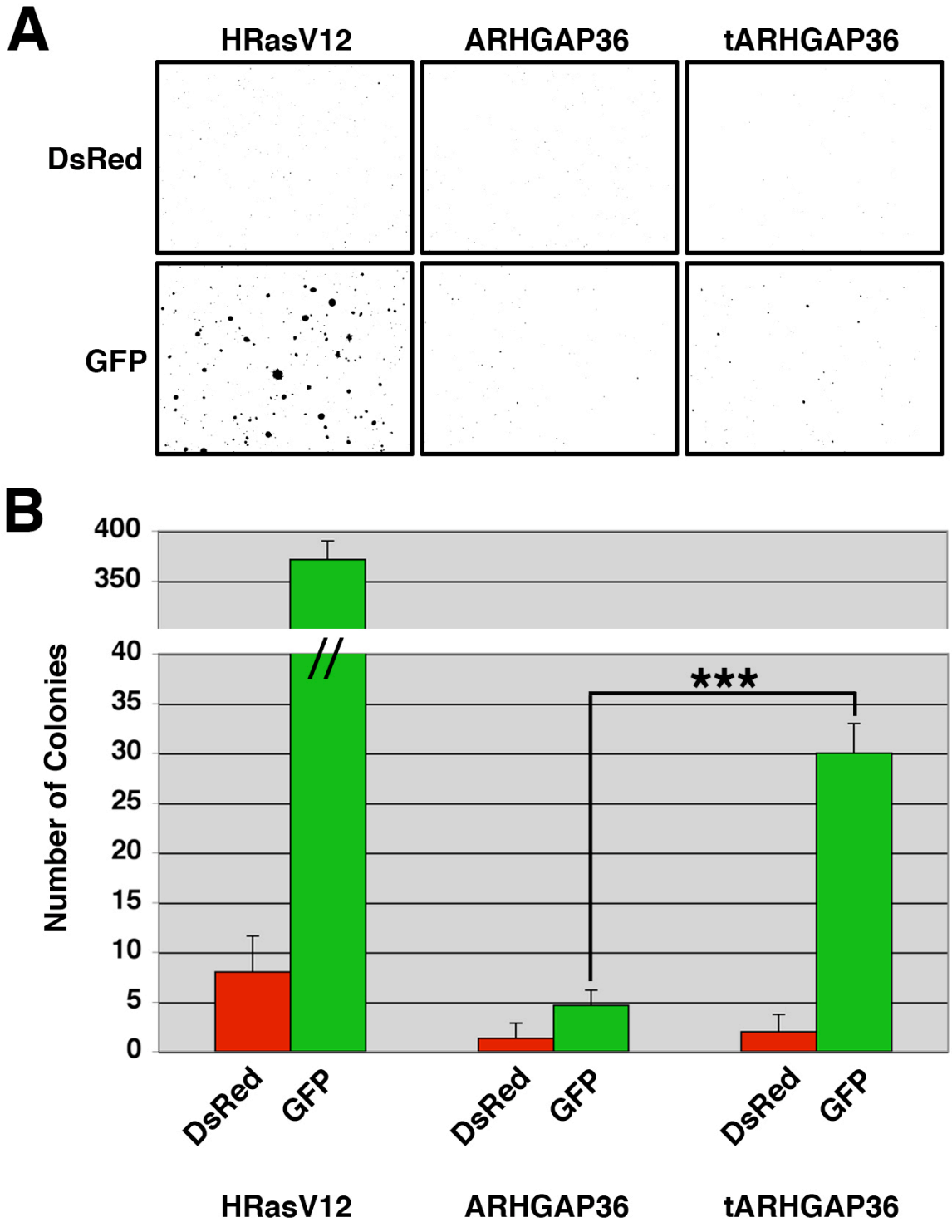
A
HRasV12
ARHGAP36
tARHGAP36
DsRed
GFP
B
400
350
40
35
30
25
20
15
10
5
0
Number of Colonies
***
DsRed
GFP
DsRed
GFP
DsRed
GFP
HRasV12
ARHGAP36
tARHGAP36

**Figure 3.3. Strategy For *in vivo* Delivery Of SB Transposons To Model Medulloblastoma Development**

(A) Scheme for PEI complexing individual transposons expressing different transgenes to inject into the cerebellum of 1-day old mice. *SB100* is transiently expressed from a phophoglycerate kinase (PGK) promoter to facilitate stable genome integration of all transposons including LUC transposon regulated by the CAGGs promoter. Transient LUC expression can be detected by live-animal bioluminescent imaging 24 hours after injection to verify successful injection of the PEI/DNA complexes. (Schematic modified from Wiesner and Decker et al., 2009). (B) Table of experimental groups describing combinations of transposon vectors injected, quantity ratio of vector combinations, total quantity and volume of DNA vectors, and total number of mice injected.

**A**

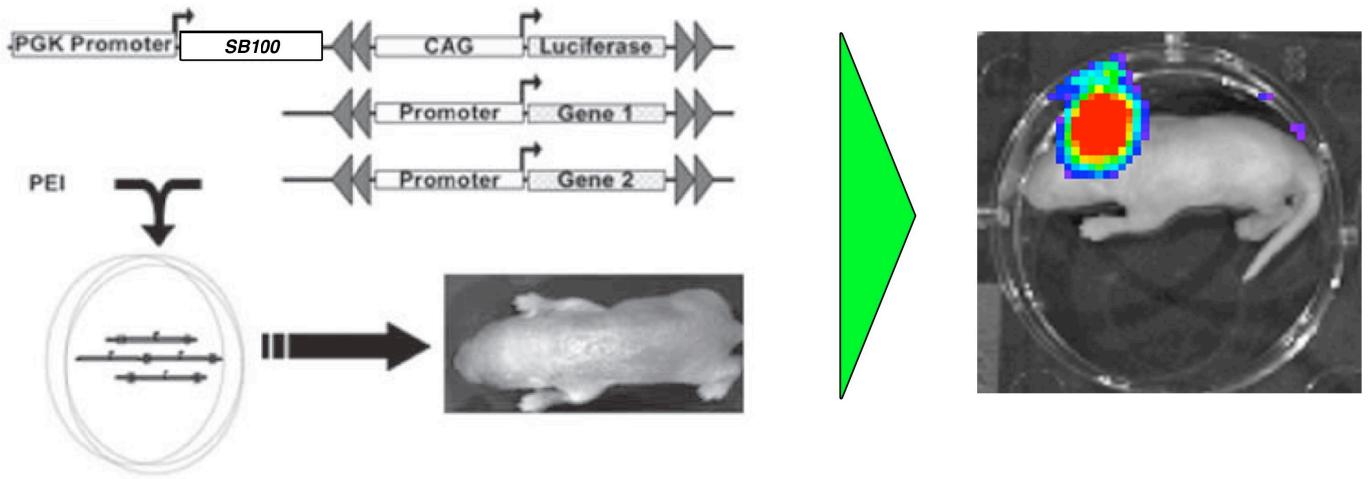


**B**

| Experimental Group | Vector 1 | Vector 2 | Vector 3 | Vector 4 | Ratio | Total DNA (µg) | Volume (µL) | Mice Injected (n) |
|---|---|---|---|---|---|---|---|---|
| LgTAg | pT2/C-*Luc*/PGK-*SB100* | pT/CMV-*SV40-LgT* | pT2/CAGGS-Empty | - | 1 to 1 to 1 | 1 | 2 | 9 |
| LgTAg + myrAKT | pT2/C-*Luc*/PGK-*SB100* | pT/CMV-*SV40-LgT* | pKT2/CLP-*myrAKT* | - | 1 to 1 to 1 | 1 | 2 | 30 |
| LgTAg + ARHGAP36 | pT2/C-*Luc*/PGK-*SB100* | pT/CMV-*SV40-LgT* | pT3.5-CAGGS-*ARHGAP36* | - | 1 to 1 to 1 | 1 | 2 | 10 |
| myrAKT + ARHGAP36 | pT2/C-*Luc*/PGK-*SB100* | pKT2/CLP-*myrAKT* | pT3.5-CAGGS-*ARHGAP36* | - | 1 to 1 to 1 | 1 | 2 | 4 |
| LgTAg + myrAKT + ARHGAP36 | pT2/C-*Luc*/PGK-*SB100* | pT/CMV-*SV40-LgT* | pKT2/CLP-*myrAKT* | pT3.5-CAGGS-*ARHGAP36* | 1 to 1 to 1 to 1 | 1 | 2 | 32 |
| LgTAg + tARHGAP36 | pT2/C-*Luc*/PGK-*SB100* | pT/CMV-*SV40-LgT* | pT3.5-CAGGS-*tARHGAP36* | - | 1 to 1 to 1 | 1 | 2 | 25 |
| myrAKT + tARHGAP36 | pT2/C-*Luc*/PGK-*SB100* | pKT2/CLP-*myrAKT* | pT3.5-CAGGS-*tARHGAP36* | - | 1 to 1 to 1 | 1 | 2 | 19 |
| LgTAg + myrAKT + tARHGAP36 | pT2/C-*Luc*/PGK-*SB100* | pT/CMV-*SV40-LgT* | pKT2/CLP-*myrAKT* | pT3.5-CAGGS-*tARHGAP36* | 1 to 1 to 1 to 1 | 1 | 2 | 14 |

**Figure 3.4. SB-Mediated Oncogene Delivery Can Induce Spontaneous Medulloblastoma In Mice**

(A) Luciferase expression detected by bioluminescent imaging indicating tumor presence. (B-C) H and E staining. (B) Sagital section of representative MB located in the fourth ventricle (arrow). (C) High power magnification of tumor in (B) depicting small, round tumor cells, rosette formation (arrows) and mitotic nuclei (arrowheads). (D-F) Immunohistochemistry illustrating positive staining for (D) LgTAg, (E) p-Akt(S473), (F) ARHGAP36. (G) MB latency among experimental groups. Scale bars = 50μm.

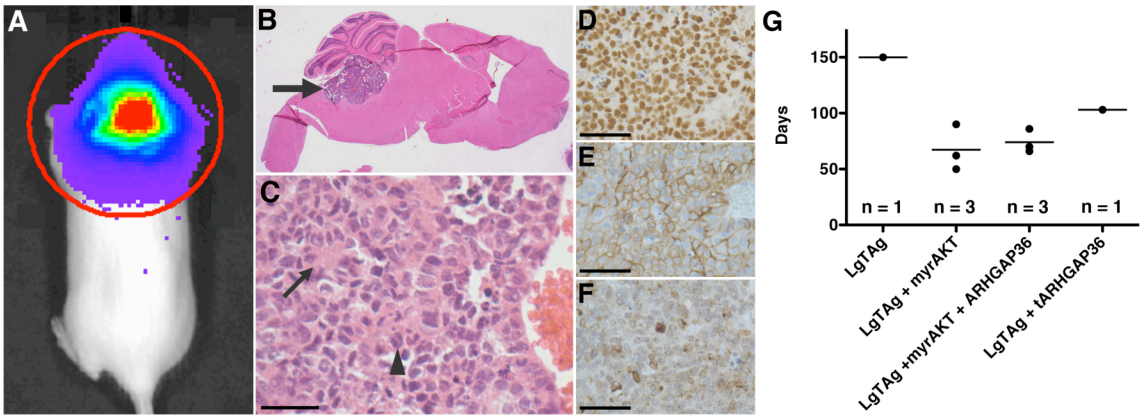
A
B
C
D
E
F
G
Days
150
100
50
0
n = 1
n = 3
n = 3
n = 1
LgTAg
LgTAg + myrAKT
LgTAg +myrAKT + ARHGAP36
LgTAg + tARHGAP36

# Chapter 4

## Conclusion and Summary

Primitive neuroectodermal tumors are malignant pediatric brain tumors that include MB and sPNET subtypes. The World Health Organization's 2007 edition for classification of central nervous system tumors defines MB and sPNET as distinct embryonal grade IV malignancies with similar undifferentiated morphologies (Louis et al., 2007). Histological analysis of these tumor types demonstrate common phenotypes of small round cells with high nucleus-to-cytoplasm ratio, and frequently observed Homer-Wright rosettes (Inda et al., 2006). Regardless of their histological similarities, patients with sPNET suffer a poorer outcome compared to MB patients even after identical therapy (Reddy et al., 2000). Part of this discrepancy can be explained by genetic differences between the two tumor types. Multiple studies over the past ten years have helped to identify distinct genetic defects stemming from genomic deletion or amplification (Burnett et al., 1997; Inda et al., 2005; Li et al. 2009; Northcott et al., 2009; Pfister et al., 2007), altered gene expression at the RNA (Cho et al., 2010; Kool et al., 2008; Northcott et al., 2011; Pomeroy et al., 2002; Thompson et al., 2006) and epigenetic levels (Inda et al., 2006; Kongkham et al., 2008). The culmination of this work has demonstrated not only molecular difference between MB and sPNET but also show molecular stratification amongst MB and sPNET themselves through gene expression or biomarker analysis that can help determine patient outcome. Additional factors that render differential tumor response include age and sex of the patient. In total, there is a lack of complete understanding of their genetic basis as yet unknown specific genetic defects may elicit clinical ramifications.

Current efforts to define the genetic heterogeneity of MB have achieved the identification of distinct molecular subgroups including those driven by SHH or WNT signaling. This has lead to testing and use of targeted therapy against the SHH pathway with a SMO antagonist (GDC-0449) in an adult patient with recurrent, metastatic MB containing somatic *PTCH1* mutation (Rudin et al., 2009). In this case the patient benefited reduced tumor burden over a 3-month period, however suffered rapid, fatal recurrence thereafter due in part to an acquired SMO mutation conferring resistance to GDC-0449 binding and SHH pathway suppression. Despite an unsuccessful result, this case illustrates the possibility of molecularly targeted MB therapy and reinforces the need for combinatorial therapies and to also understand the biological mechanisms of less understood yet more dangerous tumor subgroups. Similar action is desperately needed for sPNET as these tumors impart a dismal prognosis in a majority of patients.

We have developed here a new tissue-specific forward genetics SB transposon-mediated mouse model for tagging candidate cancer genes that drive MB and sPNET development. By virtue of insertional mutagenesis in neural and glial precursor cells using the *Nestin*-Cre transgene to activate transposition, this model has biological relevance for the MB and sPNET. We show positive SB expression in MB and sPNET prospective cells of origin including fourth ventricle stem cells and granule cells of the developing cerebellum, and subventricular stem cells of the neocortex, respectively. These experiments recapitulate histological and molecular anomalies observed in human MB and sPNET and also directly implicate genes and pathways with previously unspecified roles in PNET formation.

Notably, multiple regulators of Ras signaling were altered in sPNET corresponding with pathway activation. Although not previously directly implicated in human sPNET, other studies have shown activation of KRAS (Brüstle et al., 1992; Hader et al., 2003) or inactivation of Ras-pathway regulators (Inda and Castresana, 2007; Pfister et al., 2007) in these tumors. As we observed, P53 status and subsequent genome stability may also provide an important combinational defect in the etiology of these tumors. In addition, *ARHGAP36* was identified as a strong candidate oncogene in non-SHH/WNT driven human MB and implicates altered RhoGTPase signaling or other unknown ARHGAP36-mediated functions in the development of these molecularly poorly defined tumors. Of translational significance for sPNET and MB, predominant RAS signaling in sPNET indicates a potential therapeutic target enhancing current strategies, and ARHGAP36 itself also poses as a potential molecule for targeted therapy in MB patient subsets with confirmed elevated expression.

As *Arhgap36* was identified as a completely novel gene found to be a significant candidate oncogene for poorly defined MB, we sought to characterize its abilities for cellular transformation *in vitro*. We found that the human *ARHGAP36* isoform mimicking the transposon-mediated *Arhgap36* transcript identified in the SB-mediated mouse MB was capable to induce NIH3T3 cell transformation. These experiments provide insight into potential tumorigenic aspects of the endogenous ARHGAP36 sequence not easily identifiable by other methods. The requirement of additional sequence elements such as endogenous nuclear localization sequence and GAP domain important for correct ARHGAP36 subcellular localization and subsequent function will

be tested. Further delineation of ARHGAP36 mechanism of action will include assessment of how altered expression effects phenotype of human MB cell lines Daoy, Med8a and ONS76 and RhoGTPase signaling by measuring GTP-bound forms of potential RhoGTPase targets RhoA, Rac1 and Cdc42 in these and untransformed NIH3T3 cells. We have engineered human MB cell lines to overexpress the different ARHGAP36 isoforms for this purpose, and methods are also being developed to directly disrupt ARHGAP36 at the genomic DNA level. Furthermore, It will also be important to investigate how manipulated ARHGAP36 expression interacts with simultaneously reduced *Pten* or *p53* expression based on data from Chapter 2. A transposon overexpression construct has been designed for stable genomic integration and simultaneous long-term expression of *ARHGAP36* and the *myrAKT* described in Chapter 3. This reagent will be transfected into untransformed NIH3T3 and neural stem cells to determine how different ARHGAP36 isoforms interact with elevated AKT signaling. Others have shown that a different RhoGAP, *ARHGAP32*, does not require PI3K signaling to induce RAS- ERK1/2-mediated NIH3T3 cell transformation (Shang et al., 2007). Interestingly, ARHGAP32 was shown to induce RAS-ERK1/2-mediated NIH3T3 cell transformation through SH3 domain interaction and sequestration of the RAS suppressor p120RasGAP (Shang et al., 2007). Indeed, ARHGAP36 may contribute to RAS pathway activation by yet unknown mechanisms. RAS/MAPK pathway activation has been reported in human MB associated with increased metastasis (MacDonald et al., 2001). Similar experiments will be explored in the context ARHGAP36 overexpression. Manipulation of *p53* will be conducted by generating a transposon expression vector

carrying the $p53^{R270H}$ dominant negative CDS identical to that used in the SB insertional mutagenesis screen from Chapter 2 (Figure 2.2). This will facilitate experiments designed to determine how *ARHGAP36* isoforms cooperate with altered *p53* function for cellular transformation *in vitro*.

We have developed a new *in vivo* mouse model of MB development by adjusting transposon-mediated delivery used to generate spontaneous glioma (Wiesner and Decker et al., 2009) for oncogenes and cell types important for proper cerebellum development. These experiments implicate a functional role for *ARHGAP36* in medulloblastomagenesis, especially in the context of *LgTAg* expression demonstrating an important interaction between *ARHGAP36* and *p53* during postnatal cerebellum development and recapitulating non-Shh derived MB. Additional testing with the $p53^{R270H}$ dominant negative CDS will help decipher this interaction. Endogenous nuclear expression in a subset of primary germinal zone-derived cells indicates an important role for ARHGAP36 during normal cerebellum development and potentially subsequent adult cerebellum homeostasis. Notably, we observed cytoplasmic/membraneous ARHGAP36 expression in the SB-insertional mutagenesis-derived MB and the transposon-mediated delivery MB model suggesting cellular localization is required for ARHGAP36 oncogenic potential in part controlled by the N-terminal sequence of the endogenous protein. This model will also serve as a viable method for testing other candidate MB genes identified from the SB-insertional mutagenesis screen, especially those not previously implicated in MB development. In addition to localized delivery of ARHGAP36 overexpression to the neonatal cerebellum, we are engineering a transgenic

mouse designed to express truncated ARHGAP36 in the presence of Cre recombinase. These mice will be crossed with different transgenic mice expressing Cre in alternate cells of origin for MB including the primary germinal zone neural stem cells (*GFAP*-Cre) and GNPC derived from the rhombic lip (*Math1*-Cre) and further combined with $Pten^{flox/+}$ or $p53^{lslR270H}$ to determine oncogenic interaction and help recapitulate poorly understood MB molecular subgroups.

Our SB-mediated insertional mutagenesis mouse model also for the first time implicates uncontrolled RAS-signaling combined with defective *p53* expression as a driving event in sPNET formation. It is unknown whether the specific genes are themselves important or if the effect of Ras pathway signaling disregulation is the downstream overriding force. Also, compared to other mouse models of brain tumors incorporating Ras overexpression and deficient *p53*, the SB mutagenesis mice demonstrate specific DNA binding dysfunction of p53 is important for the development of sPNET via the dominant negative $p53^{lsl\text{-}R270H}$ allele used as a predisposing background here. These data also suggest the early *Nestin*-Cre-mediated activation of mutagenesis in multipotent precursors during early neurogenesis and thereafter important for sPNET formation versus gliomagenesis. Direct comparison to genetic anomalies found in human sPNET will help to uncover the scope of disregulated RAS activation and its role in tumor formation.

In summary, this work utilized *Sleeping Beauty* transposon insertional mutagenesis to model histological and molecular aspects of MB and sPNET development, and has revealed biologically relevant candidate molecular events in the context of these tumors

in both mouse and man. Elevated ARHGAP36 is a newly discovered genetic event important for characterizing poorly understood MB molecular subgroups. Genes with functional convergence on Ras pathway control were identified and implicated to be important for sPNET formation. Together, these data provide specific targets to potentially combine with current treatment strategies and enhance outcome for MB and sPNET patients.

## REFERENCES


2008. Comprehensive genomic characterization defines human glioblastoma genes and core pathways. *Nature* **455**: 1061-1068.

Adamson DC, Shi Q, Wortham M, Northcott PA, Di C, Duncan CG, Li J, McLendon RE, Bigner DD, Taylor MD et al. 2010. OTX2 is critical for the maintenance and progression of Shh-independent medulloblastomas. *Cancer Res* **70**: 181-191.

Attardi LD, Jacks T. 1999. The role of p53 in tumour suppression: lessons from mouse models. *Cell Mol Life Sci* **55**: 48-63.

Bender AM, Collier LS, Rodriguez FJ, Tieu C, Larson JD, Halder C, Mahlum E, Kollmeyer TM, Akagi K, Sarkar G et al. 2010. Sleeping beauty-mediated somatic mutagenesis implicates CSF1 in the formation of high-grade astrocytomas. *Cancer Res* **70**: 3557-3565.

Bhatia B, Malik A, Fernandez LA, Kenney AM. 2010. p27(Kip1), a double-edged sword in Shh-mediated medulloblastoma: Tumor accelerator and suppressor. *Cell Cycle* **9**: 4307-4314.

Bhoopathi P, Chetty C, Gujrati M, Dinh DH, Rao JS, Lakka S. 2010. Cathepsin B facilitates autophagy-mediated apoptosis in SPARC overexpressed primitive neuroectodermal tumor cells. *Cell Death Differ* **17**: 1529-1539.

Bhoopathi P, Gondi CS, Gujrati M, Dinh DH, Lakka SS. 2011. SPARC mediates Src-induced disruption of actin cytoskeleton via inactivation of small GTPases Rho-Rac-Cdc42. *Cell Signal* **23**: 1978-1987.

Binning MJ, Niazi T, Pedone CA, Lal B, Eberhart CG, Kim KJ, Laterra J, Fults DW. 2008. Hepatocyte growth factor and sonic Hedgehog expression in cerebellar neural progenitor cells costimulate medulloblastoma initiation and growth. *Cancer Res* **68**: 7838-7845.

Bossolasco M, Lebel M, Lemieux N, Mes-Masson AM. 1999. The human TDE gene homologue: localization to 20q13.1-13.3 and variable expression in human tumor cell lines and tissue. *Mol Carcinog* **26**: 189-200.

Brandes AA, Franceschi E, Tosoni A, Reni M, Gatta G, Vecht C, Kortmann RD. 2009. Adult neuroectodermal tumors of posterior fossa (medulloblastoma) and of supratentorial sites (stPNET). *Crit Rev Oncol Hematol* **71**: 165-179.

Browd SR, Kenney AM, Gottfried ON, Yoon JW, Walterhouse D, Pedone CA, Fults DW. 2006. N-myc can substitute for insulin-like growth factor signaling in a

mouse model of sonic hedgehog-induced medulloblastoma. *Cancer Res* **66**: 2666-2672.

Brustle O, Ohgaki H, Schmitt HP, Walter GF, Ostertag H, Kleihues P. 1992. Primitive neuroectodermal tumors after prophylactic central nervous system irradiation in children. Association with an activated K-ras gene. *Cancer* **69**: 2385-2392.

Burnett ME, White EC, Sih S, von Haken MS, Cogen PH. 1997. Chromosome arm 17p deletion analysis reveals molecular genetic heterogeneity in supratentorial and infratentorial primitive neuroectodermal tumors of the central nervous system. *Cancer Genet Cytogenet* **97**: 25-31.

Calderilla-Barbosa L, Ortega A, Cisneros B. 2006. Phosphorylation of dystrophin Dp71d by Ca2+/calmodulin-dependent protein kinase II modulates the Dp71d nuclear localization in PC12 cells. *J Neurochem* **98**: 713-722.

Carlson CM, Dupuy AJ, Fritz S, Roberg-Perez KJ, Fletcher CF, Largaespada DA. 2003. Transposon mutagenesis of the mouse germline. *Genetics* **165**: 243-256.

Carlson CM, Frandsen JL, Kirchhof N, McIvor RS, Largaespada DA. 2005. Somatic integration of an oncogene-harboring Sleeping Beauty transposon models liver tumor development in the mouse. *Proc Natl Acad Sci U S A* **102**: 17059-17064.

Carlson CM, Largaespada DA. 2005. Insertional mutagenesis in mice: new perspectives and tools. *Nat Rev Genet* **6**: 568-580.

Carvalho CM, Lupski JR. 2008. Copy number variation at the breakpoint region of isochromosome 17q. *Genome Res* **18**: 1724-1732.

Castellino RC, Barwick BG, Schniederjan M, Buss MC, Becher O, Hambardzumyan D, Macdonald TJ, Brat DJ, Durden DL. 2010. Heterozygosity for Pten promotes tumorigenesis in a mouse model of medulloblastoma. *PLoS One* **5**: e10849.

Chen B, Gao Y, Jiang T, Ding J, Zeng Y, Xu R, Jiang X. 2011. Inhibition of tumor cell migration and invasion through knockdown of Rac1 expression in medulloblastoma cells. *Cell Mol Neurobiol* **31**: 251-257.

Cho YJ, Tsherniak A, Tamayo P, Santagata S, Ligon A, Greulich H, Berhoukim R, Amani V, Goumnerova L, Eberhart CG et al. 2011. Integrative genomic analysis of medulloblastoma identifies a molecular subgroup that drives poor clinical outcome. *J Clin Oncol* **29**: 1424-1430.

Collier LS, Carlson CM, Ravimohan S, Dupuy AJ, Largaespada DA. 2005. Cancer gene discovery in solid tumours using transposon-based somatic mutagenesis in the mouse. *Nature* **436**: 272-276.

Crawford JR, MacDonald TJ, Packer RJ. 2007. Medulloblastoma in childhood: new biological advances. *Lancet Neurol* **6**: 1073-1085.

De Vos M, Hayward BE, Picton S, Sheridan E, Bonthron DT. 2004. Novel PMS2 pseudogenes can conceal recessive mutations causing a distinctive childhood cancer syndrome. *Am J Hum Genet* **74**: 954-964.

de Wit NJ, Burtscher HJ, Weidle UH, Ruiter DJ, van Muijen GN. 2002. Differentially expressed genes identified in human melanoma cell lines with different metastatic behaviour using high density oligonucleotide arrays. *Melanoma Res* **12**: 57-69.

Ding L, Getz G, Wheeler DA, Mardis ER, McLellan MD, Cibulskis K, Sougnez C, Greulich H, Muzny DM, Morgan MB et al. 2008. Somatic mutations affect key pathways in lung adenocarcinoma. *Nature* **455**: 1069-1075.

Dubuc AM, Northcott PA, Mack S, Witt H, Pfister S, Taylor MD. 2010. The genetics of pediatric brain tumors. *Curr Neurol Neurosci Rep* **10**: 215-223.

Dupuy AJ. 2010. Transposon-based screens for cancer gene discovery in mouse models. *Semin Cancer Biol* **20**: 261-268.

Dupuy AJ, Akagi K, Largaespada DA, Copeland NG, Jenkins NA. 2005. Mammalian mutagenesis using a highly mobile somatic Sleeping Beauty transposon system. *Nature* **436**: 221-226.

Dupuy AJ, Clark K, Carlson CM, Fritz S, Davidson AE, Markley KM, Finley K, Fletcher CF, Ekker SC, Hackett PB et al. 2002. Mammalian germ-line transgenesis by transposition. *Proc Natl Acad Sci U S A* **99**: 4495-4499.

Eberhart CG. 2007. In search of the medulloblast: neural stem cells and embryonal brain tumors. *Neurosurg Clin N Am* **18**: 59-69, viii-ix.

Eberhart CG. 2011. Molecular diagnostics in embryonal brain tumors. *Brain Pathol* **21**: 96-104.

Eberhart CG, Chaudhry A, Daniel RW, Khaki L, Shah KV, Gravitt PE. 2005. Increased p53 immunopositivity in anaplastic medulloblastoma and supratentorial PNET is not caused by JC virus. *BMC Cancer* **5**: 19.

Eberhart CG, Kepner JL, Goldthwaite PT, Kun LE, Duffner PK, Friedman HS, Strother DR, Burger PC. 2002. Histopathologic grading of medulloblastomas: a Pediatric Oncology Group study. *Cancer* **94**: 552-560.

Ebinger M, Senf L, Wachowski O, Scheurlen W. 2004. Promoter methylation pattern of caspase-8, P16INK4A, MGMT, TIMP-3, and E-cadherin in medulloblastoma. *Pathol Oncol Res* **10**: 17-21.

Fimia GM, Stoykova A, Romagnoli A, Giunta L, Di Bartolomeo S, Nardacci R, Corazzari M, Fuoco C, Ucar A, Schwartz P et al. 2007. Ambra1 regulates autophagy and development of the nervous system. *Nature* **447**: 1121-1125.

Fraser MM, Zhu X, Kwon CH, Uhlmann EJ, Gutmann DH, Baker SJ. 2004. Pten loss causes hypertrophy and increased proliferation of astrocytes in vivo. *Cancer Res* **64**: 7773-7779.

Frese KK, Tuveson DA. 2007. Maximizing mouse cancer models. *Nat Rev Cancer* **7**: 645-658.

Fruhwald MC, O'Dorisio MS, Dai Z, Tanner SM, Balster DA, Gao X, Wright FA, Plass C. 2001. Aberrant promoter methylation of previously unidentified target genes is a common abnormality in medulloblastomas--implications for tumor biology and potential clinical utility. *Oncogene* **20**: 5033-5042.

Fults DW. 2005. Modeling medulloblastoma with genetically engineered mice. *Neurosurg Focus* **19**: E7.

Gessi M, Setty P, Bisceglia M, zur Muehlen A, Lauriola L, Waha A, Giangaspero F, Pietsch T. 2011. Supratentorial primitive neuroectodermal tumors of the central nervous system in adults: molecular and histopathologic analysis of 12 cases. *Am J Surg Pathol* **35**: 573-582.

Geurts AM, Collier LS, Geurts JL, Oseth LL, Bell ML, Mu D, Lucito R, Godbout SA, Green LE, Lowe SW et al. 2006. Gene mutations and genomic rearrangements in the mouse as a result of transposon mobilization from chromosomal concatemers. *PLoS Genet* **2**: e156.

Gibson P, Tong Y, Robinson G, Thompson MC, Currle DS, Eden C, Kranenburg TA, Hogg T, Poppleton H, Martin J et al. 2010. Subtypes of medulloblastoma have distinct developmental origins. *Nature* **468**: 1095-1099.

Gilbertson RJ, Ellison DW. 2008. The origins of medulloblastoma subtypes. *Annu Rev Pathol* **3**: 341-365.

Goodrich LV, Milenkovic L, Higgins KM, Scott MP. 1997. Altered neural cell fates and medulloblastoma in mouse patched mutants. *Science* **277**: 1109-1113.

Gorlin RJ. 1987. Nevoid basal-cell carcinoma syndrome. *Medicine (Baltimore)* **66**: 98-113.

Grabundzija I, Izsvak Z, Ivics Z. 2011. Insertional engineering of chromosomes with Sleeping Beauty transposition: an overview. *Methods Mol Biol* **738**: 69-85.

Guan KL, Rao Y. 2003. Signalling mechanisms mediating neuronal responses to guidance cues. *Nat Rev Neurosci* **4**: 941-956.

Hader WJ, Drovini-Zis K, Maguire JA. 2003. Primitive neuroectodermal tumors in the central nervous system following cranial irradiation: a report of four cases. *Cancer* **97**: 1072-1076.

Hambardzumyan D, Becher OJ, Rosenblum MK, Pandolfi PP, Manova-Todorova K, Holland EC. 2008. PI3K pathway regulates survival of cancer stem cells residing in the perivascular niche following radiation in medulloblastoma in vivo. *Genes Dev* **22**: 436-448.

Hamilton SR, Liu B, Parsons RE, Papadopoulos N, Jen J, Powell SM, Krush AJ, Berk T, Cohen Z, Tetu B et al. 1995. The molecular basis of Turcot's syndrome. *N Engl J Med* **332**: 839-847.

Hartmann W, Digon-Sontgerath B, Koch A, Waha A, Endl E, Dani I, Denkhaus D, Goodyer CG, Sorensen N, Wiestler OD et al. 2006. Phosphatidylinositol 3'-kinase/AKT signaling is activated in medulloblastoma cell proliferation and is associated with reduced expression of PTEN. *Clin Cancer Res* **12**: 3019-3027.

Hayden JT, Fruhwald MC, Hasselblatt M, Ellison DW, Bailey S, Clifford SC. 2009. Frequent IDH1 mutations in supratentorial primitive neuroectodermal tumors (sPNET) of adults but not children. *Cell Cycle* **8**: 1806-1807.

Holland EC, Hively WP, DePinho RA, Varmus HE. 1998. A constitutively active epidermal growth factor receptor cooperates with disruption of G1 cell-cycle arrest pathways to induce glioma-like lesions in mice. *Genes Dev* **12**: 3675-3685.

Holland EC, Varmus HE. 1998. Basic fibroblast growth factor induces cell migration and proliferation after glia-specific gene transfer in mice. *Proc Natl Acad Sci U S A* **95**: 1218-1223.

Huang H, Reis R, Yonekawa Y, Lopes JM, Kleihues P, Ohgaki H. 1999. Identification in human brain tumors of DNA sequences specific for SV40 large T antigen. *Brain Pathol* **9**: 33-42.

Hundley JE, Koester SK, Troyer DA, Hilsenbeck SG, Subler MA, Windle JJ. 1997. Increased tumor proliferation and genomic instability without decreased apoptosis in MMTV-ras mice deficient in p53. *Mol Cell Biol* **17**: 723-731.

Inda MM, Castresana JS. 2007. RASSF1A promoter is highly methylated in primitive neuroectodermal tumors of the central nervous system. *Neuropathology* **27**: 341-346.

Inda MM, Munoz J, Coullin P, Fauvet D, Danglot G, Tunon T, Bernheim A, Castresana JS. 2006. High promoter hypermethylation frequency of p14/ARF in supratentorial PNET but not in medulloblastoma. *Histopathology* **48**: 579-587.

Inda MM, Perot C, Guillaud-Bataille M, Danglot G, Rey JA, Bello MJ, Fan X, Eberhart C, Zazpe I, Portillo E et al. 2005. Genetic heterogeneity in supratentorial and infratentorial primitive neuroectodermal tumours of the central nervous system. *Histopathology* **47**: 631-637.

Ivics Z, Hackett PB, Plasterk RH, Izsvak Z. 1997. Molecular reconstruction of Sleeping Beauty, a Tc1-like transposon from fish, and its transposition in human cells. *Cell* **91**: 501-510.

Ivics Z, Li MA, Mates L, Boeke JD, Nagy A, Bradley A, Izsvak Z. 2009. Transposon-mediated genome manipulation in vertebrates. *Nat Methods* **6**: 415-422.

Jacques TS, Swales A, Brzozowski MJ, Henriquez NV, Linehan JM, Mirzadeh Z, C OM, Naumann H, Alvarez-Buylla A, Brandner S. 2010. Combinations of genetic mutations in the adult neural stem cell compartment determine brain tumour phenotypes. *EMBO J* **29**: 222-235.

Jaffe AB, Hall A. 2002. Rho GTPases in transformation and metastasis. *Adv Cancer Res* **84**: 57-80.

Johansson FK, Brodd J, Eklof C, Ferletta M, Hesselager G, Tiger CF, Uhrbom L, Westermark B. 2004. Identification of candidate cancer-causing genes in mouse brain tumors by retroviral tagging. *Proc Natl Acad Sci U S A* **101**: 11334-11337.

Karajannis M, Allen JC, Newcomb EW. 2008. Treatment of pediatric brain tumors. *J Cell Physiol* **217**: 584-589.

Keng VW, Villanueva A, Chiang DY, Dupuy AJ, Ryan BJ, Matise I, Silverstein KA, Sarver A, Starr TK, Akagi K et al. 2009. A conditional transposon-based insertional mutagenesis screen for genes associated with mouse hepatocellular carcinoma. *Nat Biotechnol* **27**: 264-274.

Kessler JD, Hasegawa H, Brun SN, Emmenegger BA, Yang ZJ, Dutton JW, Wang F, Wechsler-Reya RJ. 2009. N-myc alters the fate of preneoplastic cells in a mouse model of medulloblastoma. *Genes Dev* **23**: 157-170.

Kongkham PN, Northcott PA, Ra YS, Nakahara Y, Mainprize TG, Croul SE, Smith CA, Taylor MD, Rutka JT. 2008. An epigenetic genome-wide screen identifies SPINT2 as a novel tumor suppressor gene in pediatric medulloblastoma. *Cancer Res* **68**: 9945-9953.

Kool J, Berns A. 2009. High-throughput insertional mutagenesis screens in mice to identify oncogenic networks. *Nat Rev Cancer* **9**: 389-399.

Kool M, Koster J, Bunt J, Hasselt NE, Lakeman A, van Sluis P, Troost D, Meeteren NS, Caron HN, Cloos J et al. 2008. Integrated genomics identifies five medulloblastoma subtypes with distinct genetic profiles, pathway signatures and clinicopathological features. *PLoS One* **3**: e3088.

Kraus JA, Felsberg J, Tonn JC, Reifenberger G, Pietsch T. 2002. Molecular genetic analysis of the TP53, PTEN, CDKN2A, EGFR, CDK4 and MDM2 tumour-associated genes in supratentorial primitive neuroectodermal tumours and glioblastomas of childhood. *Neuropathol Appl Neurobiol* **28**: 325-333.

Kwon CH, Zhao D, Chen J, Alcantara S, Li Y, Burns DK, Mason RP, Lee EY, Wu H, Parada LF. 2008. Pten haploinsufficiency accelerates formation of high-grade astrocytomas. *Cancer Res* **68**: 3286-3294.

Kwon CH, Zhu X, Zhang J, Knoop LL, Tharp R, Smeyne RJ, Eberhart CG, Burger PC, Baker SJ. 2001. Pten regulates neuronal soma size: a mouse model of Lhermitte-Duclos disease. *Nat Genet* **29**: 404-411.

Larrea MD, Wander SA, Slingerland JM. 2009. p27 as Jekyll and Hyde: regulation of cell cycle and cell motility. *Cell Cycle* **8**: 3455-3461.

Lee A, Kessler JD, Read TA, Kaiser C, Corbeil D, Huttner WB, Johnson JE, Wechsler-Reya RJ. 2005. Isolation of neural stem cells from the postnatal cerebellum. *Nat Neurosci* **8**: 723-729.

Lee Y, Kawagoe R, Sasai K, Li Y, Russell HR, Curran T, McKinnon PJ. 2007. Loss of suppressor-of-fused function promotes tumorigenesis. *Oncogene* **26**: 6442-6447.

Li M, Lee KF, Lu Y, Clarke I, Shih D, Eberhart C, Collins VP, Van Meter T, Picard D, Zhou L et al. 2009. Frequent amplification of a chr19q13.41 microRNA polycistron in aggressive primitive neuroectodermal brain tumors. *Cancer Cell* **16**: 533-546.

Li MH, Bouffet E, Hawkins CE, Squire JA, Huang A. 2005a. Molecular genetics of supratentorial primitive neuroectodermal tumors and pineoblastoma. *Neurosurg Focus* **19**: E3.

Li R, Zhang B, Zheng Y. 1997. Structural determinants required for the interaction between Rho GTPase and the GTPase-activating domain of p190. *J Biol Chem* **272**: 32830-32835.

Li Z, Dong X, Wang Z, Liu W, Deng N, Ding Y, Tang L, Hla T, Zeng R, Li L et al. 2005b. Regulation of PTEN by Rho small GTPases. *Nat Cell Biol* **7**: 399-404.

Louis DN, Ohgaki H, Wiestler OD, Cavenee WK, Burger PC, Jouvet A, Scheithauer BW, Kleihues P. 2007. The 2007 WHO classification of tumours of the central nervous system. *Acta Neuropathol* **114**: 97-109.

Lu Q, Longo FM, Zhou H, Massa SM, Chen YH. 2009. Signaling through Rho GTPase pathway as viable drug target. *Curr Med Chem* **16**: 1355-1365.

Luo L. 2000. Rho GTPases in neuronal morphogenesis. *Nat Rev Neurosci* **1**: 173-180.

Luo L, Hensch TK, Ackerman L, Barbel S, Jan LY, Jan YN. 1996. Differential effects of the Rac GTPase on Purkinje cell axons and dendritic trunks and spines. *Nature* **379**: 837-840.

MacDonald TJ, Brown KM, LaFleur B, Peterson K, Lawlor C, Chen Y, Packer RJ, Cogen P, Stephan DA. 2001. Expression profiling of medulloblastoma: PDGFRA and the RAS/MAPK pathway as therapeutic targets for metastatic disease. *Nat Genet* **29**: 143-152.

Malek R, Matta J, Taylor N, Perry ME, Mendrysa SM. 2011. The p53 inhibitor MDM2 facilitates Sonic Hedgehog-mediated tumorigenesis and influences cerebellar foliation. *PLoS One* **6**: e17884.

Marcus DM, Carpenter JL, O'Brien JM, Kivela T, Brauner E, Tarkkanen A, Virtanen I, Albert DM. 1991. Primitive neuroectodermal tumor of the midbrain in a murine model of retinoblastoma. *Invest Ophthalmol Vis Sci* **32**: 293-301.

Marino S, Krimpenfort P, Leung C, van der Korput HA, Trapman J, Camenisch I, Berns A, Brandner S. 2002. PTEN is essential for cell migration but not for fate

determination and tumourigenesis in the cerebellum. *Development* **129**: 3513-3522.

Marino S, Vooijs M, van Der Gulden H, Jonkers J, Berns A. 2000. Induction of medulloblastomas in p53-null mutant mice by somatic inactivation of Rb in the external granular layer cells of the cerebellum. *Genes Dev* **14**: 994-1004.

Mates L, Chuah MK, Belay E, Jerchow B, Manoj N, Acosta-Sanchez A, Grzela DP, Schmitt A, Becker K, Matrai J et al. 2009. Molecular evolution of a novel hyperactive Sleeping Beauty transposase enables robust stable gene transfer in vertebrates. *Nat Genet* **41**: 753-761.

Meili R, Sasaki AT, Firtel RA. 2005. Rho Rocks PTEN. *Nat Cell Biol* **7**: 334-335.

Mikkers H, Allen J, Knipscheer P, Romeijn L, Hart A, Vink E, Berns A. 2002. High-throughput retroviral tagging to identify components of specific signaling pathways in cancer. *Nat Genet* **32**: 153-159.

Miller FD, Gauthier AS. 2007. Timing is everything: making neurons versus glia in the developing cortex. *Neuron* **54**: 357-369.

Mochizuki H, Nishi T, Bruner JM, Lee PS, Levin VA, Saya H. 1992. Alternative splicing of neurofibromatosis type 1 gene transcript in malignant brain tumors: PCR analysis of frozen-section mRNA. *Mol Carcinog* **6**: 83-87.

Momota H, Shih AH, Edgar MA, Holland EC. 2008. c-Myc and beta-catenin cooperate with loss of p53 to generate multiple members of the primitive neuroectodermal tumor family in mice. *Oncogene* **27**: 4392-4401.

Mori K, Iwao K, Miyoshi Y, Nakagawara A, Kofu K, Akiyama T, Arita N, Hayakawa T, Nakamura Y. 1998. Identification of brain-specific splicing variants of the hDLG1 gene and altered splicing in neuroblastoma cell lines. *J Hum Genet* **43**: 123-127.

Newbold RF, Mokbel K. 2010. Evidence for a tumour suppressor function of SETD2 in human breast cancer: a new hypothesis. *Anticancer Res* **30**: 3309-3311.

Nitz MD, Harding MA, Smith SC, Thomas S, Theodorescu D. 2011. RREB1 transcription factor splice variants in urologic cancer. *Am J Pathol* **179**: 477-486.

Northcott PA, Korshunov A, Witt H, Hielscher T, Eberhart CG, Mack S, Bouffet E, Clifford SC, Hawkins CE, French P et al. 2011. Medulloblastoma comprises four distinct molecular variants. *J Clin Oncol* **29**: 1408-1414.

Northcott PA, Nakahara Y, Wu X, Feuk L, Ellison DW, Croul S, Mack S, Kongkham PN, Peacock J, Dubuc A et al. 2009. Multiple recurrent genetic events converge on control of histone lysine methylation in medulloblastoma. *Nat Genet* **41**: 465-472.

Northcott PA, Rutka JT, Taylor MD. 2010. Genomics of medulloblastoma: from Giemsa-banding to next-generation sequencing in 20 years. *Neurosurg Focus* **28**: E6.

Ohlfest JR, Demorest ZL, Motooka Y, Vengco I, Oh S, Chen E, Scappaticci FA, Saplis RJ, Ekker SC, Low WC et al. 2005. Combinatorial antiangiogenic gene therapy by nonviral gene transfer using the sleeping beauty transposon causes tumor regression and improves survival in mice bearing intracranial human glioblastoma. *Mol Ther* **12**: 778-788.

Okabe M, Ikawa M, Kominami K, Nakanishi T, Nishimune Y. 1997. 'Green mice' as a source of ubiquitous green cells. *FEBS Lett* **407**: 313-319.

Okabe T, Nakamura T, Nishimura YN, Kohu K, Ohwada S, Morishita Y, Akiyama T. 2003. RICS, a novel GTPase-activating protein for Cdc42 and Rac1, is involved in the beta-catenin-N-cadherin and N-methyl-D-aspartate receptor signaling. *J Biol Chem* **278**: 9920-9927.

Olive KP, Tuveson DA, Ruhe ZC, Yin B, Willis NA, Bronson RT, Crowley D, Jacks T. 2004. Mutant p53 gain of function in two mouse models of Li-Fraumeni syndrome. *Cell* **119**: 847-860.

Oliver TG, Read TA, Kessler JD, Mehmeti A, Wells JF, Huynh TT, Lin SM, Wechsler-Reya RJ. 2005. Loss of patched and disruption of granule cell development in a pre-neoplastic stage of medulloblastoma. *Development* **132**: 2425-2439.

Orellana C, Martinez F, Hernandez-Marti M, Castel V, Canete A, Prieto F, Badia L. 1998. A novel TP53 germ-line mutation identified in a girl with a primitive neuroectodermal tumor and her father. *Cancer Genet Cytogenet* **105**: 103-108.

Packer RJ, MacDonald T, Vezina G. 2008. Central nervous system tumors. *Pediatr Clin North Am* **55**: 121-145, xi.

Packer RJ, Vezina G. 2008. Management of and prognosis with medulloblastoma: therapy at a crossroads. *Arch Neurol* **65**: 1419-1424.

Parsons DW, Li M, Zhang X, Jones S, Leary RJ, Lin JC, Boca SM, Carter H, Samayoa J, Bettegowda C et al. 2011. The genetic landscape of the childhood cancer medulloblastoma. *Science* **331**: 435-439.

Pazzaglia S, Tanori M, Mancuso M, Rebessi S, Leonardi S, Di Majo V, Covelli V, Atkinson MJ, Hahn H, Saran A. 2006. Linking DNA damage to medulloblastoma tumorigenesis in patched heterozygous knockout mice. *Oncogene* **25**: 1165-1173.

Pearson AD, Craft AW, Ratcliffe JM, Birch JM, Morris-Jones P, Roberts DF. 1982. Two families with the Li-Fraumeni cancer family syndrome. *J Med Genet* **19**: 362-365.

Perry A, Miller CR, Gujrati M, Scheithauer BW, Zambrano SC, Jost SC, Raghavan R, Qian J, Cochran EJ, Huse JT et al. 2009. Malignant gliomas with primitive neuroectodermal tumor-like components: a clinicopathologic and genetic study of 53 cases. *Brain Pathol* **19**: 81-90.

Pfister S, Remke M, Castoldi M, Bai AH, Muckenthaler MU, Kulozik A, von Deimling A, Pscherer A, Lichter P, Korshunov A. 2009. Novel genomic amplification targeting the microRNA cluster at 19q13.42 in a pediatric embryonal tumor with abundant neuropil and true rosettes. *Acta Neuropathol* **117**: 457-464.

Pfister S, Remke M, Toedt G, Werft W, Benner A, Mendrzyk F, Wittmann A, Devens F, von Hoff K, Rutkowski S et al. 2007. Supratentorial primitive neuroectodermal tumors of the central nervous system frequently harbor deletions of the CDKN2A locus and other genomic aberrations distinct from medulloblastomas. *Genes Chromosomes Cancer* **46**: 839-851.

Pfister SM, Korshunov A, Kool M, Hasselblatt M, Eberhart C, Taylor MD. 2010. Molecular diagnostics of CNS embryonal tumors. *Acta Neuropathol* **120**: 553-566.

Phi JH, Kim JH, Eun KM, Wang KC, Park KH, Choi SA, Kim YY, Park SH, Cho BK, Kim SK. 2010. Upregulation of SOX2, NOTCH1, and ID1 in supratentorial primitive neuroectodermal tumors: a distinct differentiation pattern from that of medulloblastomas. *J Neurosurg Pediatr* **5**: 608-614.

Pomeroy SL, Tamayo P, Gaasenbeek M, Sturla LM, Angelo M, McLaughlin ME, Kim JY, Goumnerova LC, Black PM, Lau C et al. 2002. Prediction of central nervous system embryonal tumour outcome based on gene expression. *Nature* **415**: 436-442.

Prakash SK, Paylor R, Jenna S, Lamarche-Vane N, Armstrong DL, Xu B, Mancini MA, Zoghbi HY. 2000. Functional analysis of ARHGAP6, a novel GTPase-activating protein for RhoA. *Hum Mol Genet* **9**: 477-488.

Qiu RG, Chen J, McCormick F, Symons M. 1995. A role for Rho in Ras transformation. *Proc Natl Acad Sci U S A* **92**: 11781-11785.

Raffel C, McComb JG, Bodner S, Gilles FE. 1989. Benign brain stem lesions in pediatric patients with neurofibromatosis: case reports. *Neurosurgery* **25**: 959-964.

Rahrmann EP, Collier LS, Knutson TP, Doyal ME, Kuslak SL, Green LE, Malinowski RL, Roethe L, Akagi K, Waknitz M et al. 2009. Identification of PDE4D as a proliferation promoting factor in prostate cancer using a Sleeping Beauty transposon-based somatic mutagenesis screen. *Cancer Res* **69**: 4388-4397.

Rao G, Pedone CA, Del Valle L, Reiss K, Holland EC, Fults DW. 2004. Sonic hedgehog and insulin-like growth factor signaling synergize to induce medulloblastoma formation from nestin-expressing neural progenitors in mice. *Oncogene* **23**: 6156-6162.

Rauen KA, Banerjee A, Bishop WR, Lauchle JO, McCormick F, McMahon M, Melese T, Munster PN, Nadaf S, Packer RJ et al. 2011. Costello and cardio-facio-cutaneous syndromes: Moving toward clinical trials in RASopathies. *Am J Med Genet C Semin Med Genet* **157**: 136-146.

Reddy AT, Janss AJ, Phillips PC, Weiss HL, Packer RJ. 2000. Outcome for children with supratentorial primitive neuroectodermal tumors treated with surgery, radiation, and chemotherapy. *Cancer* **88**: 2189-2193.

Reilly KM, Loisel DA, Bronson RT, McLaughlin ME, Jacks T. 2000. Nf1;Trp53 mutant mice develop glioblastoma with evidence of strain-specific effects. *Nat Genet* **26**: 109-113.

Rogers HA, Miller S, Lowe J, Brundler MA, Coyle B, Grundy RG. 2009. An investigation of WNT pathway activation and association with survival in central nervous system primitive neuroectodermal tumours (CNS PNET). *Br J Cancer* **100**: 1292-1302.

Rubin AL, Arnstein P, Rubin H. 1990. Physiological induction and reversal of focus formation and tumorigenicity in NIH 3T3 cells. *Proc Natl Acad Sci U S A* **87**: 10005-10009.

Rudin CM, Hann CL, Laterra J, Yauch RL, Callahan CA, Fu L, Holcomb T, Stinson J, Gould SE, Coleman B et al. 2009. Treatment of medulloblastoma with hedgehog pathway inhibitor GDC-0449. *N Engl J Med* **361**: 1173-1178.

Russo C, Pellarin M, Tingby O, Bollen AW, Lamborn KR, Mohapatra G, Collins VP, Feuerstein BG. 1999. Comparative genomic hybridization in patients with supratentorial and infratentorial primitive neuroectodermal tumors. *Cancer* **86**: 331-339.

Sahai E, Marshall CJ. 2002. RHO-GTPases and cancer. *Nat Rev Cancer* **2**: 133-142.

Sanz-Moreno V, Gadea G, Ahn J, Paterson H, Marra P, Pinner S, Sahai E, Marshall CJ. 2008. Rac activation and inactivation control plasticity of tumor cell movement. *Cell* **135**: 510-523.

Schuller U, Heine VM, Mao J, Kho AT, Dillon AK, Han YG, Huillard E, Sun T, Ligon AH, Qian Y et al. 2008. Acquisition of granule neuron precursor identity is a critical determinant of progenitor cell competence to form Shh-induced medulloblastoma. *Cancer Cell* **14**: 123-134.

Senchenko VN, Krasnov GS, Dmitriev AA, Kudryavtseva AV, Anedchenko EA, Braga EA, Pronina IV, Kondratieva TT, Ivanov SV, Zabarovsky ER et al. 2011. Differential expression of CHL1 gene during development of major human cancers. *PLoS One* **6**: e15612.

Sers C, Emmenegger U, Husmann K, Bucher K, Andres AC, Schafer R. 1997. Growth-inhibitory activity and downregulation of the class II tumor-suppressor gene H-rev107 in tumor cell lines and experimental tumors. *J Cell Biol* **136**: 935-944.

Shakhova O, Leung C, van Montfort E, Berns A, Marino S. 2006. Lack of Rb and p53 delays cerebellar development and predisposes to large cell anaplastic medulloblastoma through amplification of N-Myc and Ptch2. *Cancer Res* **66**: 5190-5200.

Shang X, Moon SY, Zheng Y. 2007. p200 RhoGAP promotes cell proliferation by mediating cross-talk between Ras and Rho signaling pathways. *J Biol Chem* **282**: 8801-8811.

Sjoblom T, Jones S, Wood LD, Parsons DW, Lin J, Barber TD, Mandelker D, Leary RJ, Ptak J, Silliman N et al. 2006. The consensus coding sequences of human breast and colorectal cancers. *Science* **314**: 268-274.

Starr TK, Allaei R, Silverstein KA, Staggs RA, Sarver AL, Bergemann TL, Gupta M, O'Sullivan MG, Matise I, Dupuy AJ et al. 2009. A transposon-based genetic screen in mice identifies genes altered in colorectal cancer. *Science* **323**: 1747-1750.

Swartling FJ, Grimmer MR, Hackett CS, Northcott PA, Fan QW, Goldenberg DD, Lau J, Masic S, Nguyen K, Yakovenko S et al. 2010. Pleiotropic role for MYCN in medulloblastoma. *Genes Dev* **24**: 1059-1072.

Symons M, Segall JE. 2009. Rac and Rho driving tumor invasion: who's at the wheel? *Genome Biol* **10**: 213.

Tabori U, Baskin B, Shago M, Alon N, Taylor MD, Ray PN, Bouffet E, Malkin D, Hawkins C. 2010. Universal poor survival in children with medulloblastoma harboring somatic TP53 mutations. *J Clin Oncol* **28**: 1345-1350.

Tang X, Tian Z, Chueh PJ, Chen S, Morre DM, Morre DJ. 2007. Alternative splicing as the basis for specific localization of tNOX, a unique hydroquinone (NADH) oxidase, to the cancer cell surface. *Biochemistry* **46**: 12337-12346.

Taylor MD, Mainprize TG, Rutka JT. 2000. Molecular insight into medulloblastoma and central nervous system primitive neuroectodermal tumor biology from hereditary syndromes: a review. *Neurosurgery* **47**: 888-901.

Thompson MC, Fuller C, Hogg TL, Dalton J, Finkelstein D, Lau CC, Chintagumpala M, Adesina A, Ashley DM, Kellie SJ et al. 2006. Genomics identifies medulloblastoma subgroups that are enriched for specific genetic alterations. *J Clin Oncol* **24**: 1924-1931.

Traenka C, Remke M, Korshunov A, Bender S, Hielscher T, Northcott PA, Witt H, Ryzhova M, Felsberg J, Benner A et al. 2010. Role of LIM and SH3 protein 1 (LASP1) in the metastatic dissemination of medulloblastoma. *Cancer Res* **70**: 8003-8014.

Tronche F, Kellendonk C, Kretz O, Gass P, Anlag K, Orban PC, Bock R, Klein R, Schutz G. 1999. Disruption of the glucocorticoid receptor gene in the nervous system results in reduced anxiety. *Nat Genet* **23**: 99-103.

Varela I, Tarpey P, Raine K, Huang D, Ong CK, Stephens P, Davies H, Jones D, Lin ML, Teague J et al. 2011. Exome sequencing identifies frequent mutation of the SWI/SNF complex gene PBRM1 in renal carcinoma. *Nature* **469**: 539-542.

Varley JM, Evans DG, Birch JM. 1997. Li-Fraumeni syndrome--a molecular and clinical review. *Br J Cancer* **76**: 1-14.

Verhaak RG, Hoadley KA, Purdom E, Wang V, Qi Y, Wilkerson MD, Miller CR, Ding L, Golub T, Mesirov JP et al. 2010. Integrated genomic analysis identifies clinically relevant subtypes of glioblastoma characterized by abnormalities in PDGFRA, IDH1, EGFR, and NF1. *Cancer Cell* **17**: 98-110.

Vogel KS, Klesse LJ, Velasco-Miguel S, Meyers K, Rushing EJ, Parada LF. 1999. Mouse tumor model for neurofibromatosis type 1. *Science* **286**: 2176-2179.

Wechsler-Reya RJ, Scott MP. 1999. Control of neuronal precursor proliferation in the cerebellum by Sonic Hedgehog. *Neuron* **22**: 103-114.

Werbowetski-Ogilvie TE, Seyed Sadr M, Jabado N, Angers-Loustau A, Agar NY, Wu J, Bjerkvig R, Antel JP, Faury D, Rao Y et al. 2006. Inhibition of medulloblastoma cell invasion by Slit. *Oncogene* **25**: 5103-5112.

Wetmore C, Eberhart DE, Curran T. 2001. Loss of p53 but not ARF accelerates medulloblastoma in mice heterozygous for patched. *Cancer Res* **61**: 513-516.

Wiesner SM, Decker SA, Larson JD, Ericson K, Forster C, Gallardo JL, Long C, Demorest ZL, Zamora EA, Low WC et al. 2009. De novo induction of genetically engineered brain tumors in mice using plasmid DNA. *Cancer Res* **69**: 431-439.

Woo S, Gomez TM. 2006. Rac1 and RhoA promote neurite outgrowth through formation and stabilization of growth cone point contacts. *J Neurosci* **26**: 1418-1428.

Wu X, Northcott PA, Croul S, Taylor MD. 2011. Mouse models of medulloblastoma. *Chin J Cancer* **30**: 442-449.

Xiao A, Yin C, Yang C, Di Cristofano A, Pandolfi PP, Van Dyke T. 2005. Somatic induction of Pten loss in a preclinical astrocytoma model reveals major roles in disease progression and avenues for target discovery and validation. *Cancer Res* **65**: 5172-5180.

Yang H, Zhang C, Zhao X, Wu Q, Fu X, Yu B, Shao Y, Guan M, Zhang W, Wan J et al. 2010. Analysis of copy number variations of BS69 in multiple types of hematological malignancies. *Ann Hematol* **89**: 959-964.

Yang ZJ, Ellis T, Markant SL, Read TA, Kessler JD, Bourboulas M, Schuller U, Machold R, Fishell G, Rowitch DH et al. 2008. Medulloblastoma can be initiated by deletion of Patched in lineage-restricted progenitors or stem cells. *Cancer Cell* **14**: 135-145.

Yuan L, Santi M, Rushing EJ, Cornelison R, MacDonald TJ. 2010. ERK activation of p21 activated kinase-1 (Pak1) is critical for medulloblastoma cell migration. *Clin Exp Metastasis* **27**: 481-491.

Yue Q, Groszer M, Gil JS, Berk AJ, Messing A, Wu H, Liu X. 2005. PTEN deletion in Bergmann glia leads to premature differentiation and affects laminar organization. *Development* **132**: 3281-3291.

Yusa K, Zhou L, Li MA, Bradley A, Craig NL. 2011. A hyperactive piggyBac transposase for mammalian applications. *Proc Natl Acad Sci U S A* **108**: 1531-1536.

Zavarella S, Nakada M, Belverud S, Coniglio SJ, Chan A, Mittler MA, Schneider SJ, Symons M. 2009. Role of Rac1-regulated signaling in medulloblastoma invasion. Laboratory investigation. *J Neurosurg Pediatr* **4**: 97-104.

Zhen HN, Zhang X, Bu XY, Zhang ZW, Huang WJ, Zhang P, Liang JW, Wang XL. 1999. Expression of the simian virus 40 large tumor antigen (Tag) and formation of Tag-p53 and Tag-pRb complexes in human brain tumors. *Cancer* **86**: 2124-2132.

Zindy F, Nilsson LM, Nguyen L, Meunier C, Smeyne RJ, Rehg JE, Eberhart C, Sherr CJ, Roussel MF. 2003. Hemangiosarcomas, medulloblastomas, and other tumors in Ink4c/p53-null mice. *Cancer Res* **63**: 5420-5427.